European Community's Framework Programme 6

EUROPEAN EXTREMELY LARGE TELESCOPE DESIGN STUDY

Document title:	*Multi-Instruments Measurement Campaign, Paranal*
Document number:	ELT-TRE-UNI-12300-0001
Issue No	1
Date	*07/04/2009*

Prepared by A. Ziad

Approved by J. Vernin

Released by J. Vernin

European Organisation for Astronomical Research in the Southern Hemisphere

LABORATOIRE FIZEAU

Université Nice Sophia Antipolis

Report on:

Multi-instruments Measurement Campaign

Paranal, CHILE

(17-26 December 2007)

Prepared by

Wassila DALI ALI (November 2008)

Institutes participating to the Paranal campaign:

ESO:	IAC:	CTIO:	FIZEAU (NICE Univ.)
M. Sarazin	J. M. Delgado	A. Tokovinin	A. Ziad
J. Navarrete.		E. Bustos	J. Borgnino
G. Lombardi.			A. Berdja.
			J. Maire
			W. Dali Ali

Table of contents

I. Introduction:

The Extremely Large Telescope is a new concept proposed by the European organisation ESO that consists on the construction of giant telescope. It comes up as reply to the much advanced tools needed in these next decades as the detection of exoplanets. ESO focuses its efforts on the design of a telescope with 42 m diameter. This will offer at the same time a very large surface of light collection of a thousand m^2, and a very high angular resolution that would reach 0.001 to 0.6 arc-seconds in the optical wavelengths.
The optical interferometers with very large baseline also allow the possibility to reach such resolutions which increase with the baseline as well as the diameter size in case of monolithic mirror. However, the interferometers have a smaller collecting surface and the field of view is relatively restricted. The combination of unprecedented acuity and light gathering power of the future ELTs will not only provide unique images of objects at all scales, from solar and extra-solar planets to the first points of light in our Universe; it will also allows detailed spectral analysis, thus revealing their nature, motions and characteristics. These important advantages give the ELT the statute of the most performant optical instrument in ground-based astronomy field.

The realisation of such device needs huge efforts to face the technical complexity. However, as all terrestrial telescopes, the ELT suffers from one major problem, which is atmospheric turbulence. This last degrades the wave front coming from luminous source objects while traversing the turbulent layer. Hence, the power of resolution of the telescope is strongly decreased than its instrumental limit. The internal adaptive optics systems (AO) were planned to correct these effects, but their performance is strongly depending on the site quality.

For such telescope size, the site qualification takes an important part in the projects studies, as the choice of the site, the wavefront behaviour at large scales of the E-ELT size and the impact of the surface layer on image quality. Indeed, the site evaluation has not to be limited to the “classical” parameters but also to asses more deeply the properties of the wavefront at large scales.

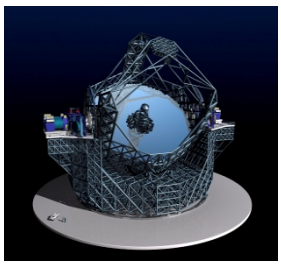

Figure1: ELT prototype image

For this aim, a campaign of observations was organised and accomplished in December 2007 at Paranal using exclusively an optical methods to measure the wavefront properties at different scales, with several site-testing instruments. First, standard instruments ESO-DIMM & GSM were used for the wavefront characterization at the small scales. The NAOS AO system which provides statistics on the wavefront behaviour up to the UT size was used for intermediate scales. The VLTI/AMBER interferometer was used to study the wavefront at large scales. A second type of instruments was dedicated to the measurement of the vertical atmospheric turbulence distribution, which is needed in the modelling of wavefront at ground level as Cut-SCIDAR, LuSci, MASS and MOSP.
The use of these different instruments comes to reduce the misinterpretation of the results, and to give simultaneously, spatial and temporal information on various scales. And allows the comparison between the data, then a better understand of the wavefront behaviour.

This campaign had a privilege of a participation of the most known site-testing instruments and high Angular Resolution techniques (NAOS AO and VLTI/AMBER).

Second objective of this study is the modelling of the wavefront at different scales of turbulence and to check the theoretical model in grate scale. This was possible since the used instruments are sensitive to various scale of turbulence presented next as:

ESO & NICE

In this section we make a brief description of each instrument, their installation and the general conditions of observations during the campaign. We talk about the pertinence of the use of each instrument in this study and the measured parameters. After we present the different results of all observations night by night after the global statistics concerning the campaign.

II. Instruments participating to the 2007 Paranal campaign:

2.1 Cute-SCIDAR: SCIntillation Detection And Ranging

The principle of generalized SCIDAR is based on the extraction of the spatial correlation of the scintillation images of binary stars. The CDD detector that records these scintillation patterns is placed in the virtual plane of analysis conjugated to some negative altitude making SCIDAR sensitive to turbulence at all altitudes. The upgrade version of Cute-SCIDAR instrument for Paranal has been developed by IAC. The new performances are to provide the temporal evolution of turbulence profiles in real time with and without dome seeing contribution, and the remote control of the instrument during this campaign.
It was mounted at The VLTI Auxiliary Telescope 4 (AT4) (see Figure 2). After solving some technical problems, the Cute-SCIDAR reached full accuracy in November 2007.

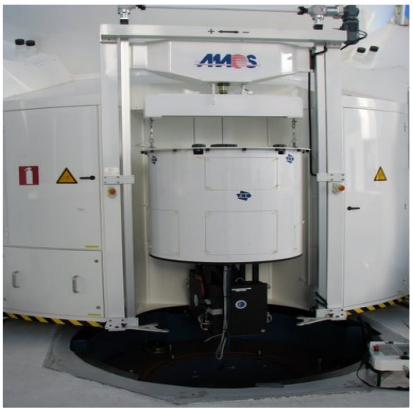

Figure 2: Cute-SCIDAR installation AT Paranal

During observations, the instrument pointed a double star target transiting between -2 hrs and +2 hrs with respect to the meridian. Typically observe stars brighter than 5.0 mag in *V*-band. The more the double star is separated; the better is the resolution of the instrument. For this reason the minimum allowed separation is 7.0 arcseconds. In the southern hemisphere, at the latitude of Paranal, there is a limited number of binary systems of this kind, so only two or three targets are observed by every night. The vertical sampling of the profile is on a 300 m grid from some altitude bellow the mountain to 1900m above the see.

2.2 ESO-DIMM: Differential Image Motion Monitor:

It is based on the statistics study of the AA distortions of the wavefront. Working in permanent at Paranal since 1986 (Sarazin M. , 1986), it was the main element of the instrumentation developed for VLT site evaluation campaign. It consists on a 35cm diameter masked telescope. ESO-DIMM is placed on a 6m height tower (see figure3).

Figure 3: the automated ESO-DIMM at the VLT Observatory with its daytime protection enclosure at Paranal 2007.

At the entrance pupil plan, the starlight passes through two circular sub-apertures. A prism with very small deviation angle is placed at one of apertures in order to split the starlight into tow beams, forming then in the focal plan two images of one star. The measurement of the differential image motion will separate the effect of atmospheric turbulence from the telescope vibration effect. Using Kolmogorov model, the seeing defined as the full width at half maximum (FWHM) of the atmospheric long exposure is related to the variance of the differential image motion through circular apertures using an analytical model. The final estimate of the seeing is the average of both parallel and perpendicular motion (Sarazin & Roddier, 1991). ESO-DIMM updates the seeing every minute

2.3 IAC-DIMM:

Another version of DIMM was also used in this campaign; it is the IAC-DIMM, which is very similar to ESO-DIMM, with the same physical basis, but transformed to become a commercial product. The main difference are the less sensitivity to aberration, the focal length was increased and equipped with an intensified CCD to avoid the temporal convolution (Vernin & Munoz-Tunon, 1995).

2.4 GSM (Generalized Seeing Monitor)

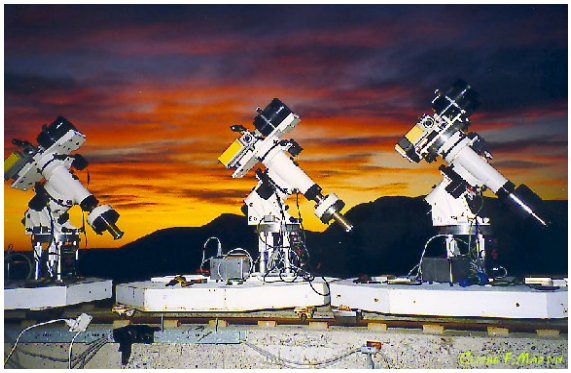

Figure 4: GSM instrument at Calern, Nice.

The Generalized Seeing Monitor is dedicated to the measurement of parameters that characterize the optical properties of wavefront. These parameters are deduced from the analyses of spatio-temporal statistic of the angle of arrival (AA) fluctuations. Parameters of interest are the seeing, outer scale of turbulence, isoplanatic angle and coherence time. The experiment consists of several independent synchronized modules measuring angle of arrival fluctuations at different points of the wavefront with 10 cm telescopes. Usually GSM consists of 4 separate modules but exclusively for this campaign 6 were used. Two are placed on the same mount to measure the seeing like DIMM configuration (Ziad & al., 2000).

2.5 LuSci (Lunar Scintillometer)

Figure 5: LuSci instrument at Paranal Dec2007

To separate the ground layer contribution in the seeing degradation, a new instrument was used in this campaign, which is LuSci. This last has a same principle than SHABAR (SHadow Band Ranging) for the solar scintillation measurement. LuSci uses the Moon as

an extended source. The normalized scintillation covariance is measured over a set of detectors at fixed separations (baselines). Each baseline has sensitivity to turbulence of a given altitude range (Hickson and Lanzetta, 2004).

The signal is averaged over the increasing projected size of the source at large heights of the turbulent layer. This limits the sensitivity to high altitudes.
The covariance C (b) at baseline b, measures C_n^2 (z) with a weighting function W(z ,b).This last is dependent on the detector configuration (size, baseline separation and orientation) as well as lunar phase. In this campaign, LuSci had detectors spaced linearly in such a way to have the turbulence profile at ranges of 3, 6, 30 and 256m above ground. We note that during the campaign the instrument was almost totally automated (Tokovinin, 2007).

2.6 MASS: (Multi Aperture Scintillation Sensor)

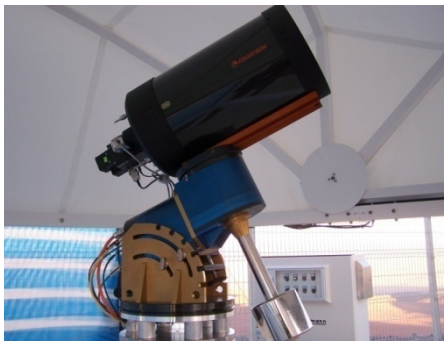

Figure 6: MASS instrument at Paranal 2007

The MASS instrument measures the scintillation. The light from a single bright star is received by a system of 4 concentric apertures (the inner aperture A of 2 cm diameter, and the annular apertures B, C, and D surrounding it, with the outer diameter of D about 8 cm). The beam splitting between annular apertures is done by internal optics (Kornilov & Tokovinin, 2001) . Scintillation in each aperture is detected with photo-multipliers with 1 ms exposure time. This last depend on the turbulence altitude; then a different apertures and their combinations act as spatial filters, separating contributions of corresponding altitudes. Consequently, MASS gives the turbulence profile C_N^2, the coherence time and the isoplanatic angle. However MASS does not sense the near-ground turbulence and does not work under strong scintillation.

2.7 MOSP: (Monitor of Outer Scale Profile)

Figure 7: MOSP instrument (left) and GSM (right) at Paranal Dec 2007.

MOSP is the only instrument able to extract of outer scale profiles. The principle of the instrument is based on the measurement of the fluctuations of Angle of Arrival (AA) to different angular separations by observation of the lunar limb. It consists on, the determination of the spatio-angular correlations of these fluctuations to measure the conditions of turbulence in different atmospheric layers. The AA fluctuations are measured perpendicularly to the lunar limb, leading to transverse correlations for different angular separations along the moon edge.

The instrument is composed of a small telescope (29cm of diameter) having a large focal length (10m), equipped with a PixelFly camera CCD and a Barlow lens to extend the focal distance. This increases the sensitivity of the monitor to the fluctuation of the lunar edge. In order to freeze atmospheric effects on lunar edge image motion, the exposure time was set to 1 or 2ms (Maire & al., 2006) .

2.8 NAOS /AO: (Nasmyth Adaptive Optics System (NAOS))

Figure 8: NACO instrument mounted at UT4 Paranal

Installed in the Nasmyth B focus of the 4th VLT Unit Telescope at the Paranal Observatory in Chile and has been operated since October 2002. NACO provides multimode, adaptive optics corrected observations in the range of 1 – 5micrometer. NAOS is an Adaptive Optics (AO) system designed to work with natural guide stars, extended objects and, in the close future, with a laser guide stars. Its unique feature is that it is capable of wavefront sensing in both visible and infrared light. It uses with the High-Resolution Near IR Camera (CONICA) which is an infrared imager and spectrograph. The observing modes it supports include: imaging in broad- and narrow-band filters, long slit spectroscopy, coronography with different occulting masks. Developed by ONERA group, this AO system allows the calculation without any loop opening to automatically monitor and provide the atmospheric turbulence optical parameters(seeing, $\mathcal{L}_0$,and coherence time). This method is based on the reconstruction of the open-loop data from DM and tip-tilt mirror voltages and residual wavefront slopes for closed-loop data (see T. Fusco et al., 2004). The optical turbulence parameters calculated will be compared with those measured by the instruments operating in same time during this campaign.
This will advance our knowledge on the difference in the seeing conditions observed between the UTs and the site –testing monitors at Paranal.

2.9 VLTI interferometer using AMBER: (Astronomical Multi-Beam combiner).

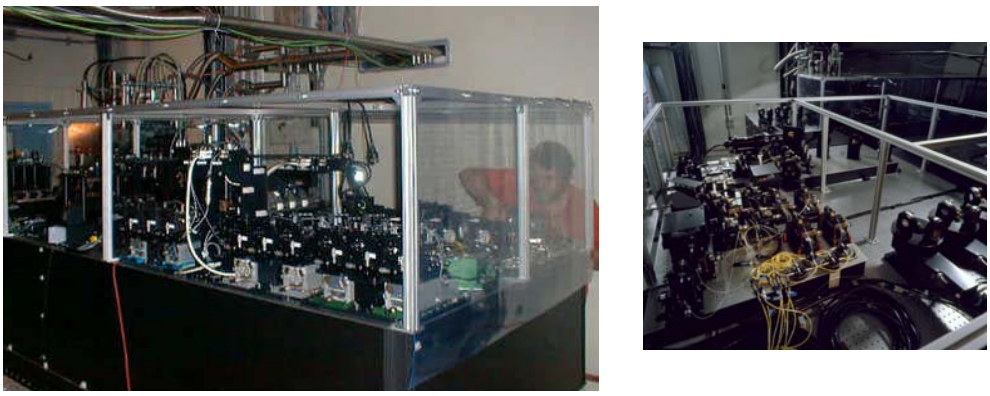

Figure 9: AMBER instrument (left), and fringe tracker FINITO (right)

Interferometric measurements with large baselines are appropriate for the wavefront study at large scales. Indeed, measurements of the optical pathlength difference (OPD) between the two arms of an interferometer lead to the phase structure function which is characteristic of the wavefront. For this task, we are interesting on the VLTI-AMBER interferometer measurement since we can observe simultaneously with 3 different baselines.

AMBER is a three-beam combiner working in the near-infrared (J, H and K band). It features a set of monomode fibre into which the incoming light is injected in order to have a clean plane wavefronts before combination. A set of collimated and mutually parallel beams are focused by a common optical element in a common Airy pattern that contains fringes with same principle than the GI2T interferometer (J. Maire et al. 2006, A&A).

The two or three beams are coming from the UTs located in non-redundant way and the auxiliary telescopes ATs which can be located in large number of station; providing then, a big choice of baselines configurations.

The OPD fluctuation that appear as spatial fluctuations of the dispersed fringes, are related to the value of outer scale (Roddier, 1981), thus the simultaneous measurements of outer scale $\mathcal{L}_0$ by GSM and MOSP in this campaign helps one to separate the instrumental contribution from atmospheric one.

During the observation AMBER was equipped with an external fringe tracker FINITO (figure9); to the OPD correction in real time. The performance of this system can be then tested by comparing the different parameters calculated with other instruments, in particular the coherence time which is provided by GSM, ESO-DIMM and MASS.

2.10 METEO station:

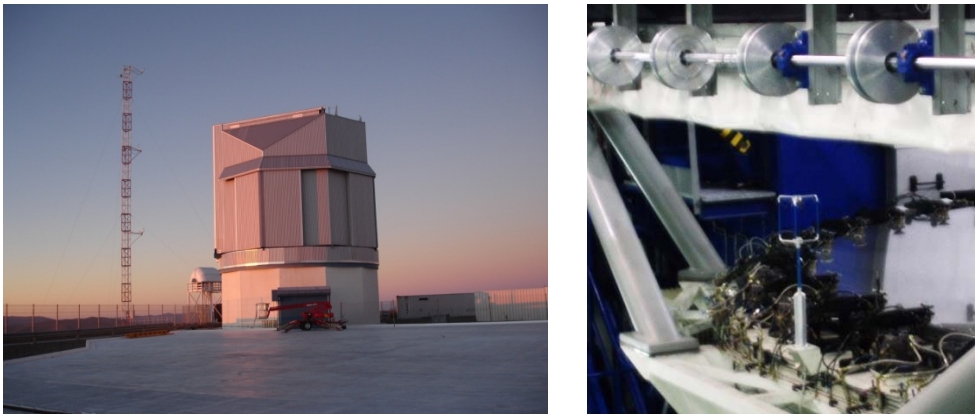

Figure 10: the meteorological station outside dome (left), and thermal probes inside dome UT4 (right)

To complete our study for this campaign, we collected data from several facilities in the site outside domes near the instruments (figure.10) where is placed the meteorological tower positioned at the North side of the Paranal telescope platform. It delivers mean wind speeds and direction at 10 and 40 m height averaged on 1 minute (60 values/hour for 24 hours by day), and the wind speed standard deviation. We collected also the temperature data inside dome at UT4 in order to follow the internal distribution of temperature and for correlation with seeing data. Another meteorological station archive is to be used in this campaign. It is from the ECMWF data for all the period of observation.

III. Conditions of Campaign observations

The conditions were adequate for this campaign with all nights were clear. The observations started at the expected date, i.e., 17 December 2007 and continued for 10 nights until 26th with the most instruments observing except some shorts cuts for certain of them. We resume the running time for all instrument in the next table:

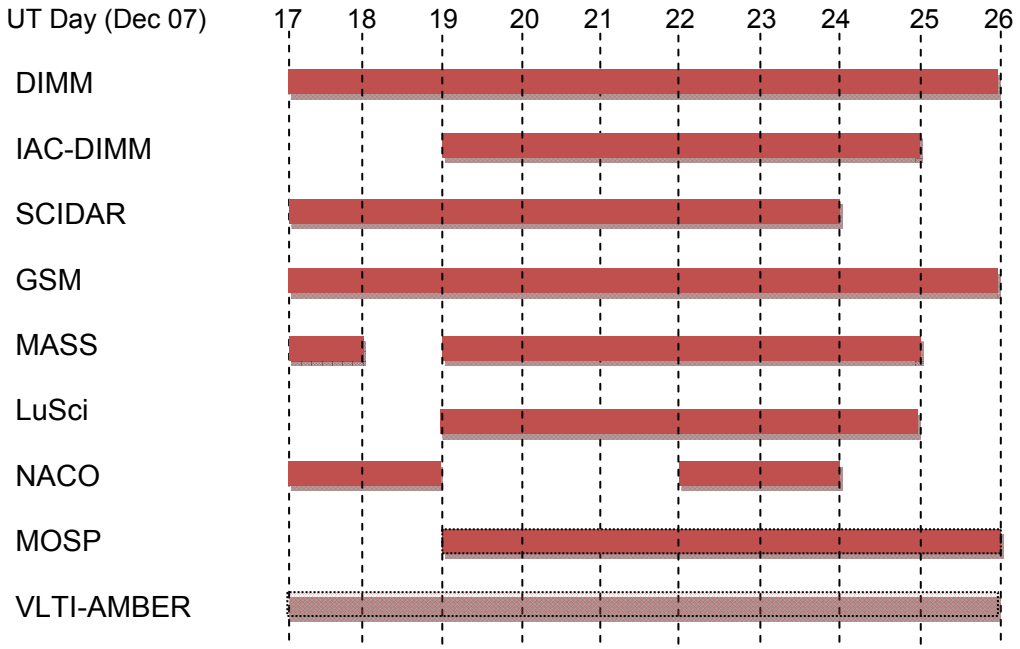

Table 1: Running period of the Paranal Campaign instruments

As we can see, the full instrument's operation has been from the night of 19th to 24rd. So for this study, we can focus on this period to make comparisons between the instruments produced data. A list of targets was provided. The instruments GSM, MOSP, MASS and LuSci (located at around 1m high from ground level) were installed as we can see in (figure 11) near the ESO-DIMM tower (located at 6 m high).

For GSM with 6 baselines and MOSP it was necessary to built two pillars in addition of those made for the Dec-98 campaign. We note that GSM and MOSP were installed and tested two days before starting observations. LuSci was installed on Dec 18th and started observations on the same night whereas Cute-SCIDAR and MASS were installed before and DIMM is permanently operating in the site.

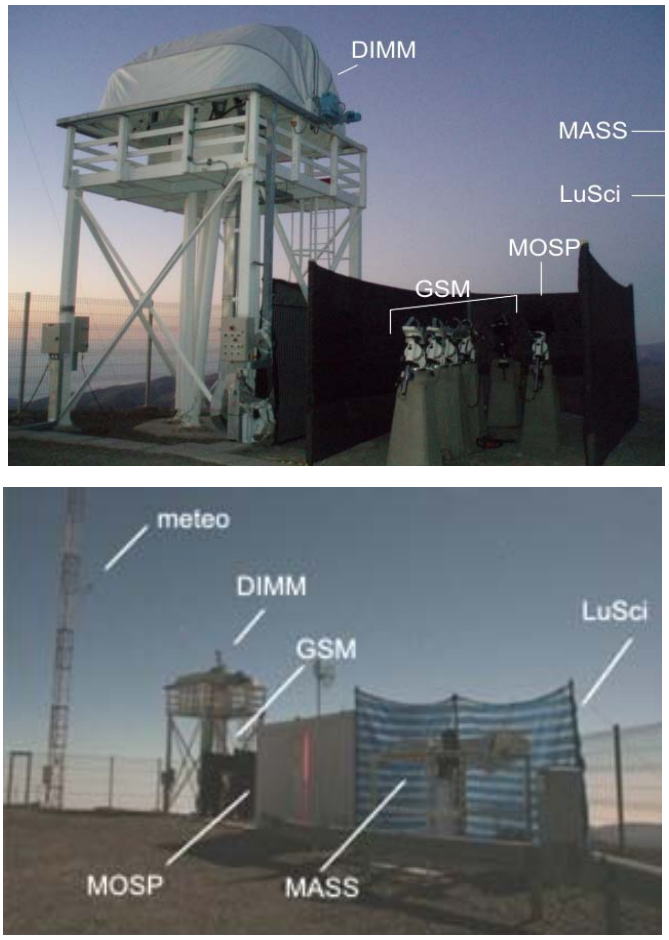

Figure 11: Instruments location during the Campaign Dec 2007 Paranal

IV. Presentation of the campaign results

In this section we present the characteristic parameter given by each instrument. After, we make a comparison between the parameters values calculated by each instrument given below:

Cute-SCIDAR ---------- V(h), $C_N^2(h)$, ε_0, θ_0, τ_0

ESO-DIMM ---------- ε_0, θ_0 , τ_0

IAC-DIMM ---------- ε_0

GSM ---------- ε_0, L_0, θ_0, τ_0

LUSCI ---------- ε_0

MOSP ---------- $L_0(h)$, $C_N^2(h)$, ε_0

NAOS/AO ---------- ε_0, L_0, τ_0

VLTI/AMBER ---------- OPD, ε_0, L_0

where $C_N^2(h)$ is the refractive index structure constant &V(h) wind speed given at altitude h, L_0 the outer scale, ε_0 the seeing, θ_0 the isoplanatic angle and τ_0 the coherence time.

We present in next section the measurement of each parameter given by each instrument for the whole campaign, the corresponding histograms and a table summarizing results and some necessary information as the temperature and wind speed. After we give the temporal evolution night by night the histograms for each parameters, each instrument and finally tables summarizing produced data by giving the median value and the rang of variation.

4.1 Outer scale measurement:

Outer scale profile measured with MOSP:

So, for this report we are not going to present detailed results because The MOSP data reduction needs more time, we just give the result of two nights and the method that we use to extract the profile of outer scale.

To estimate the turbulence outer scale profile $\mathcal{L}_0 h(h)$ during this campaign, we analyzed the wavefront AA fluctuations from image motion of the limb of the moon obtained by means of the MOSP instrument. For the extraction of the height dependence of outer scale, we used a simulated annealing algorithm using $Ch_n^2(h)$ profiles measured simultaneously with SCIDAR see (figure11). The value of $\mathcal{L}_0(h)$ is then integrated on the ground. Thus, a comparison with measurements of the outer scale using the GSM is given in (figure 13). In addition we discuss the results obtained in relation to their implications in Adaptive Optics and in Long-Baseline Interferometer (figure 12).

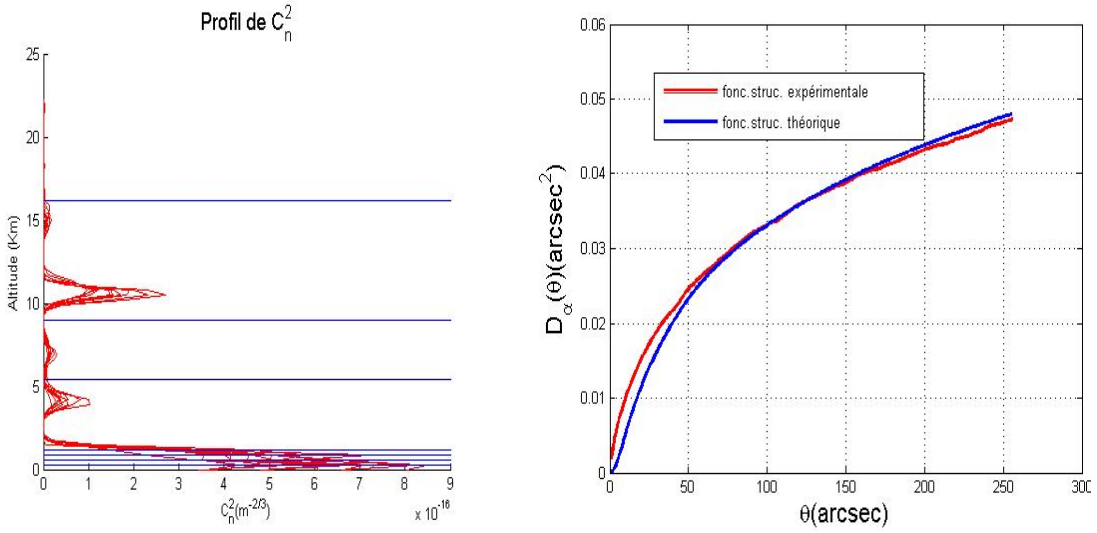

Figure 12: (left) profile of $Ch_n^2(h)$, (right) the adjustment of the experiment and theoretical structure function

we show in (figure 12) the more adequate choice of the atmospheric layer repartition to adujst the experimantal deduced strcuture function to the theorotical structure function with the a this algorithm.

The results we obtain are presented in (figure13), for tow night 19th and 23rd where we note qualitatively same profile comparing two nights with more great value of $\mathcal{L}_0 h(h)$ for the 23rd (measured at 5 UT). So, we can attribute this good coherence scale for this night

to the stabilisation of turbulence noted with the other instruments at this part of night. Indeed, the profile given for this time shows that a larger value of 60m was reached after decreasing to 5m at the low altitude (<1000m) this join our conclusion about the surface layer stabilisation seen by other instruments. The outer scale in the low atmospheric layers is smaller than the high atmosphere.

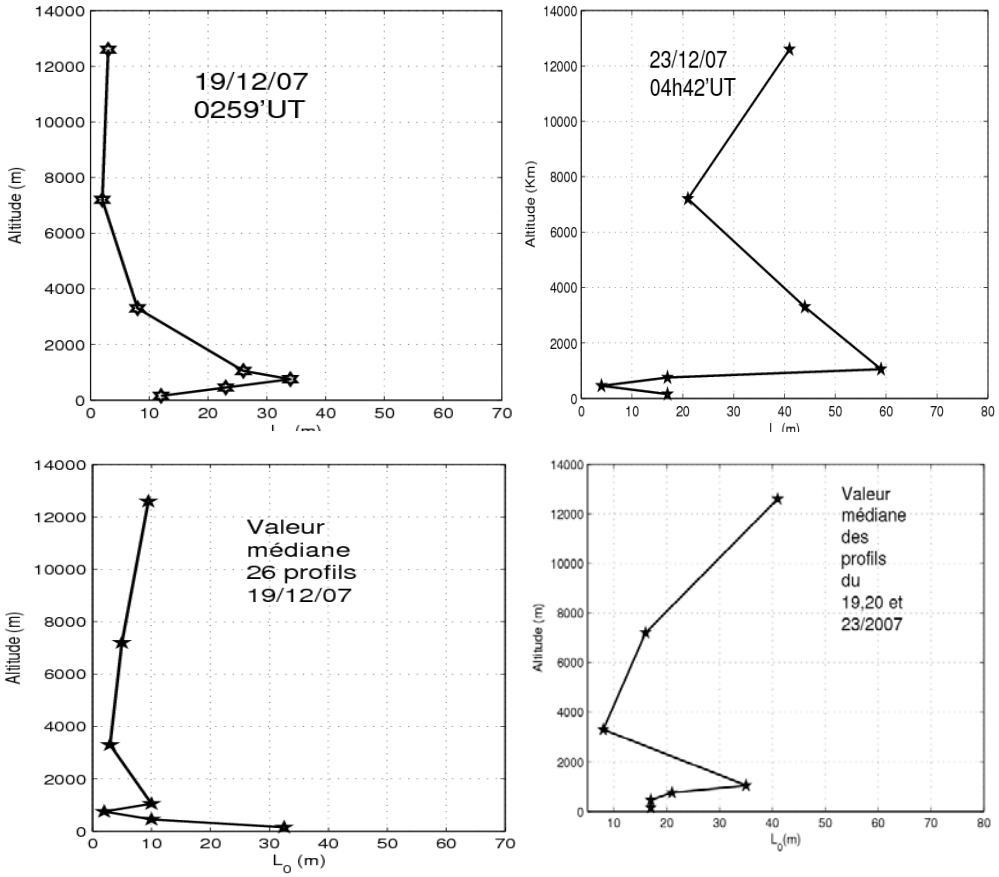

Figure 13: profile of $\mathcal{L}_0 h(h)$ for the nights 19 and 23 Dec 2007

The implications in Adaptive Optics of this study result come when calculating the variance of the Zernike polynomials coefficients using the outer scale profiles shows that modes amplitude is important for a small diameter (fig14). As consequence of this, it is not necessary; to add a mirror with the subsystems which would take into account the correction of the modes of low order, the tip-tilt for example.

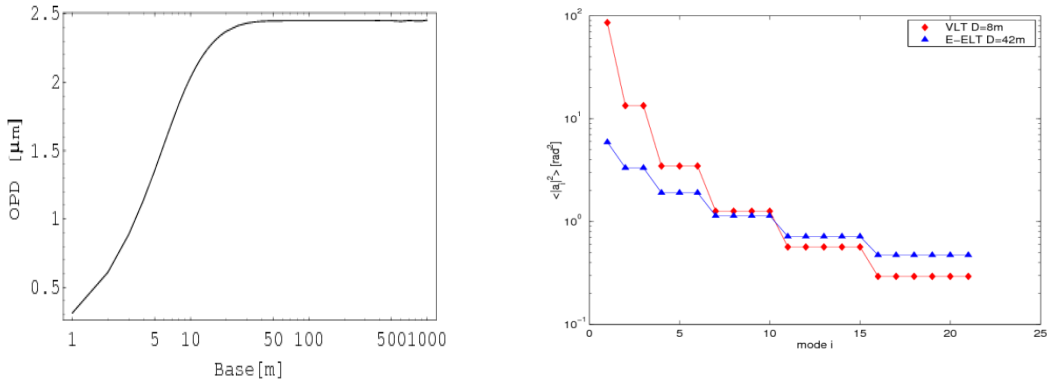

Figure 14: (left) OPD deduced value, (right) the mode amplitude using outer scale profiles

In the other hand, the calculation of the variance of OPD fluctuations, with the obtained profiles, shows that for long bases of 40m amplitude of the variance does not exceed 2.5 µm, (figure 14). That allows, for example, to determinate a maximum of the fringes displacement which is taken into account in the interferometers dimensioning.

Measurement of outer scale with AMBER:

The atmospheric turbulence causes, principally, a loss of the fringes' contrast, the effect of the differential piston, corresponding to a temporal shift of the arrival wave front on each telescope, involve random fluctuations of the optical path difference (OPD) and thus a random translation of the fringes. By measuring the OPD standard deviation which is proportional to the structure function of the phase D_φ(F. Roddier 81), we can estimate the value of the outer scale $\mathcal{L}_0$:

$$\sigma_{OPD} = \frac{\lambda}{2\pi}\sqrt{D_\varphi(B, \mathcal{L}_0)} \quad (1)$$

where B base line and λ wavelength

A part of this study is dedicated to the reduction of VLTI/AMBER data, the third long-base line of this instrument used simultaneously allow us to retrieve this parameter which is important to describe the space properties of the wave front at large scales. To make a comparison of the measured value of outer scale during this campaign a study is in hand of AMBER data. For this aim, a set of data was requested and a processing data method was checked by our team to extract the OPD and deduce outer scale value. For that, we are going to use the method presented by (Maire & al., 2007).

So in this report, we don't have yet the requested data from AMBER, so we will make some comparison of the current value given by the monitors and those measured by AMBER previously.

figure (15) gives the evolution of OPDs fluctuation according to given baseline, using equation (1) we deduce the outer scale for each baseline as it is shown in figure(15). We not that the value of outer scale given by the interferometer are relatively high than those measured by GSM this can be explained by the instrumental contribution, furthermore the atmospheric turbulence conditions. Indeed, the difference in values for each baseline configuration, supposes a dome contribution and instrumental effect if we consider the isotropy in the atmospheric turbulence affecting a three telescopes.

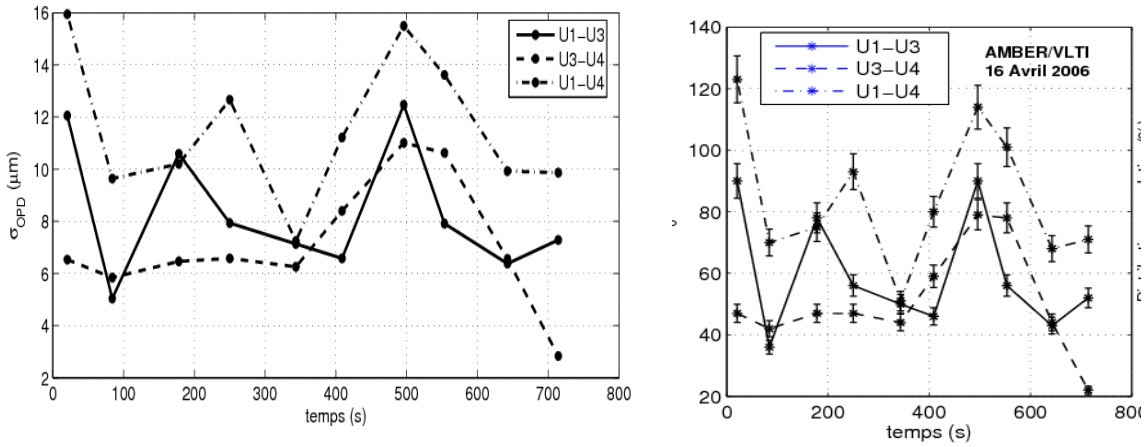

Figure 15 : (left) OPD time evolution, (right) outer scale velue given by AMBER for the night of 16 April 2006.

For the aim to separate the contribution of instruments, we are learning the possibility of the use of PRIMA to calculate the outer scale parameter. Indeed, PRIMA is equipped with laser metrology (figure 16) that allows the separation of instrument piston. First discussion with the PRIMA project stuff, on the possibility to work in special constraints for the commissioning of the instrument, motivates us to invest in this way since it will be possible to operate with FSU (Fringe Sensor Unite) open loop in both cases of keeping AO systems off or on. It will be interesting to collect a data for this opportune period of PRIMA commissioning. This will allow us not only the characterization of the outer scale parameter given by Interferometry but also to make in evidence the contribution of dome seeing.

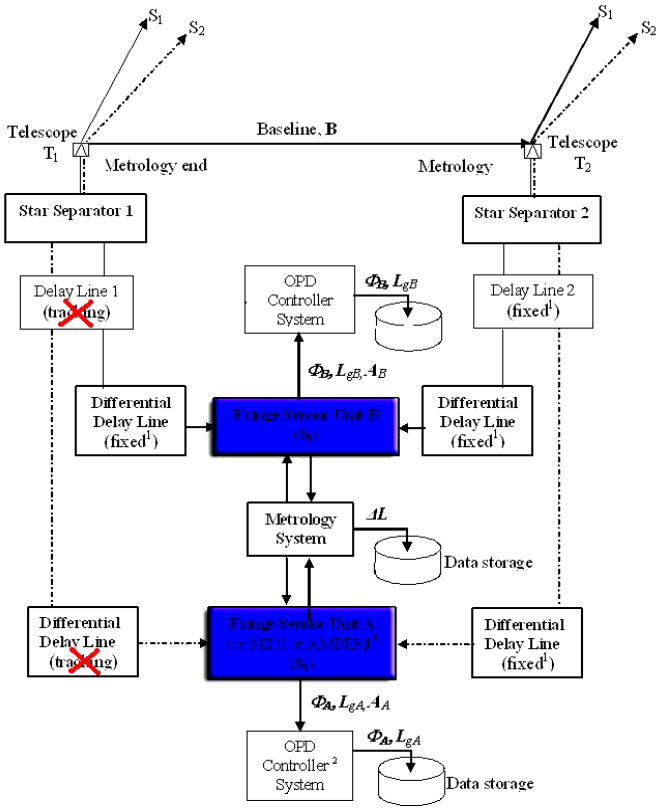

Figure 16 : schema of the principle of using PRIMA

In the following part we give tables summarizing the data produced by all instruments for all the nights during this campaign. We give also the average value of temperature, wind speed and indicate the cloud presence.

Measurement of outer scale with GSM for all Campaign:

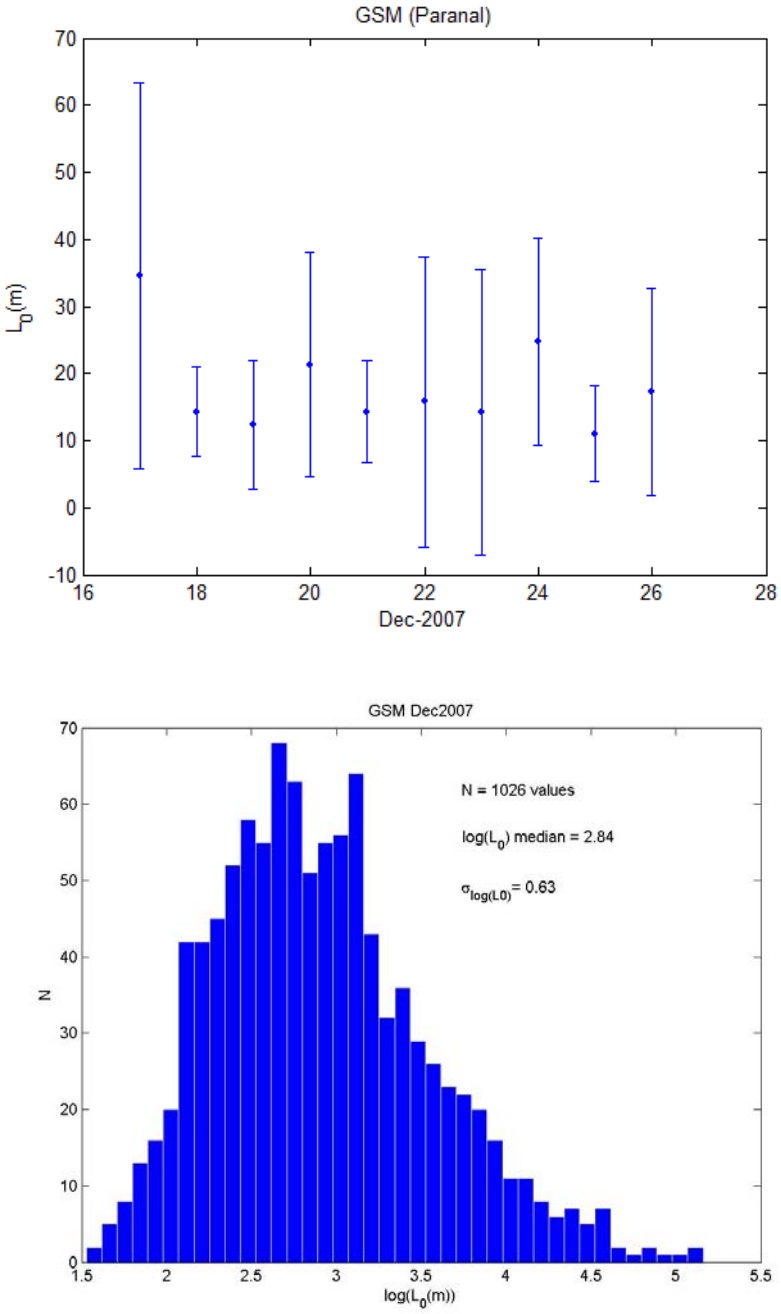

Figure 17: outer scale bar errors for all the campaign (above), histogram of the outer scale measurement (down) given by GSM.

4.2 Measurement of seeing for all campaign:

Seeing measured by Cute-SCIDAR:

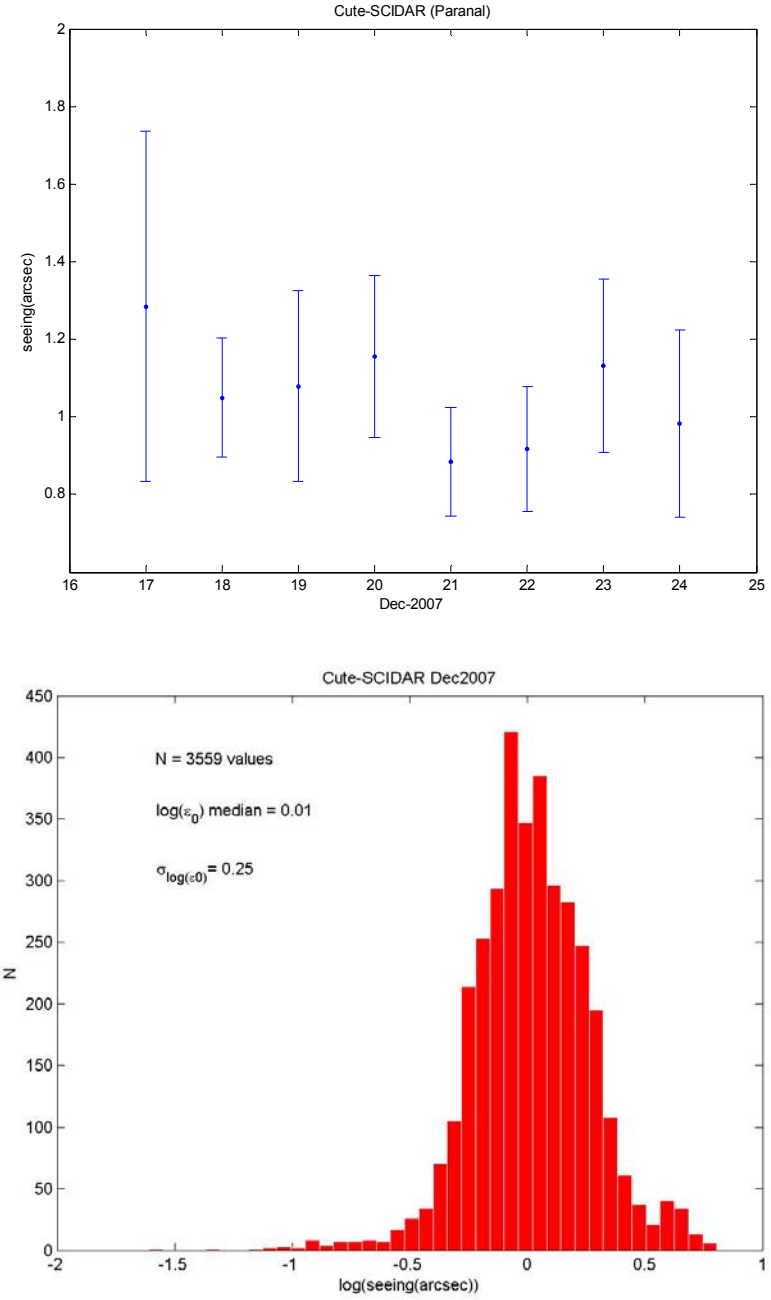

Figure 18: seeing bar errors for all the campaign (above), histogram of the seeing measurement (down) given by Cute- SCIDAR.

Seeing measured by ESO-DIMM:

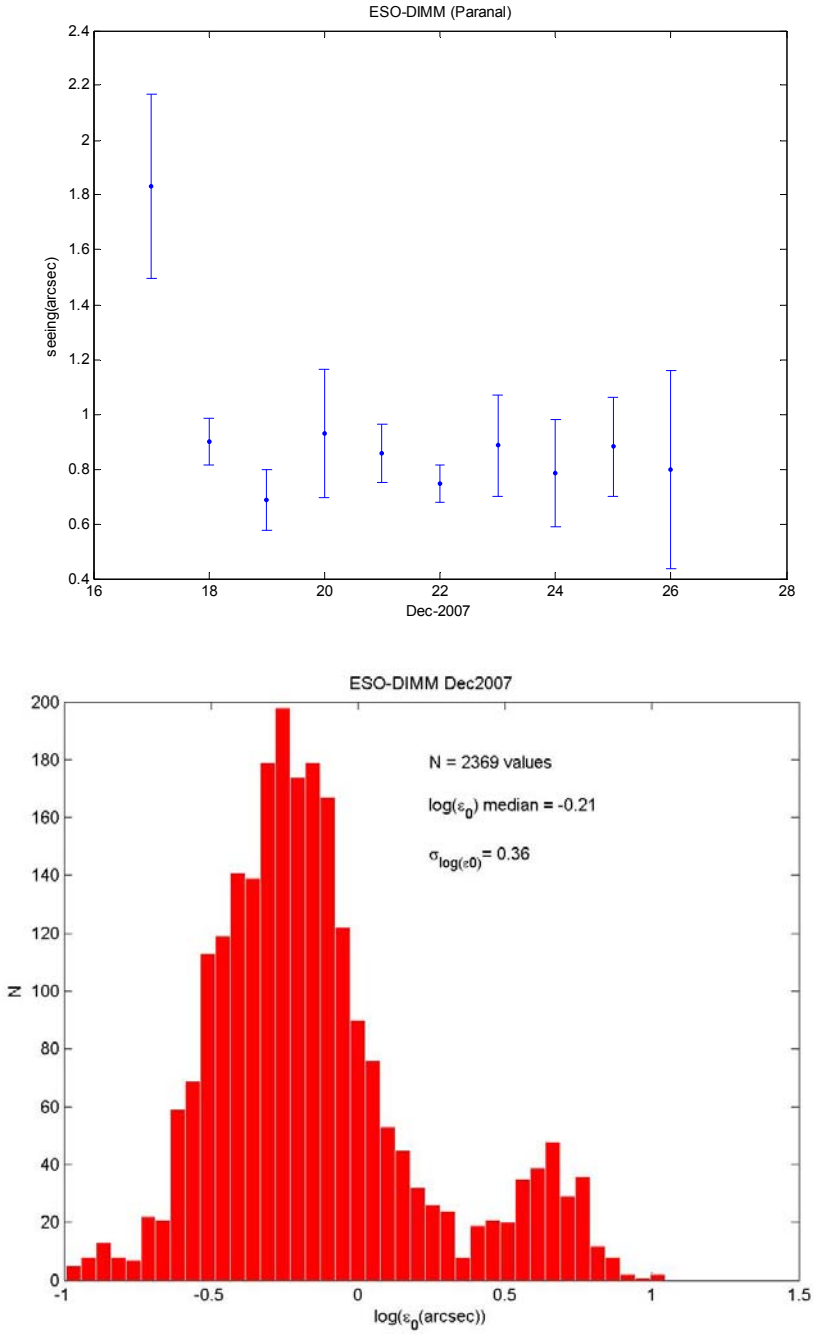

Figure 19: seeing bar errors for all the campaign (above), histogram of the seeing measurement (down) given by ESO-DIMM.

Seeing measured by IAC-DIMM:

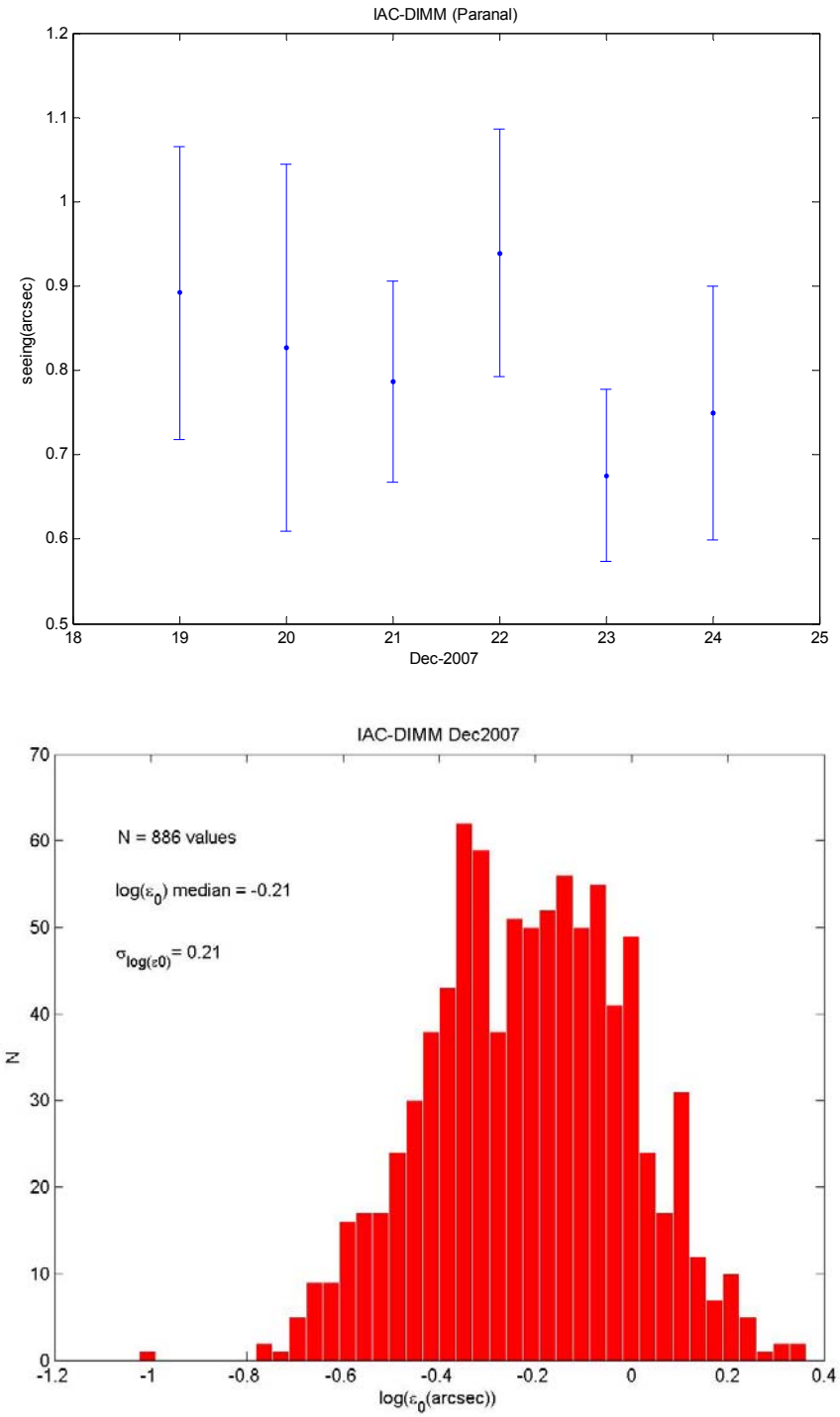

Figure 20: seeing bar errors for all the campaign (above), histogram of the seeing measurement (down) given by IAC-DIMM.

Seeing measured by GSM:

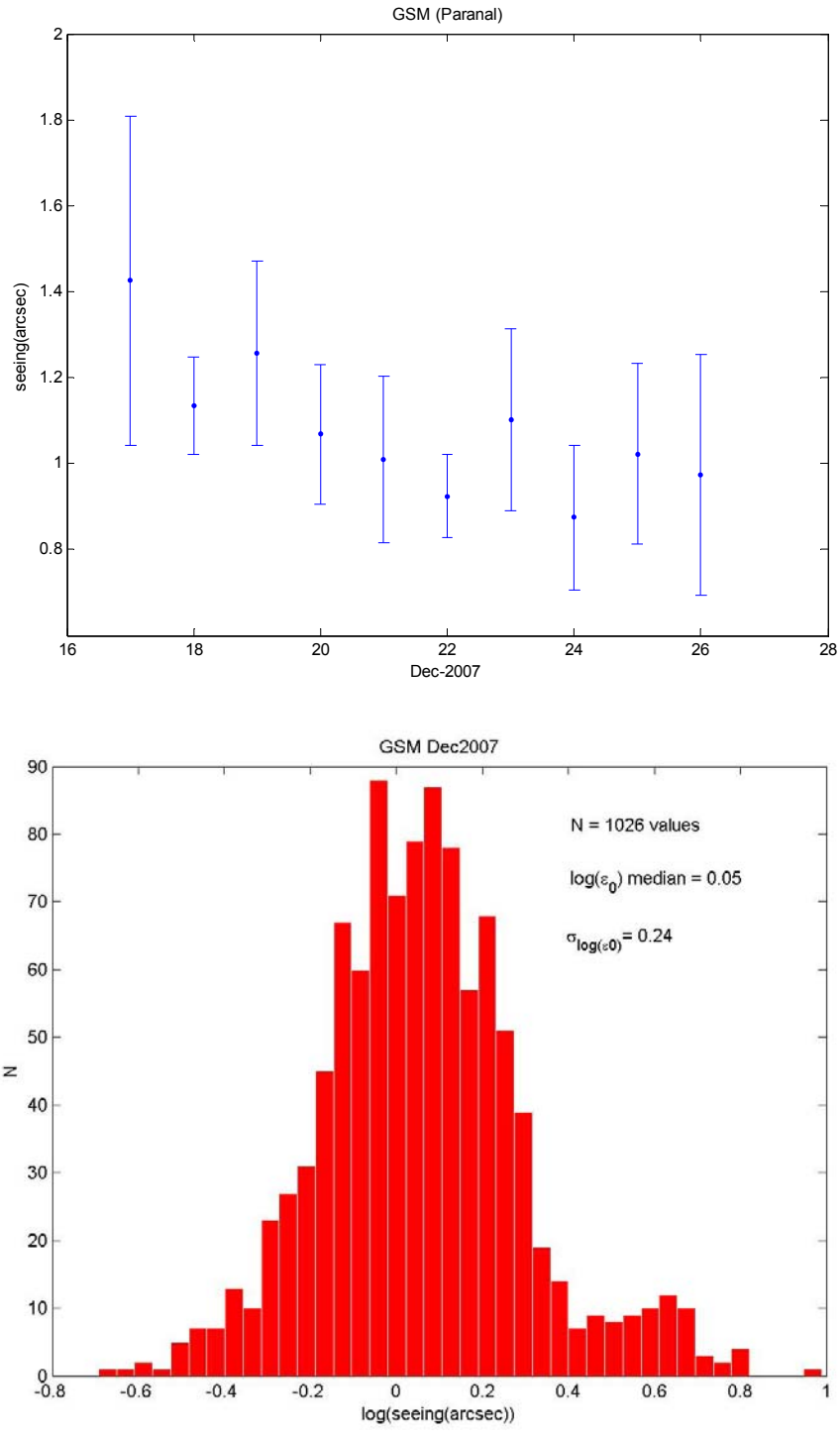

Figure 21: seeing bar errors for all the campaign (above), histogram of the seeing measurement (down) given by GSM.

Seeing measured by LuSci:

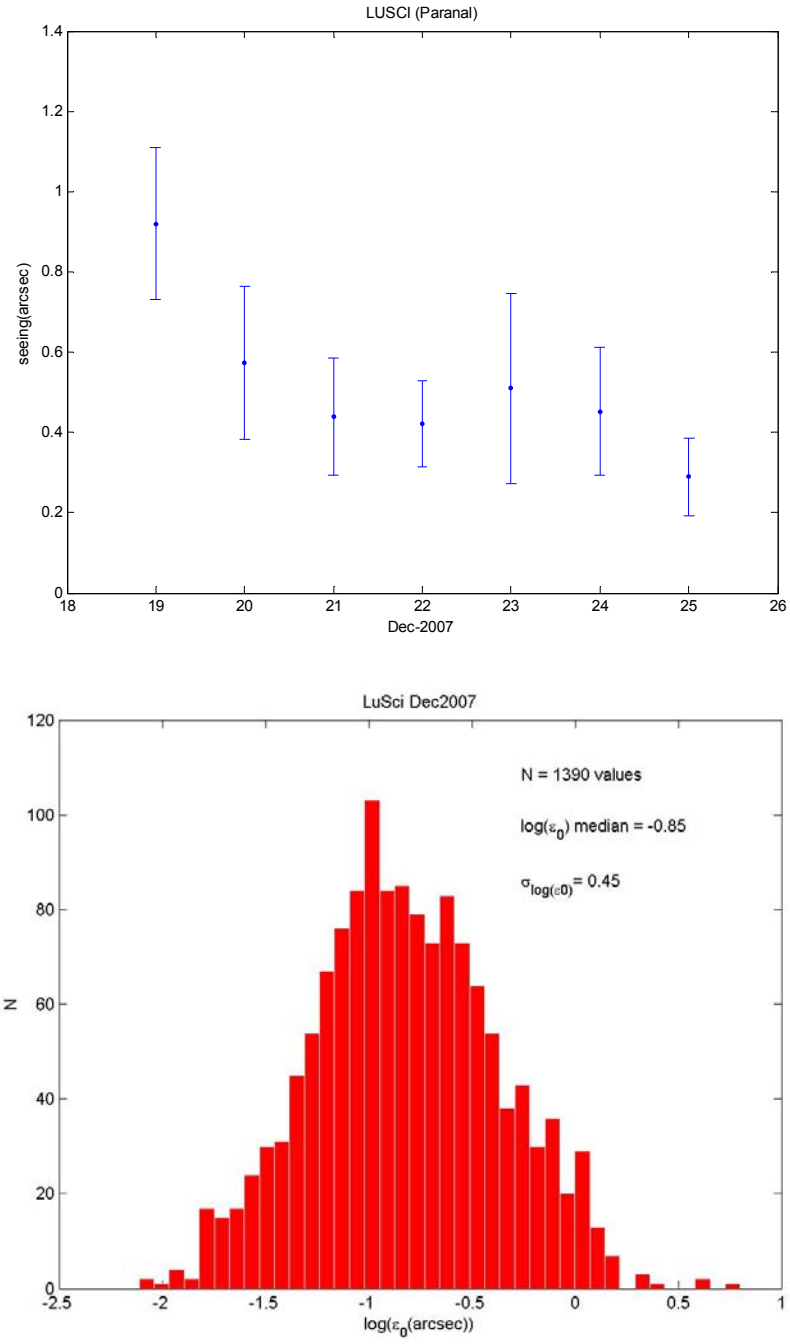

Figure 22: seeing bar errors for all the campaign (above), histogram of the seeing measurement (down) given by LuSci.

Seeing measured by MASS:

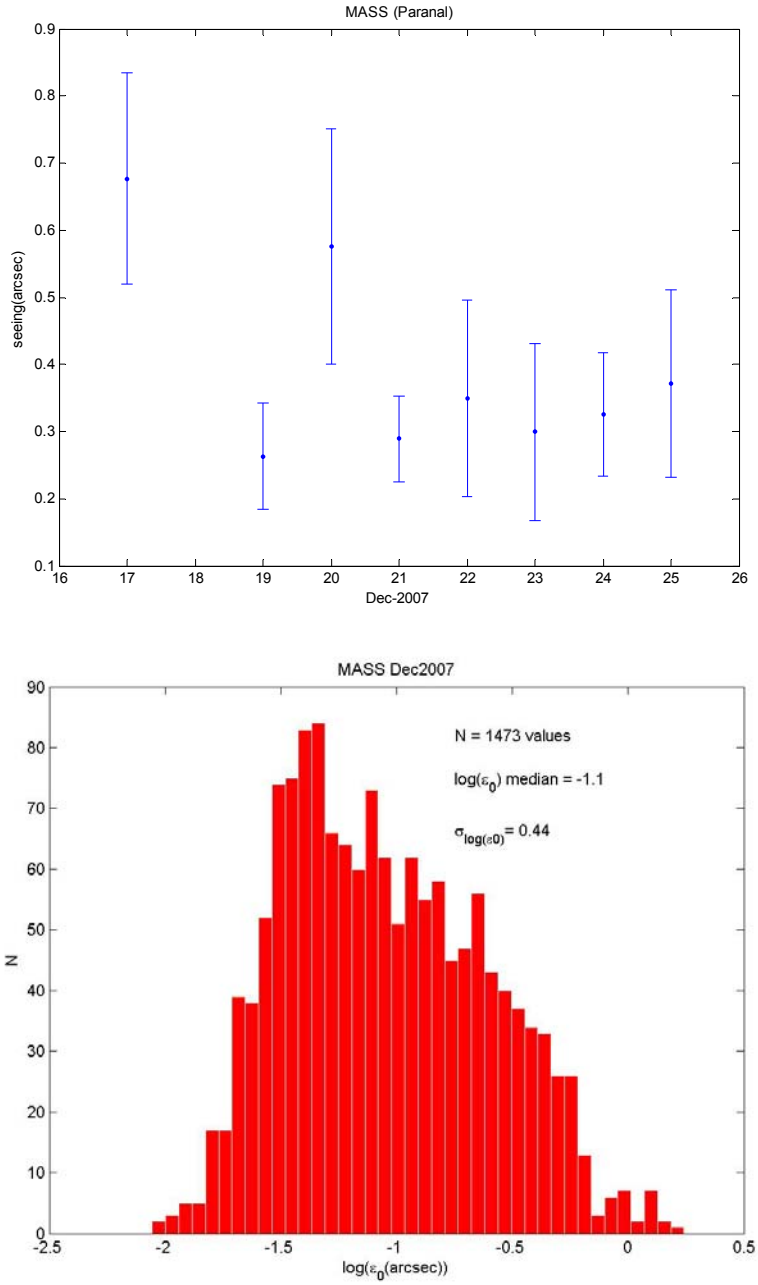

Figure 23: seeing bar errors for all the campaign (above), histogram of the seeing measurement (down) given by MASS.

4.3 Measurement of the coherence time for all campaign:

Coherence time by ESO-DIMM:

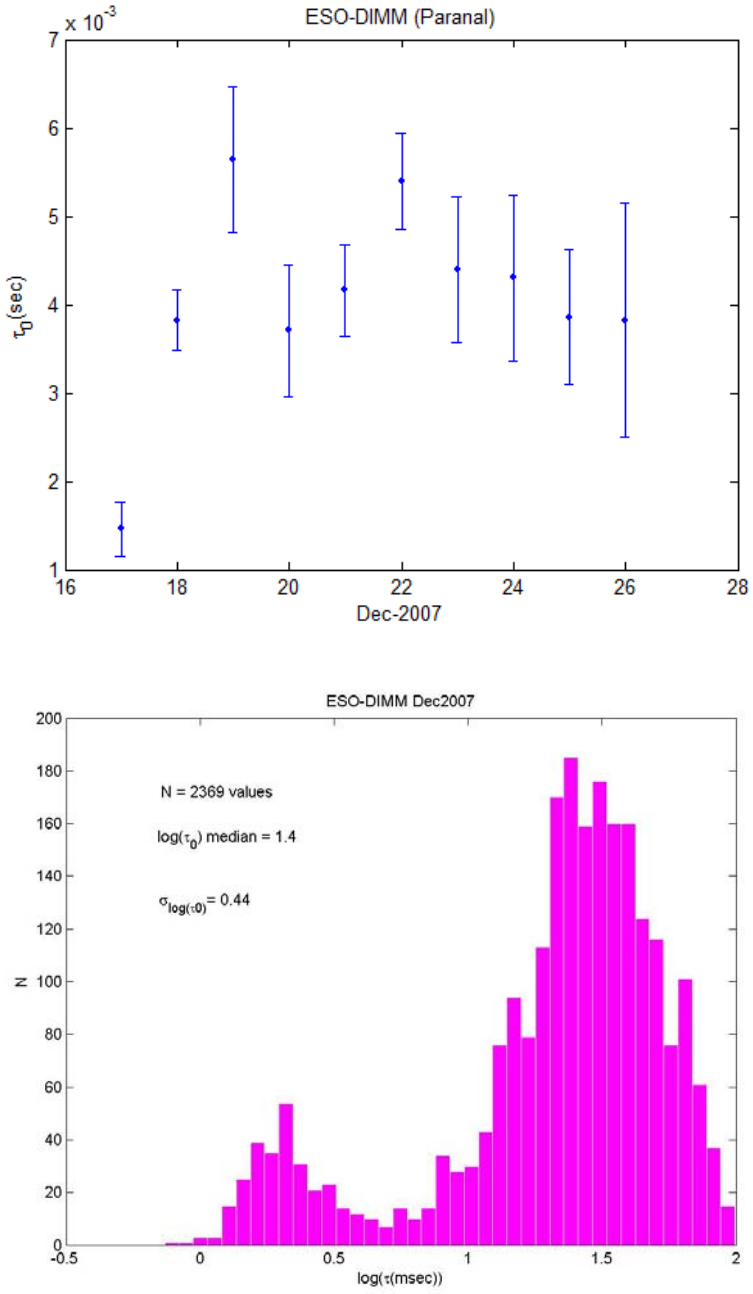

Figure 24: coherence time bar errors for all the campaign (above), histogram of the coherence time measurement (down) given by ESO-DIMM.

Coherence time by GSM:

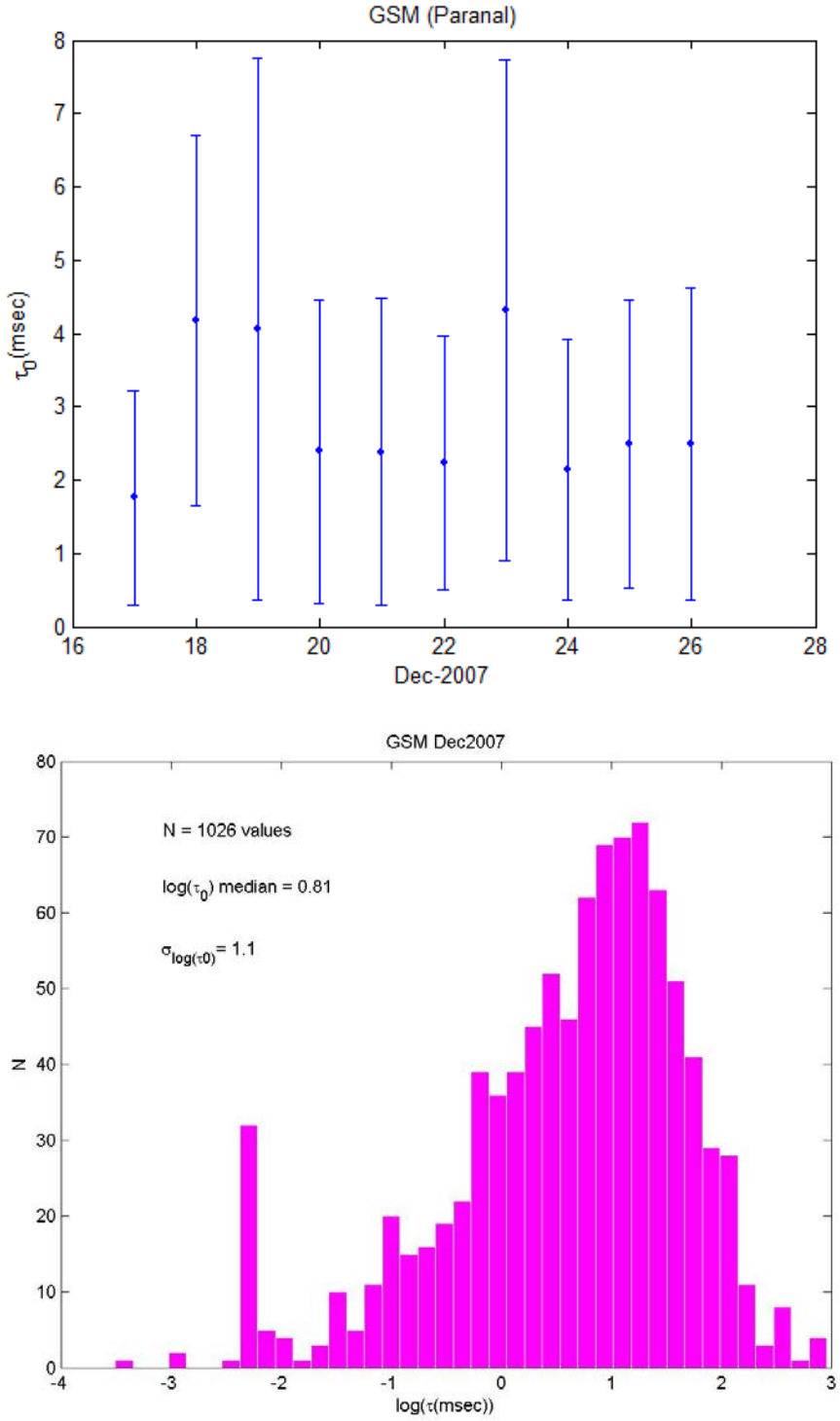

Figure 25: coherence time bar errors for all the campaign (above), histogram of the coherence time measurement (down) given by GSM

Coherence time by MASS:

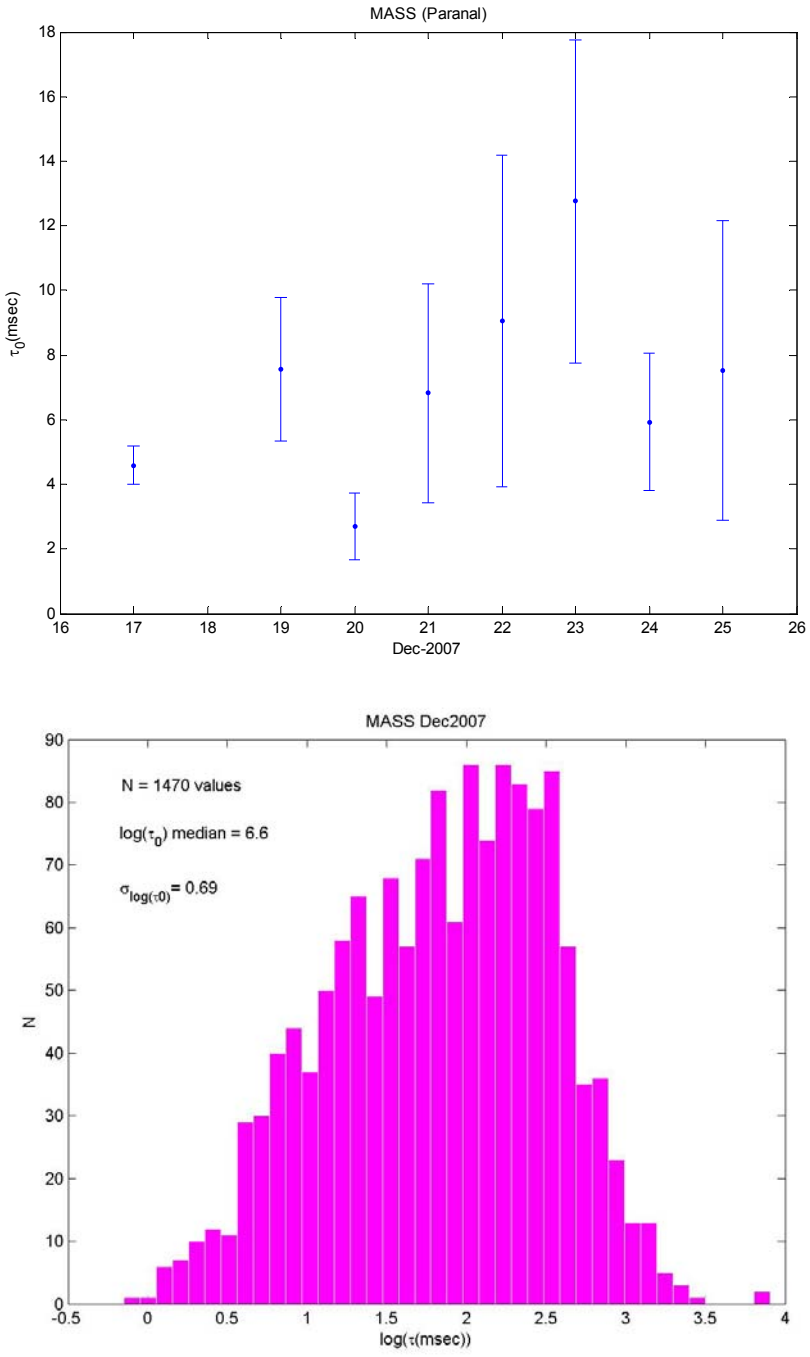

Figure 26: coherence time bar errors for all the campaign (above), histogram of the coherence time measurement (down) given by MASS.

4.4 Measurement of Isoplanatic angle for all campaign:

Isoplanatic angle by Cute-SCIDAR:

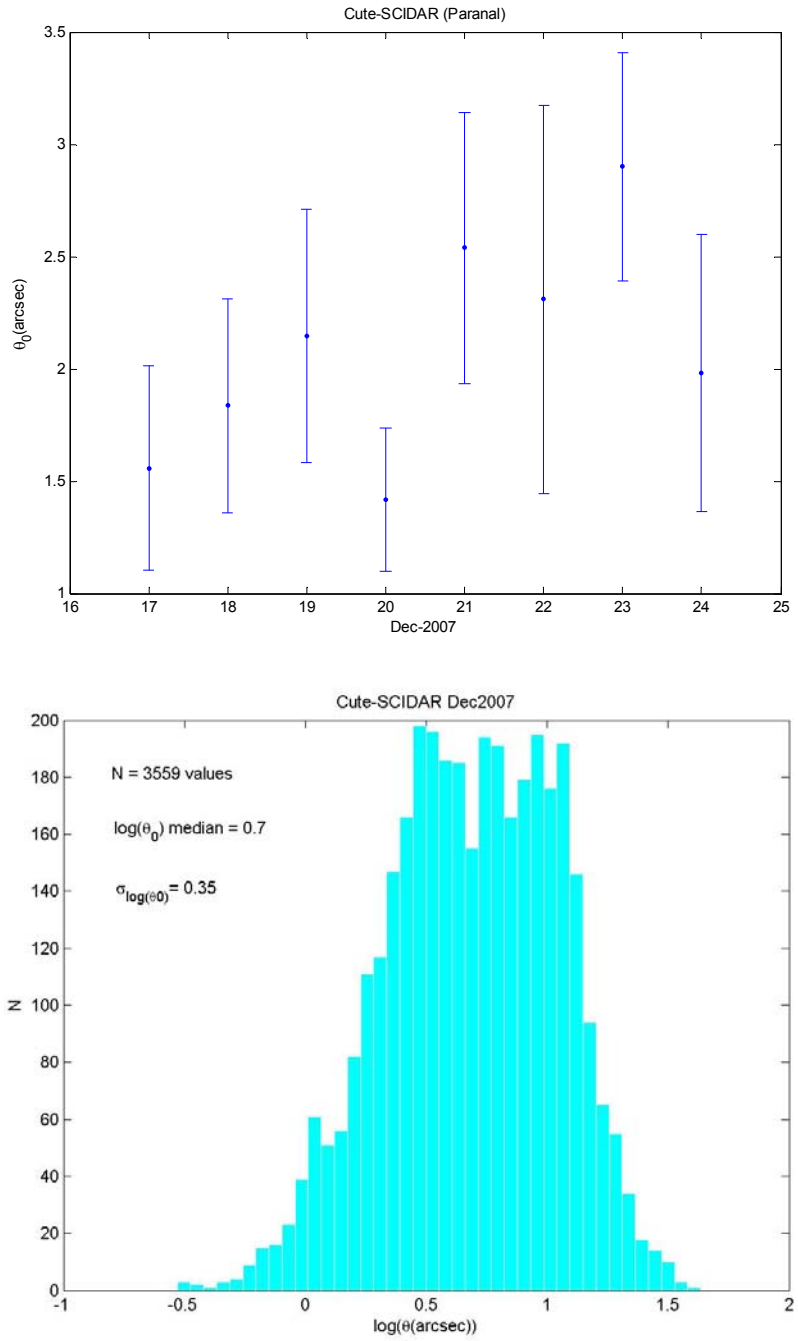

Figure 27: isoplanatic angle bar errors for all the campaign (above), histogram of the isoplanatic angle measurement (down) given by Cute-SCIDAR.

Isoplanatic angle by ESO-DIMM:

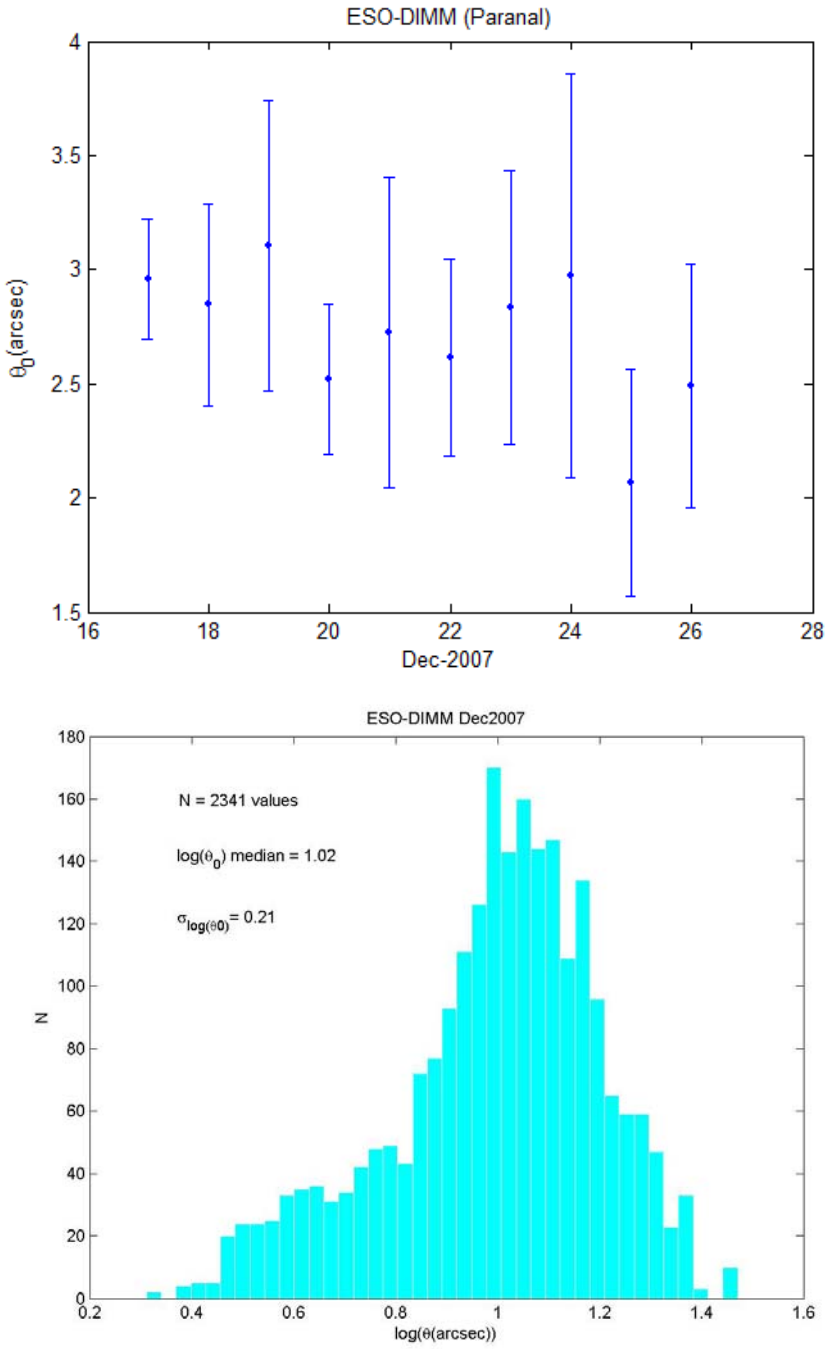

Figure 28: isoplanatic angle bar errors for all the campaign (above), histogram of the isoplanatic angle measurement (down) given by ESO-DIMM.

Isoplanatic angle by GSM:

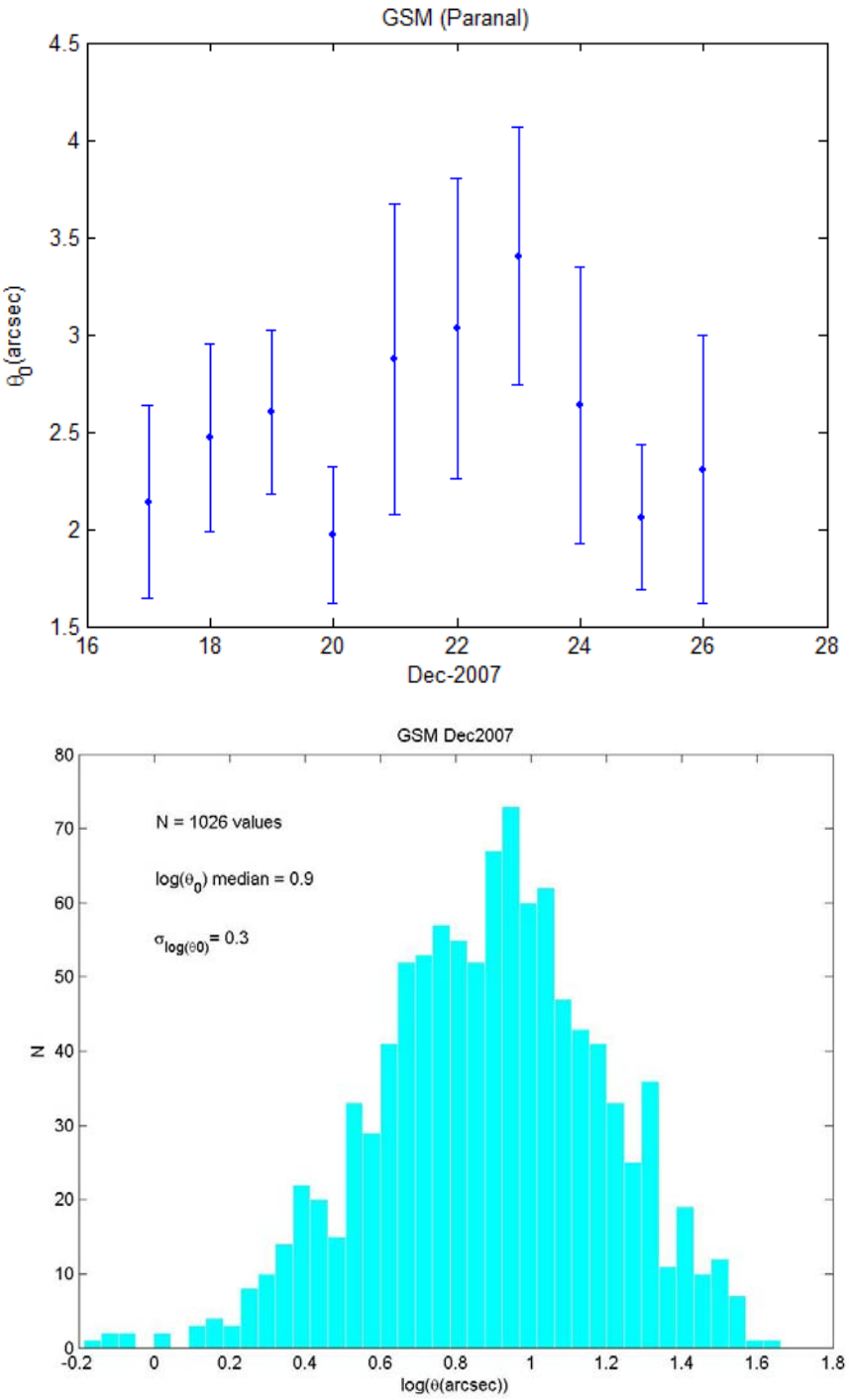

Figure 29: isoplanatic angle bar errors for all the campaign (above), histogram of the isoplanatic angle measurement (down) given by GSM.

Isoplanatic angle by MASS:

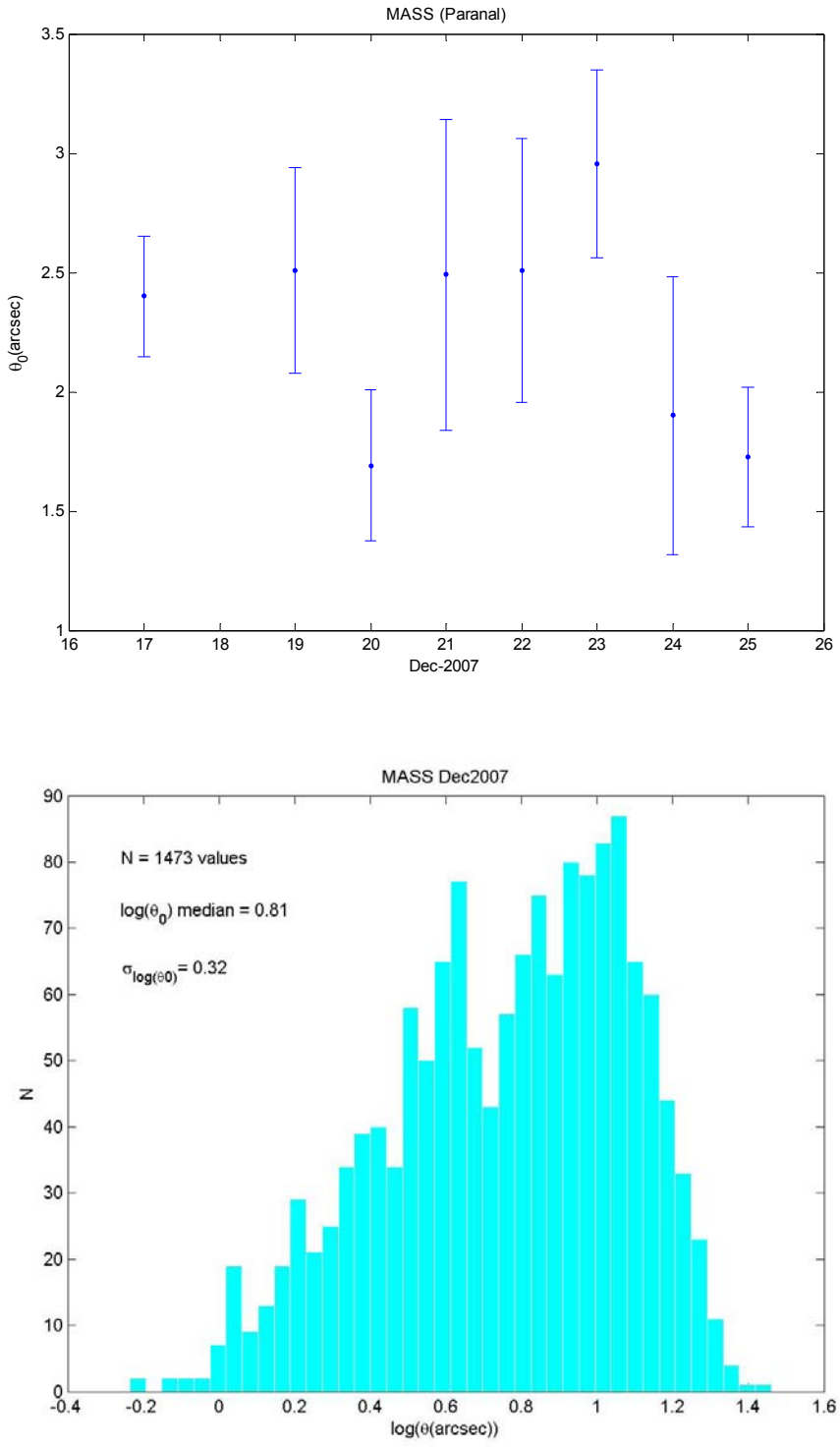

Figure 30: isoplanatic angle bar errors for all the campaign (above), histogram of the isoplanatic angle measurement (down) given by MASS.

4.5 Table of Campaign results for all parameter and all instruments:

Result-Table of Dec2007 Paranal Campaign

Instrument	ε_0 tot(arcsec)	θ_0 (arcsec)	τ_0 (msec)	L_0 (m)
Cute-SCIDAR	0.20 -- 1.01-- 2.24	0.59 -- 2.01-- 5.13	--	--
ESO-DIMM	0.37 -- 0.81-- 2.84	1.37 -- 2.77-- 4.35	0.88 -- 4.11-- 7.36	--
IAC-DIMM	0.36 -- 0.81-- 1.44	--	--	--
GSM	0.50 -- 1.05-- 2.69	0.83 -- 2.45-- 5.27	0.03 -- 2.24-- 19.30	4.60 --17.10-- 174.30
LuSci	0.12 -- 0.43-- 2.23	--	--	--
MASS	0.13 -- 0.33-- 1.27	0.79 -- 2.24-- 4.31	0.86 -- 6.61-- 49.74	--
Meteo-station	temp 30m(°C):	temp 02m(°C)		wind speed 30m (m/s)
	8.96 -- 11.64-- 13.24	8.09 -- 11.49-- 13.28		0.33 -- 7.46-- 14.03

Figure 31: table summarizing the results of the campaign. For each instrument, we calculate the median value of measured parameter and the corresponding rang of variation. We give also the averaged temperature at 30 and 2 meters above ground measured by a meteo station.

For the detailed result night by night for each parameter and each instrument we present in the next part of this report the time evolution of the parameters, the associated histograms and a table summarizing the result for each instrument for the 10 nights.

V. Result of campaign night by night:

Cute-SCIDAR:

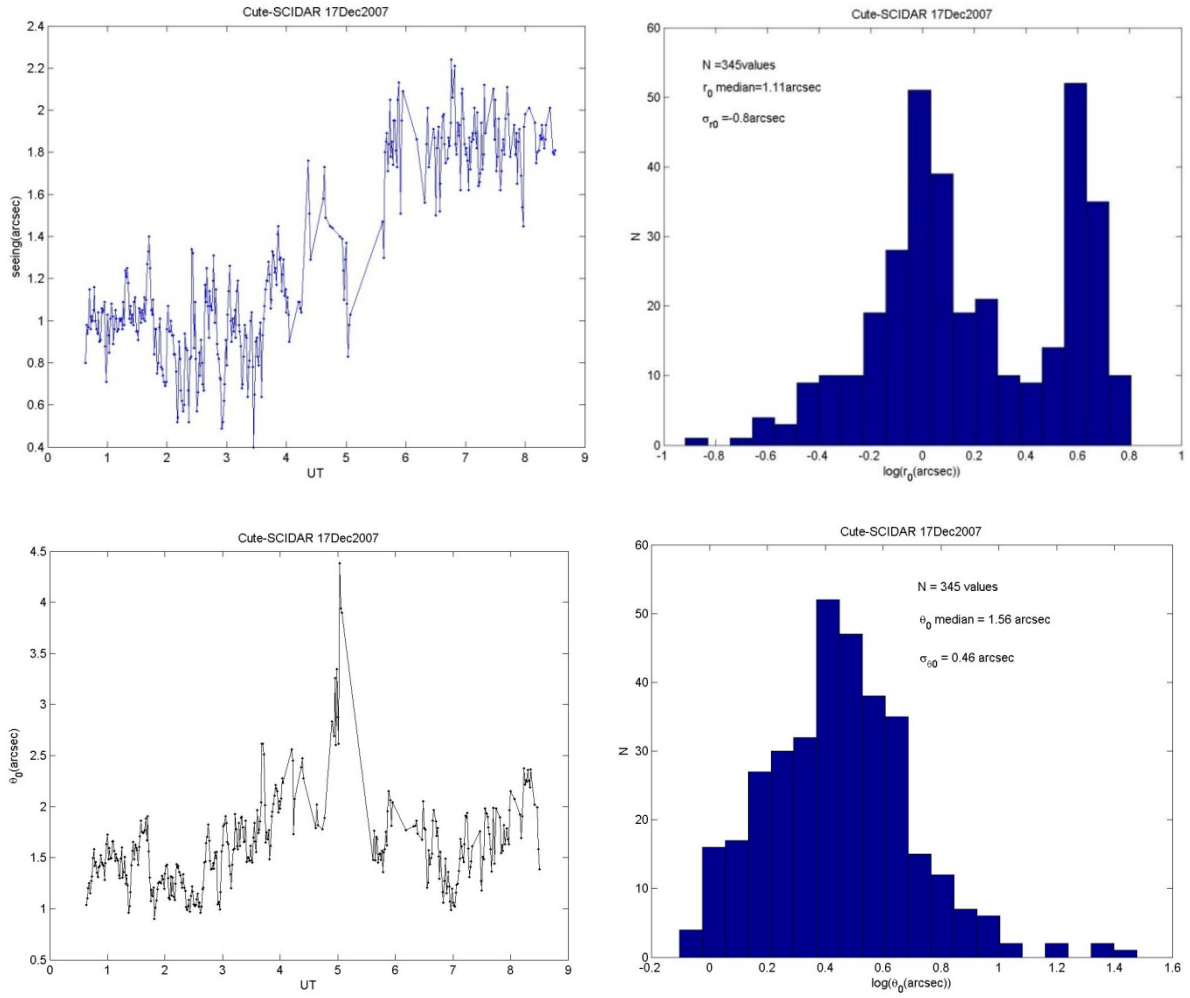

Cute-SCIDAR17Dec2007 at Paranal

night: 17 Dec2007	Median	Rang
seeing tot(arcsec)	1.11	0.4 -- 2.24
θ_0 (arcsec)	1.56	0.901 -- 4.38

Figure 31: Cute-SCIDAR (seeing and isoplanatic angle) 17 December 2007.

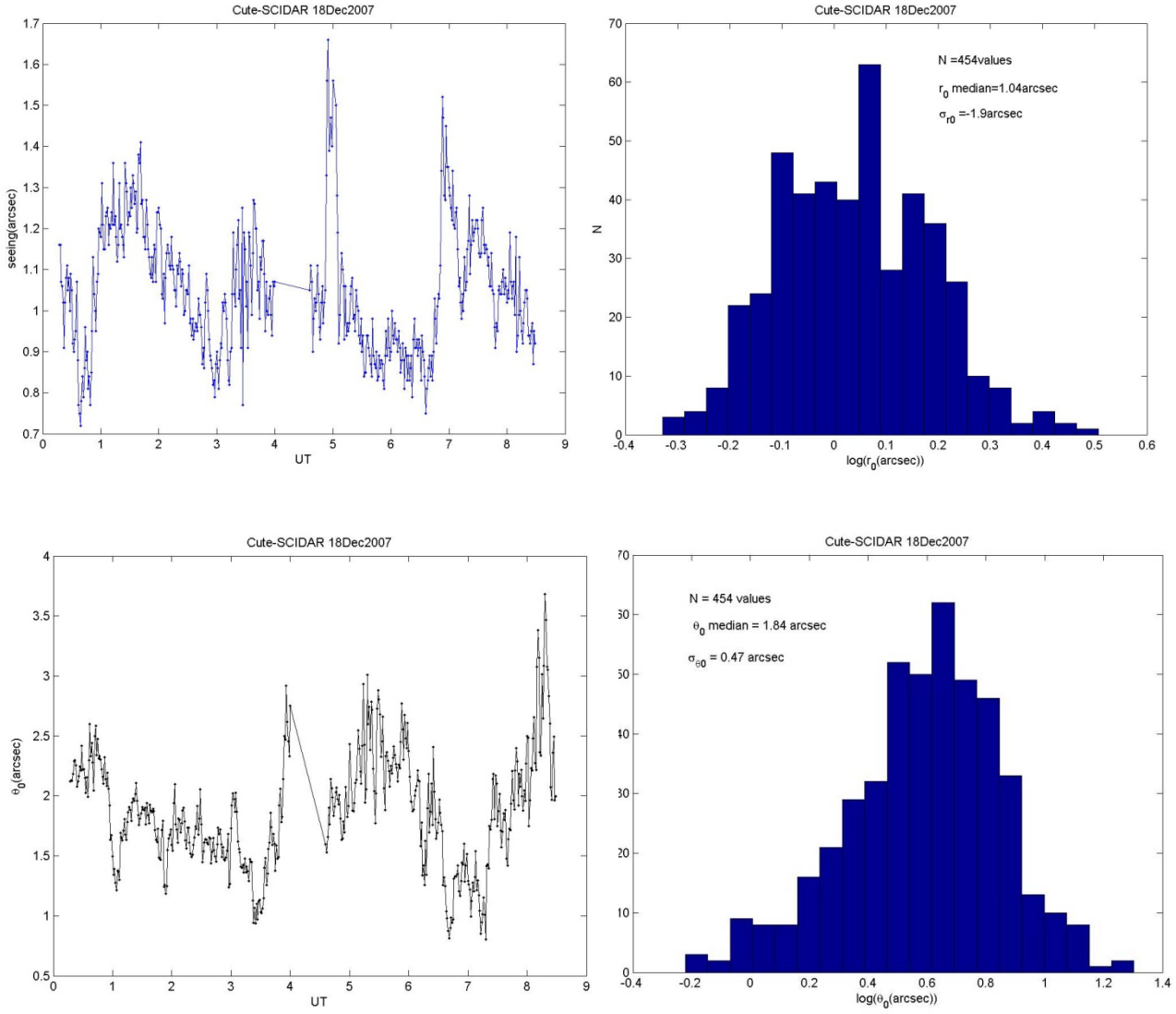

Cute-SCIDAR18Dec2007 at Paranal

night: 18 Dec2007	Median	Rang
seeing tot(arcsec)	1.04	0.72 -- 1.66
θ_0 (arcsec)	1.84	0.801 -- 3.68

Figure 32: Cute-SCIDAR (seeing and isoplanatic angle) 18December 2007.

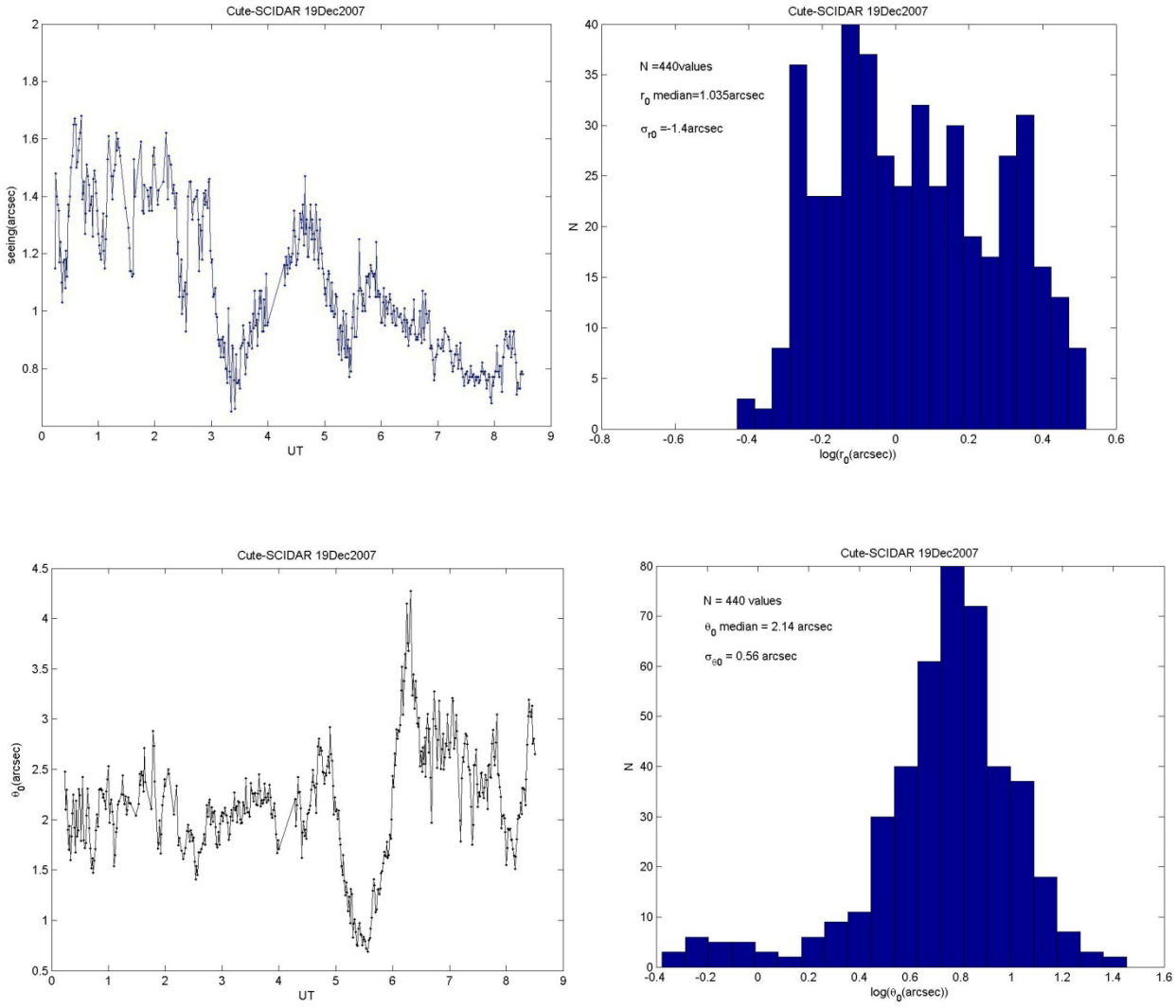

Cute-SCIDAR19Dec2007 at Paranal

night: 19 Dec2007	Median	Rang
seeing tot(arcsec)	1.04	0.65 -- 1.68
θ_0 (arcsec)	2.14	0.686 -- 4.27

Figure 33: Cute-SCIDAR (seeing and isoplanatic angle) 19 December 2007.

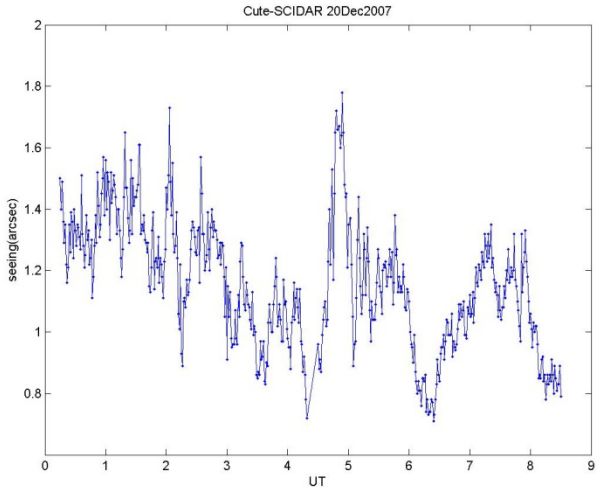

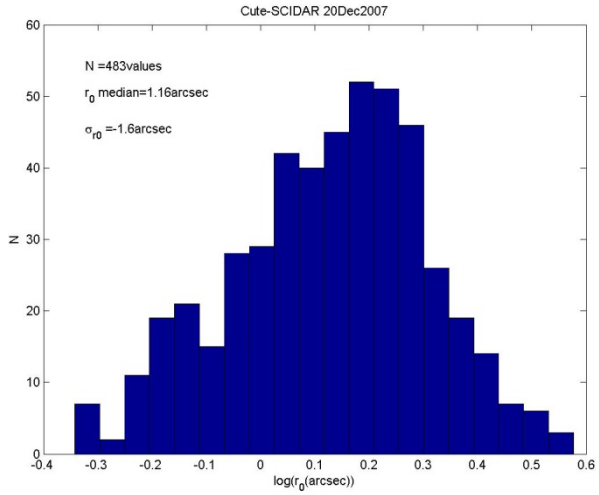

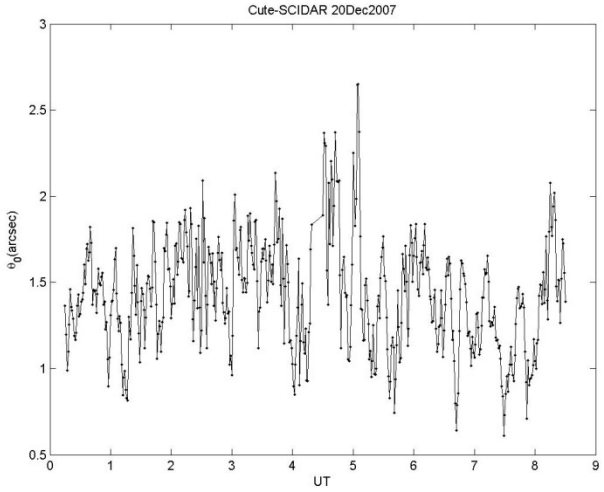

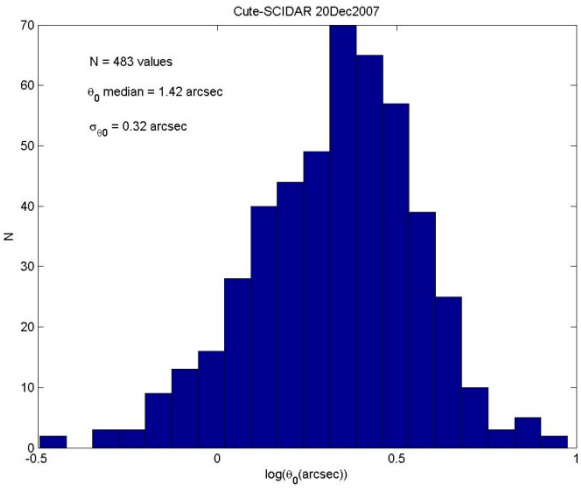

Cute-SCIDAR20Dec2007 at Paranal

night: 20 Dec2007	Median	Rang
seeing tot(arcsec)	1.16	0.71 -- 1.78
θ_0 (arcsec)	1.42	0.61 -- 2.65

Figure 34: Cute-SCIDAR (seeing and isoplanatic angle) 20 December 2007.

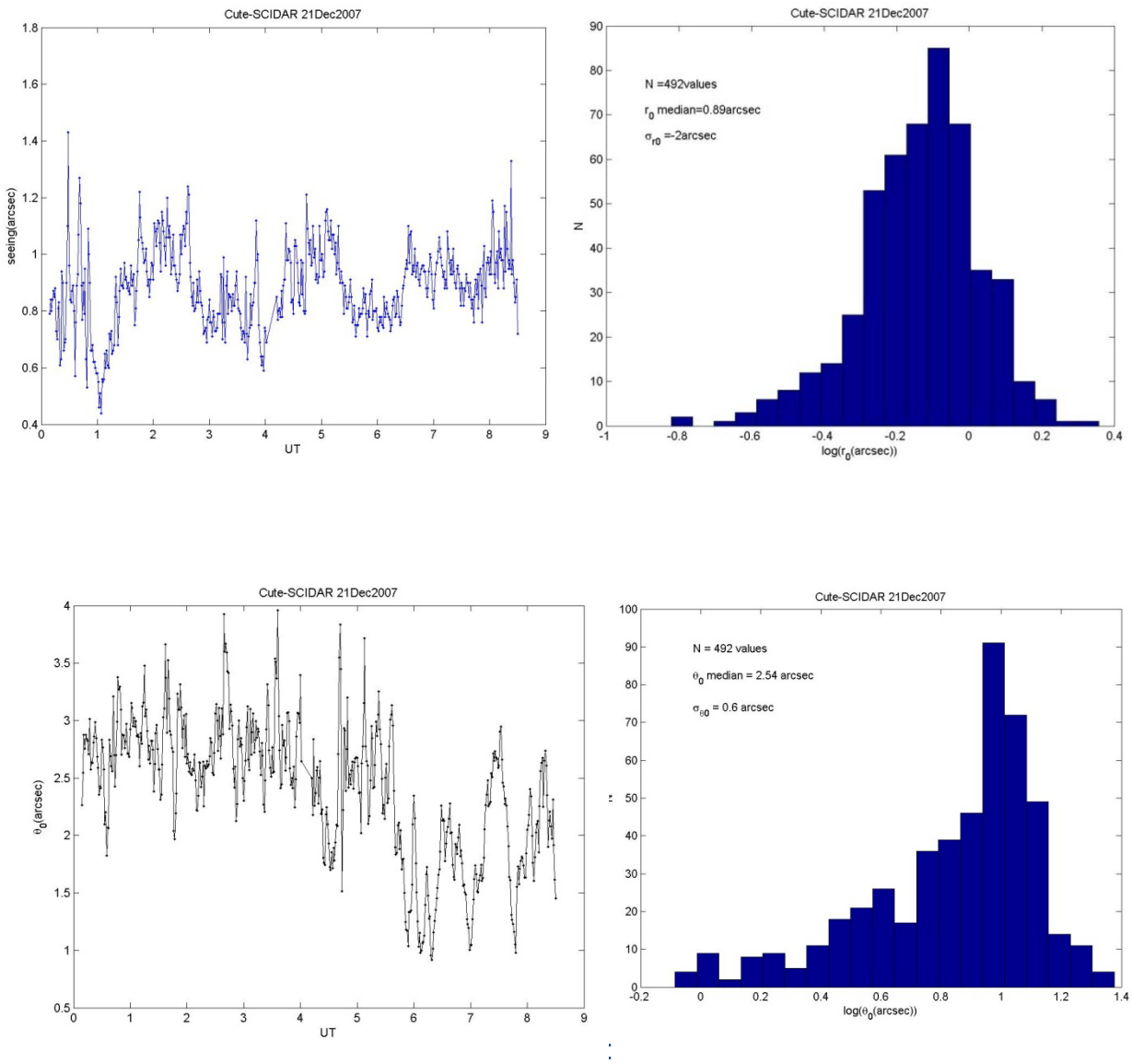

Cute-SCIDAR21Dec2007 at Paranal

night: 21 Dec2007	Median	Rang
seeing tot(arcsec)	0.89	0.44 -- 1.43
θ_0 (arcsec)	2.54	0.918 -- 3.96

Figure 35: Cute-SCIDAR (seeing and isoplanatic angle) 21 December 2007.

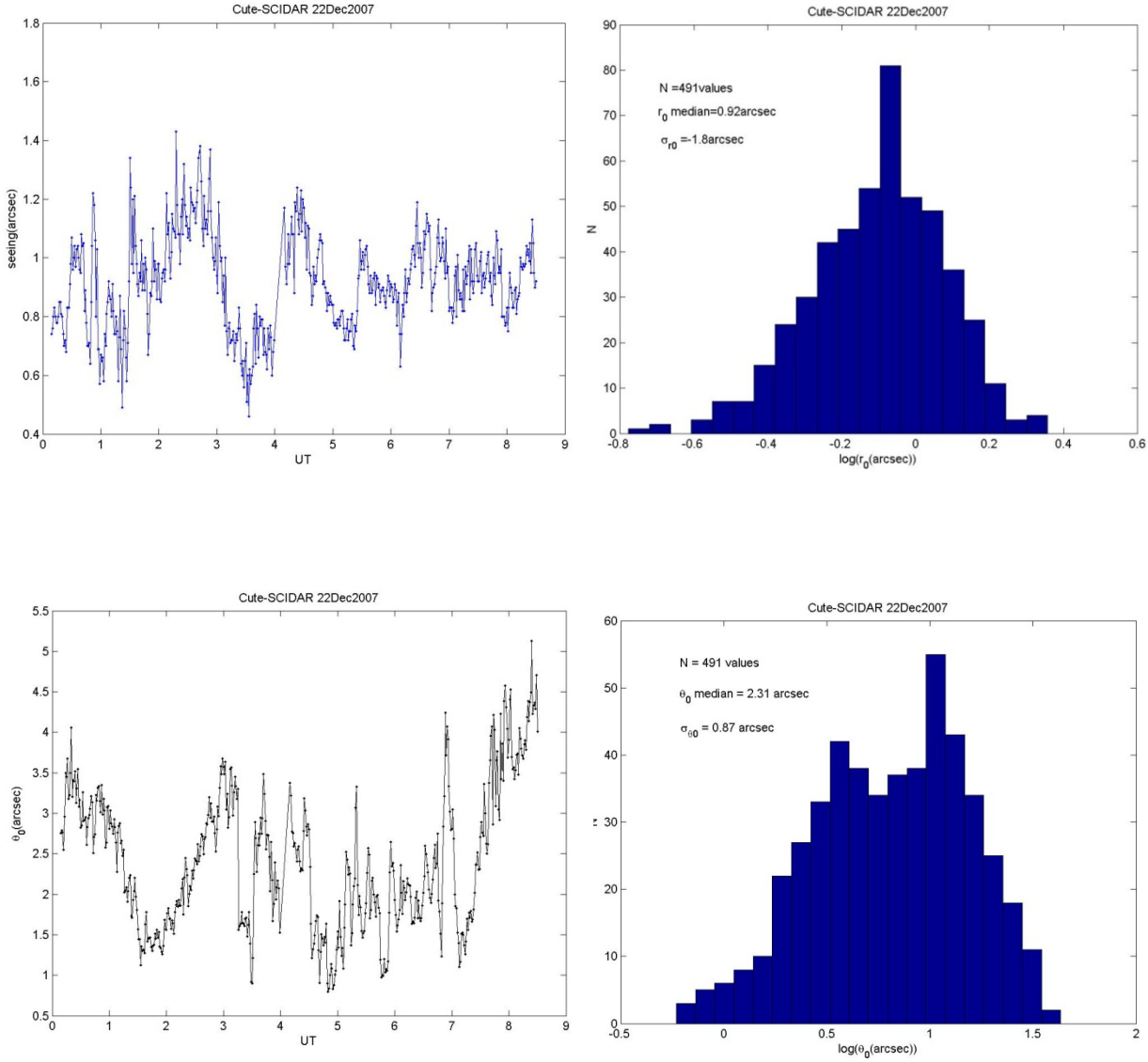

Cute-SCIDAR22Dec2007 at Paranal

night: 22 Dec2007	Median	Rang
seeing tot(arcsec)	0.92	0.46 -- 1.43
θ_0 (arcsec)	2.31	0.794 -- 5.13

Figure 36: Cute-SCIDAR (seeing and isoplanatic angle) 22 December 2007.

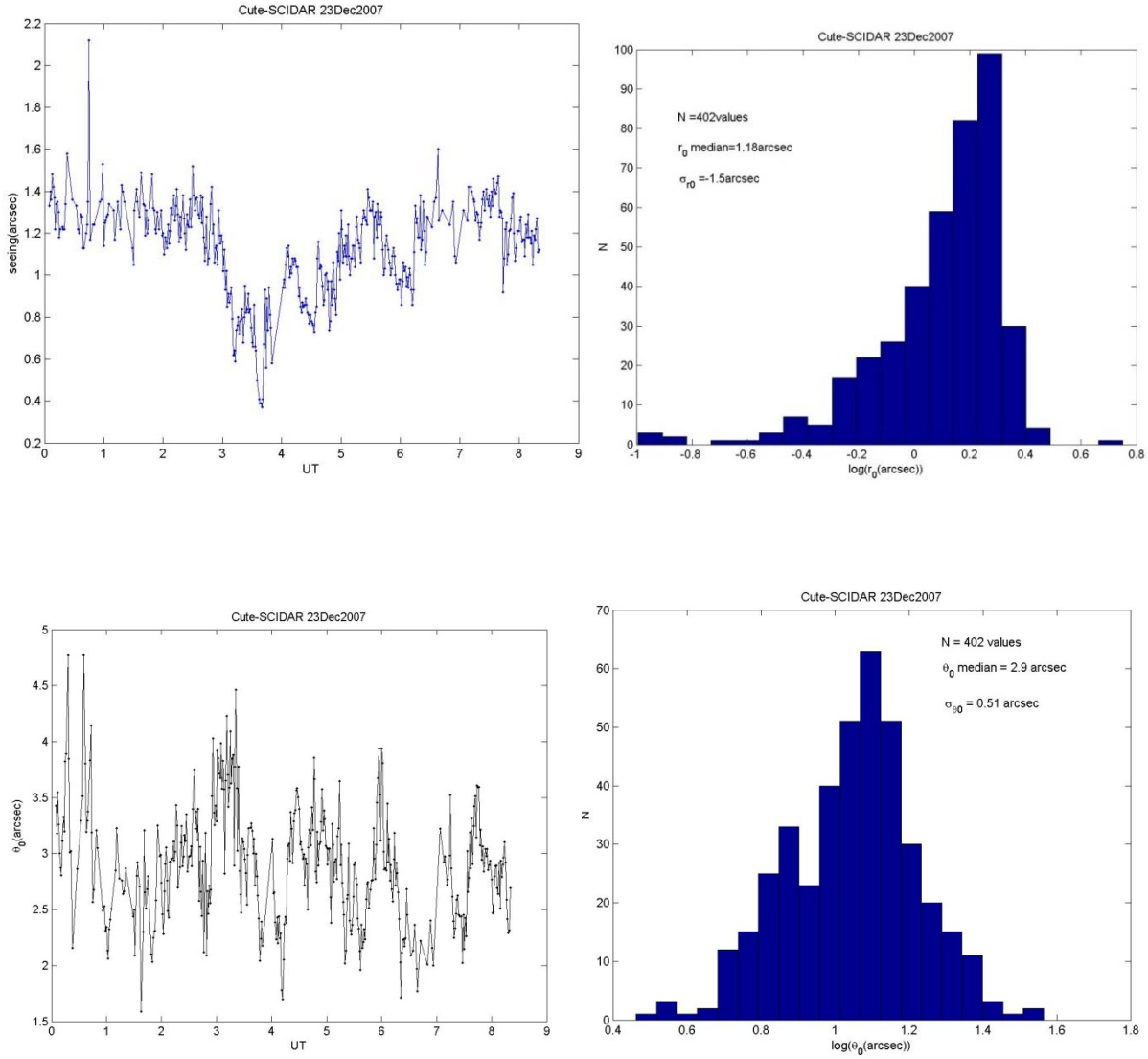

Cute-SCIDAR23Dec2007 at Paranal

night: 23 Dec2007	Median	Rang
seeing tot(arcsec)	1.18	0.37 -- 2.12
θ_0 (arcsec)	2.9	1.59 -- 4.78

Figure 37: Cute-SCIDAR (seeing and isoplanatic angle) 23 December 2007.

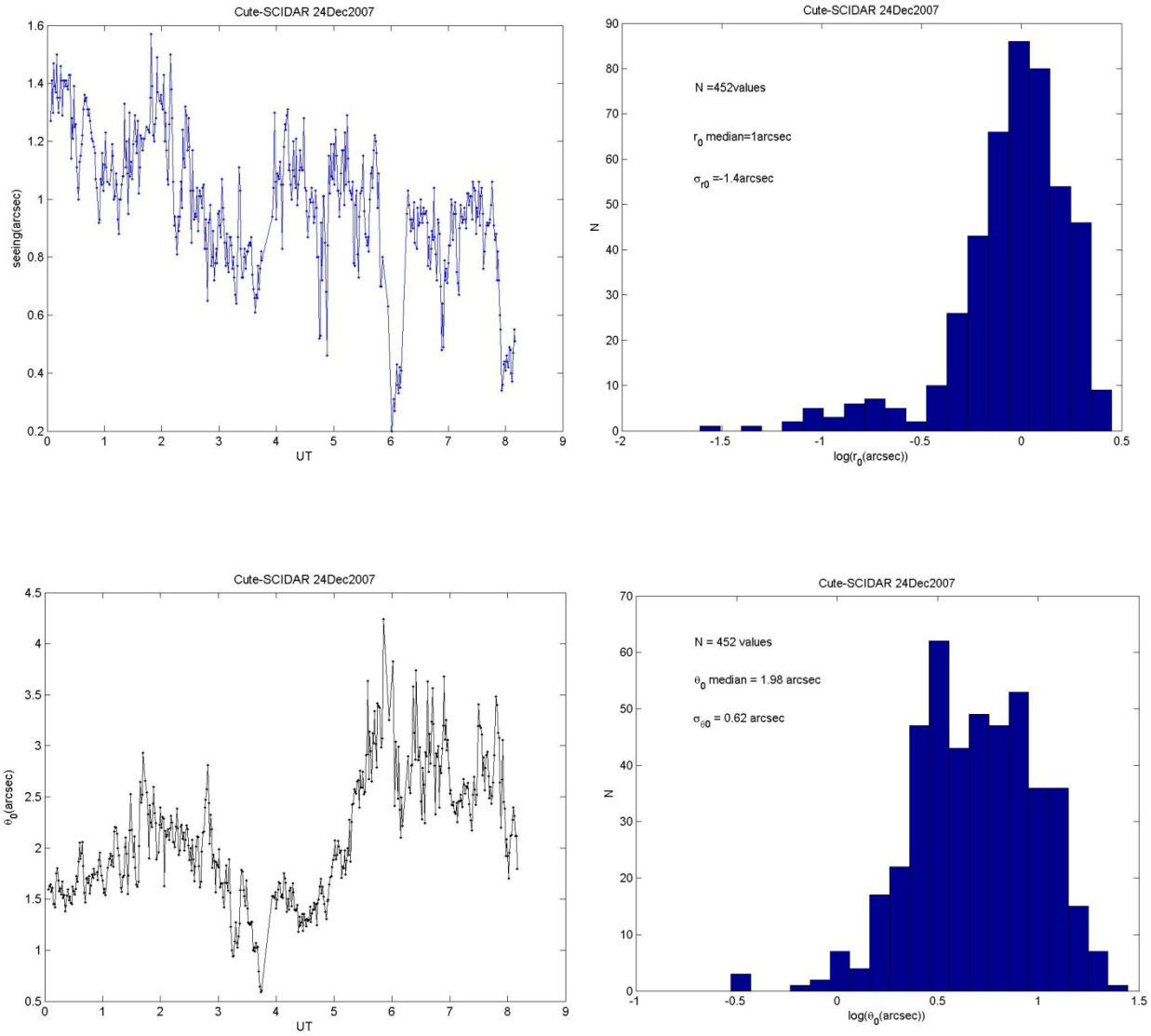

Cute-SCIDAR24Dec2007 at Paranal

night: 24 Dec2007	Median	Rang
seeing tot(arcsec)	1	0.2 -- 1.57
θ_0 (arcsec)	1.98	0.589 -- 4.24

Figure 38: Cute-SCIDAR (seeing and isoplanatic angle) 24 December 2007.

ESO-DIMM:

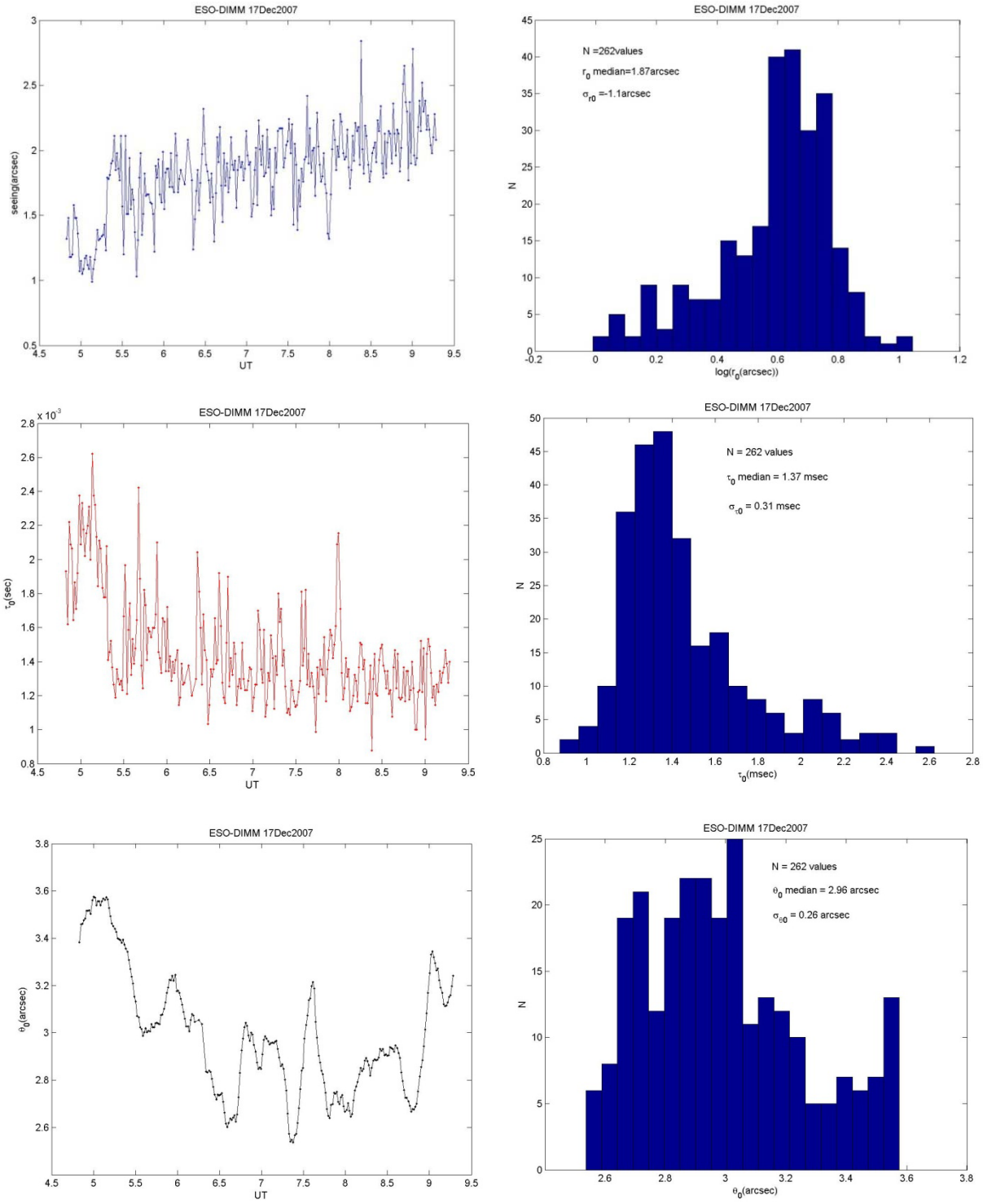

Figure 39: ESO-DIMM (seeing , coherence time and isoplanatic angle) 17 December 2007.

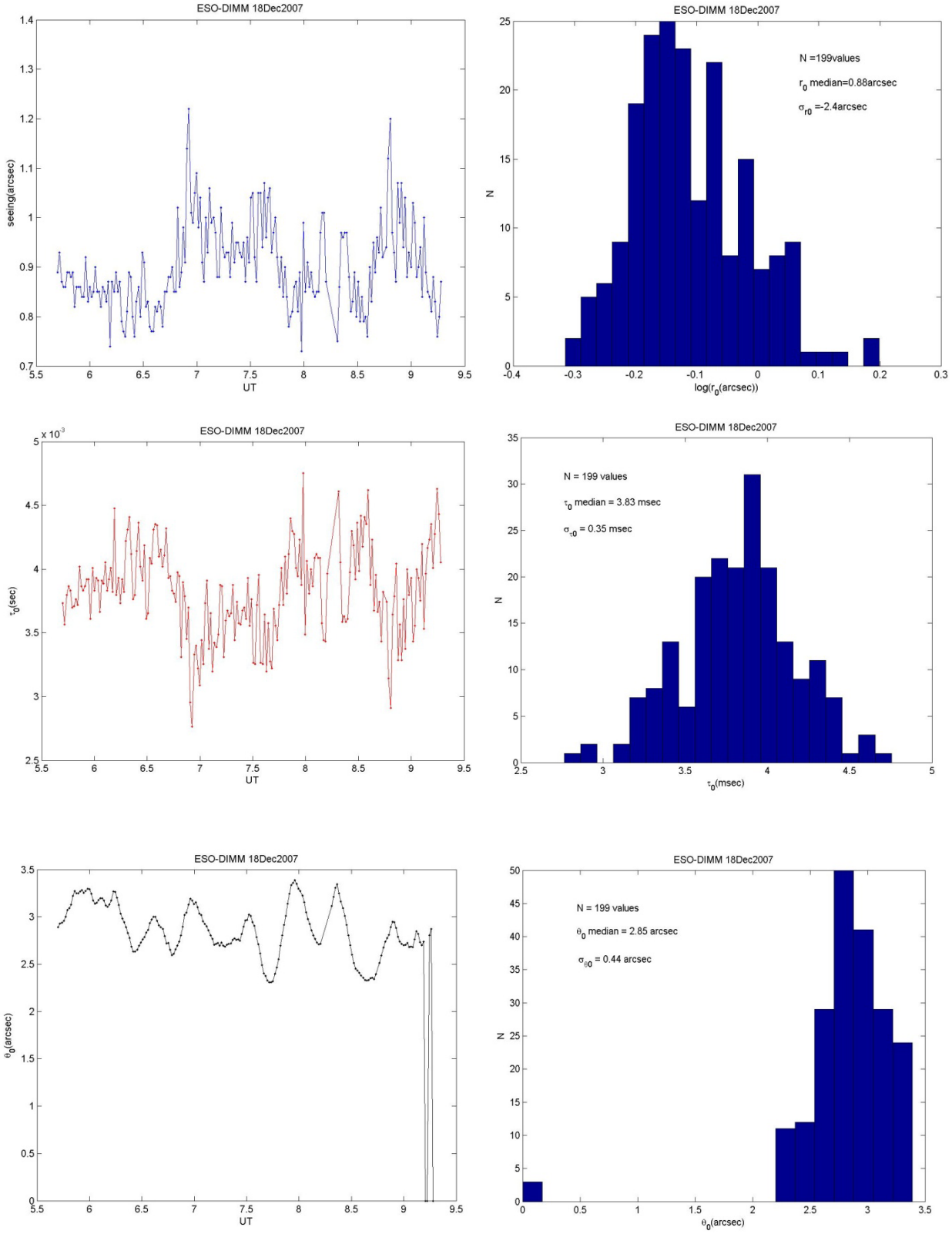

Figure 40: ESO-DIMM (seeing , coherence time and isoplanatic angle) 18 December 2007.

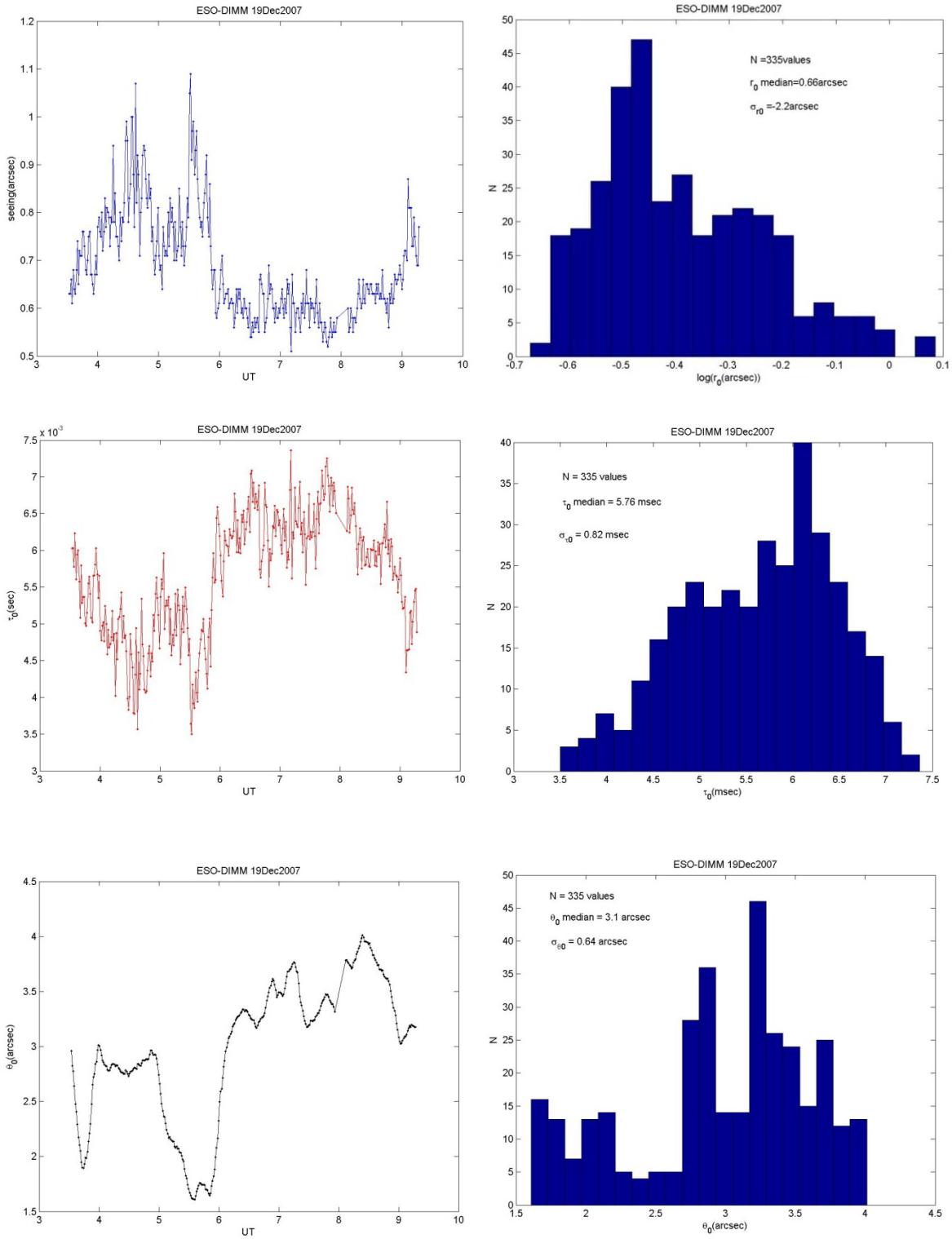

Figure 41: ESO-DIMM (seeing , coherence time and isoplanatic angle) 19 December 2007.

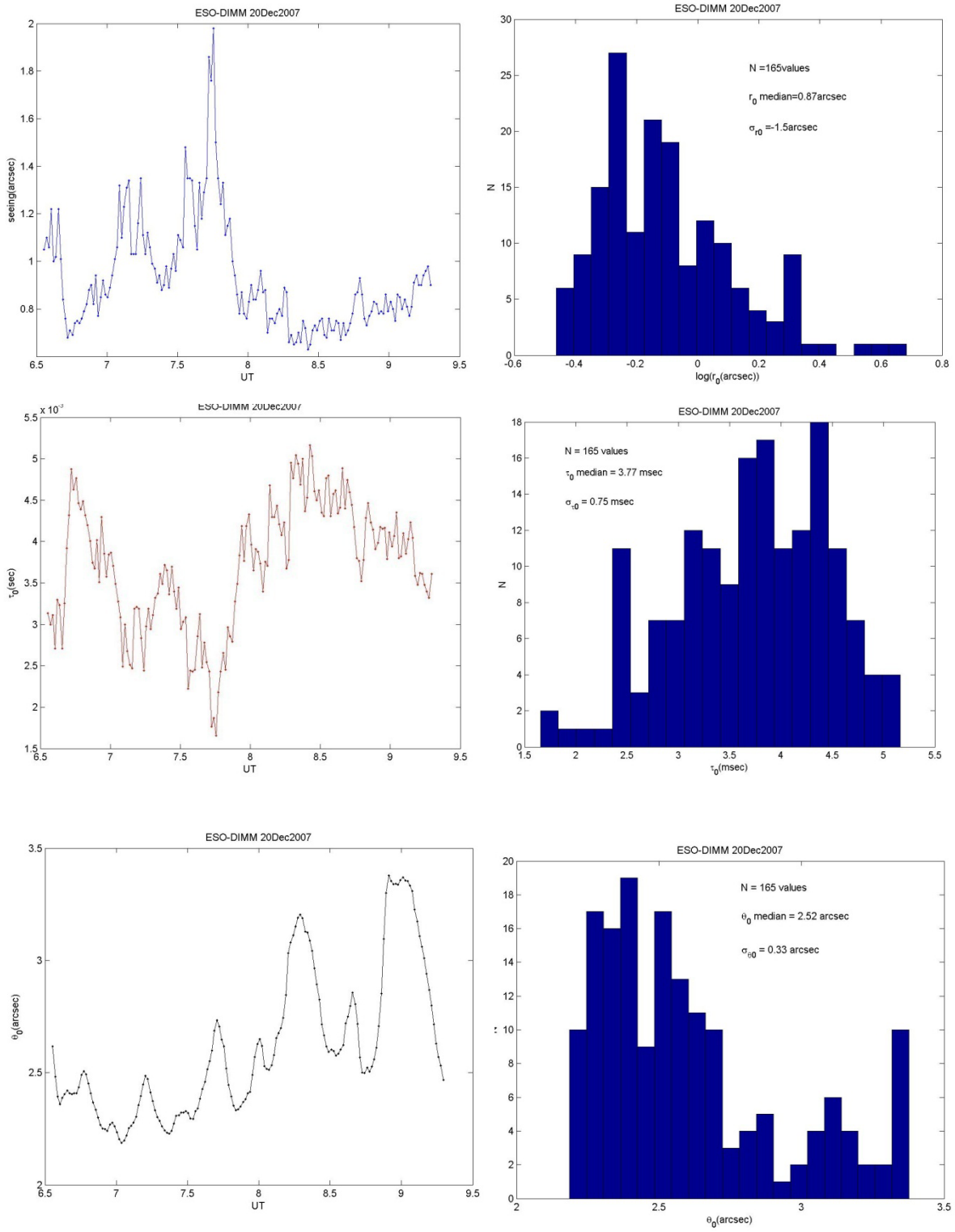

Figure 42: ESO-DIMM (seeing , coherence time and isoplanatic angle) 20 December 2007.

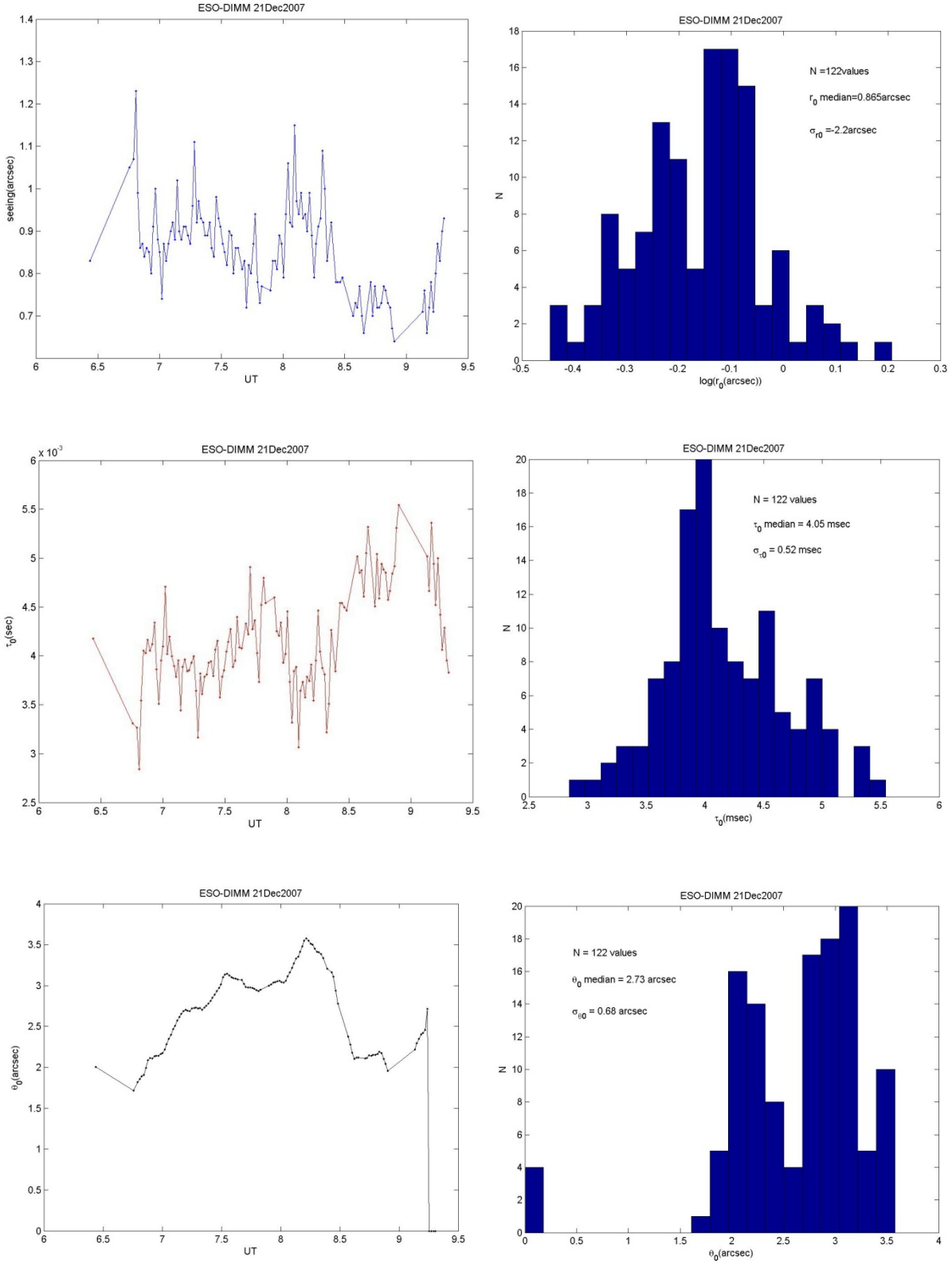

Figure 43: ESO-DIMM (seeing , coherence time and isoplanatic angle) 21December 2007.

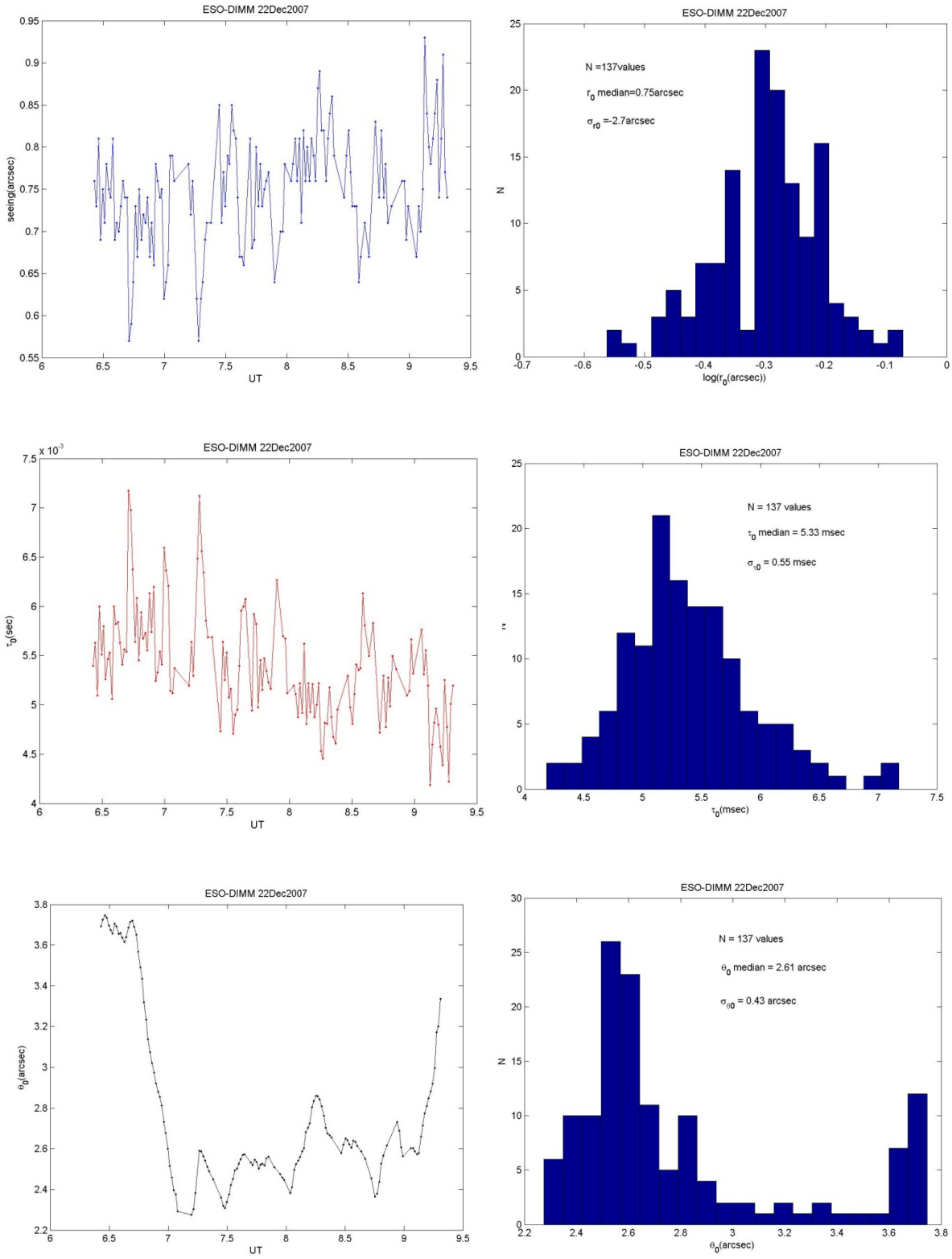

Figure 44: ESO-DIMM (seeing , coherence time and isoplanatic angle) 22 December 2007.

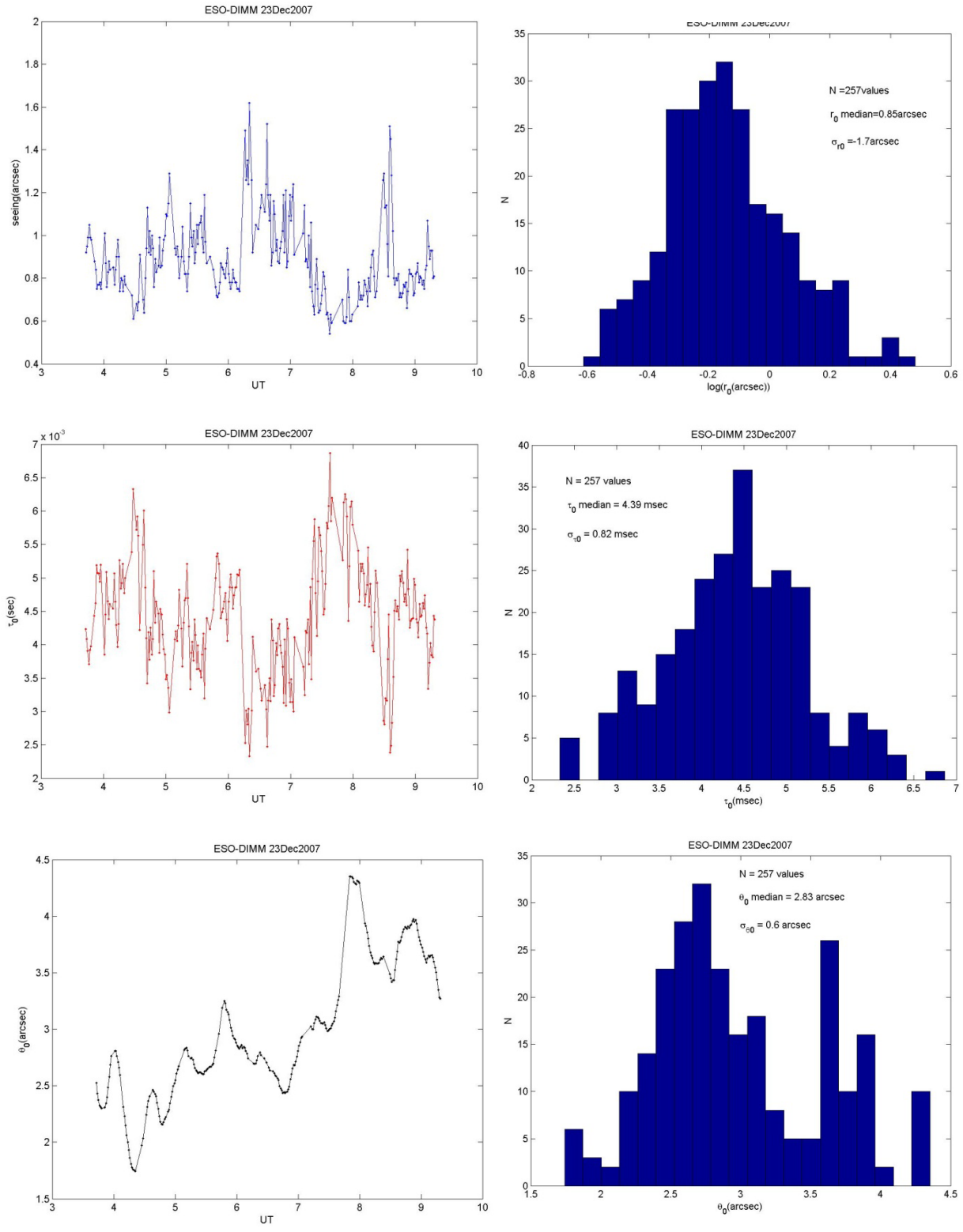

Figure 45: ESO-DIMM (seeing , coherence time and isoplanatic angle) 23 December 2007.

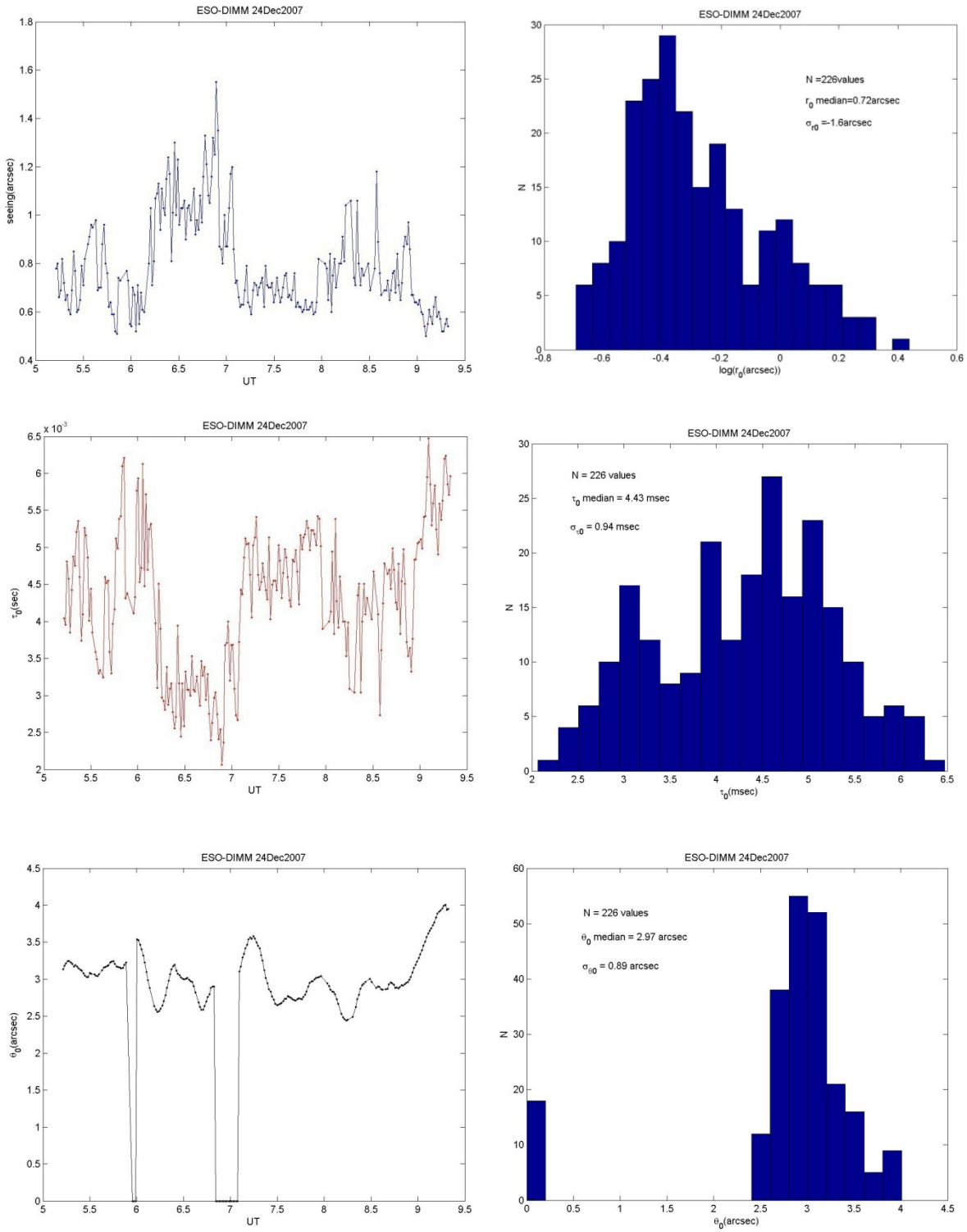

Figure 46: ESO-DIMM (seeing , coherence time and isoplanatic angle) 24 December 2007.

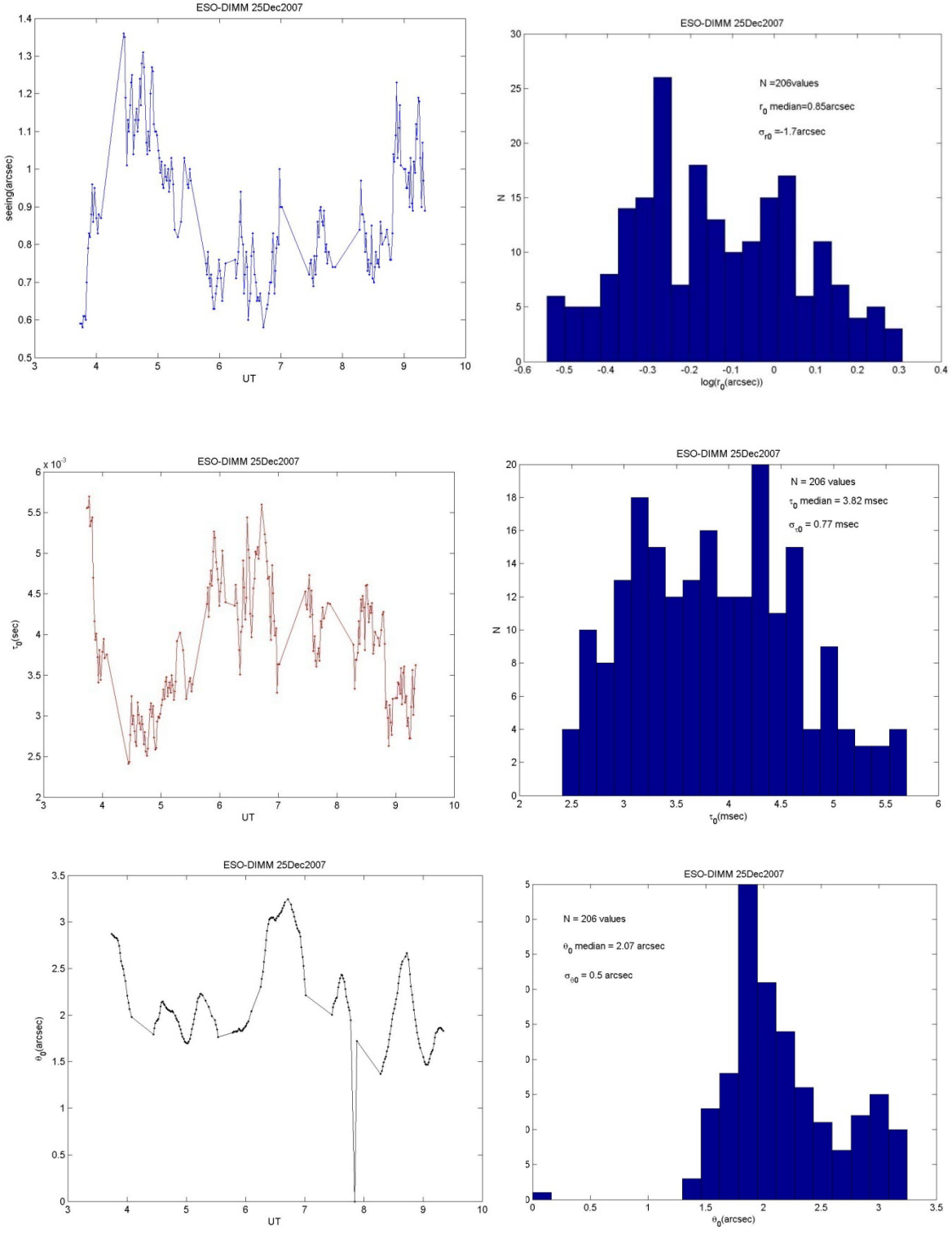

Figure 47: ESO-DIMM (seeing , coherence time and isoplanatic angle) 25 December 2007.

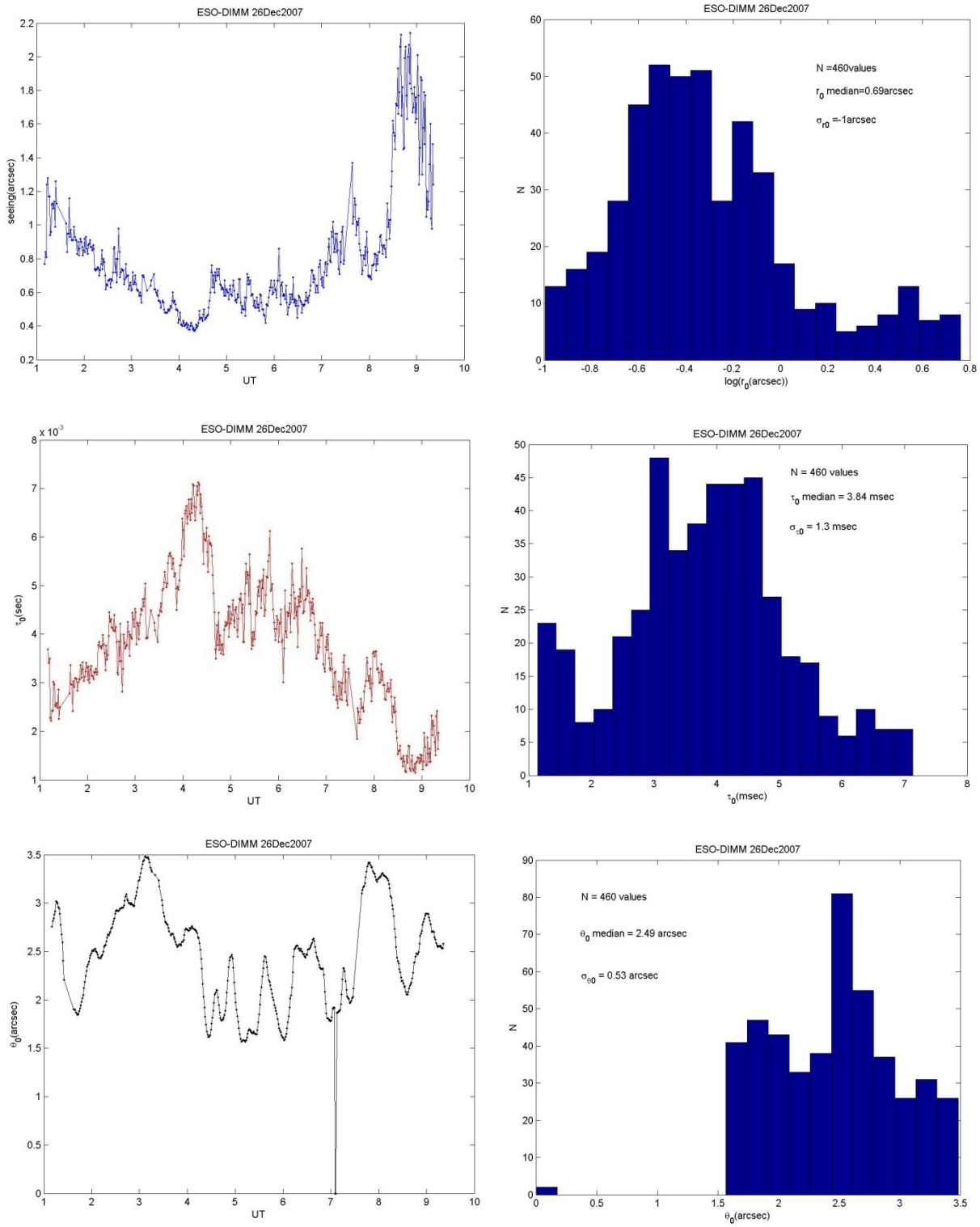

Figure 48: ESO-DIMM (seeing , coherence time and isoplanatic angle) 26 December 2007.

ESO-DIMM 17 Dec2007 at Paranal

night: 17 Dec2007	Median	Rang
seeing tot(arcsec)	1.87	0.99 -- 2.84
θ_0 (arcsec)	2.96	2.54 -- 3.58
τ_0 (msec)	1.37	0.877 -- 2.62

ESO-DIMM 19 Dec2007 at Paranal

night: 19 Dec2007	Median	Rang
seeing tot(arcsec)	0.66	0.51 -- 1.09
θ_0 (arcsec)	3.1	1.61 -- 4.01
τ_0 (msec)	5.76	3.5 -- 7.36

ESO-DIMM 18 Dec2007 at Paranal

night: 18 Dec2007	Median	Rang
seeing tot(arcsec)	0.88	0.73 -- 1.22
θ_0 (arcsec)	2.85	0 -- 3.39
τ_0 (msec)	3.83	2.77 -- 4.75

ESO-DIMM 20 Dec2007 at Paranal

night: 20 Dec2007	Median	Rang
seeing tot(arcsec)	0.87	0.63 -- 1.98
θ_0 (arcsec)	2.52	2.19 -- 3.38
τ_0 (msec)	3.77	1.66 -- 5.16

ESO-DIMM 21 Dec2007 at Paranal

night: 21 Dec2007	Median	Rang
seeing tot(arcsec)	0.865	0.64 -- 1.23
θ_0 (arcsec)	2.73	0 -- 3.57
τ_0 (msec)	4.05	2.84 -- 5.54

ESO-DIMM 22 Dec2007 at Paranal

night: 22 Dec2007	Median	Rang
seeing tot(arcsec)	0.75	0.57 -- 0.93
θ_0 (arcsec)	2.61	2.27 -- 3.75
τ_0 (msec)	5.33	4.19 -- 7.17

ESO-DIMM 23 Dec2007 at Paranal

night: 23 Dec2007	Median	Rang
seeing tot(arcsec)	0.85	0.54 -- 1.62
θ_0 (arcsec)	2.83	1.74 -- 4.35
τ_0 (msec)	4.39	2.33 -- 6.86

ESO-DIMM 24 Dec2007 at Paranal

night: 24 Dec2007	Median	Rang
seeing tot(arcsec)	0.72	0.5 -- 1.55
θ_0 (arcsec)	2.97	0 -- 4.01
τ_0 (msec)	4.43	2.07 -- 6.47

ESO-DIMM 25 Dec2007 at Paranal

night: 25 Dec2007	Median	Rang
seeing tot(arcsec)	0.85	0.58 -- 1.36
θ_0 (arcsec)	2.07	0 -- 3.25
τ_0 (msec)	3.82	2.41 -- 5.7

ESO-DIMM 26 Dec2007 at Paranal

night: 26 Dec2007	Median	Rang
seeing tot(arcsec)	0.69	0.37 -- 2.14
θ_0 (arcsec)	2.49	0 -- 3.48
τ_0 (msec)	3.84	1.14 -- 7.13

IAC-DIMM:

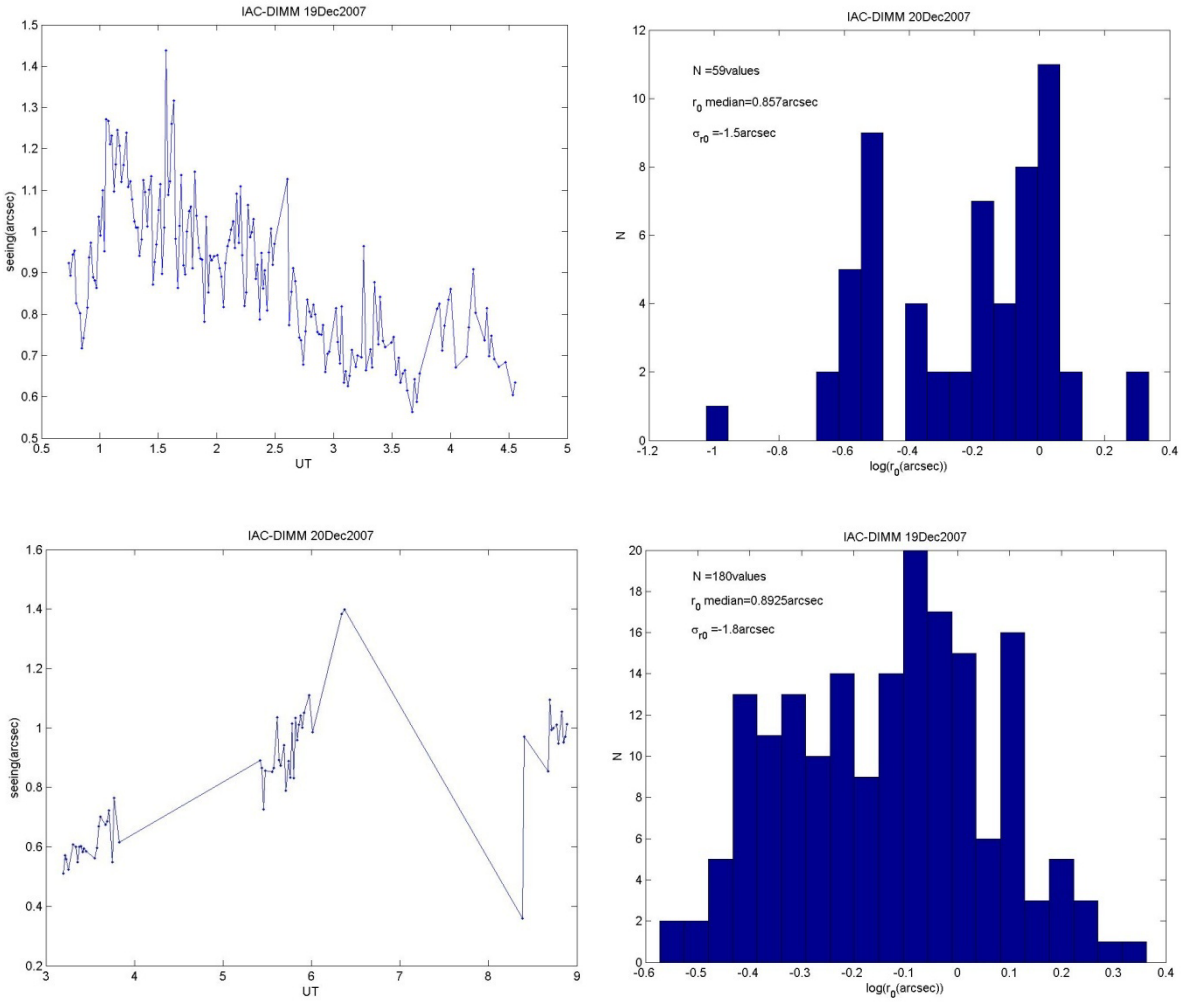

IAC-DIMM 19 Dec2007 at Paranal

night: 19 Dec2007	Median	Rang
seeing tot(arcsec)	0.893	0.564 -- 1.44

IAC-DIMM 20 Dec2007 at Paranal

night: 20 Dec2007	Median	Rang
seeing tot(arcsec)	0.857	0.359 -- 1.4

Figure 49: IAC-DIMM (seeing) 19-20 December 2007.

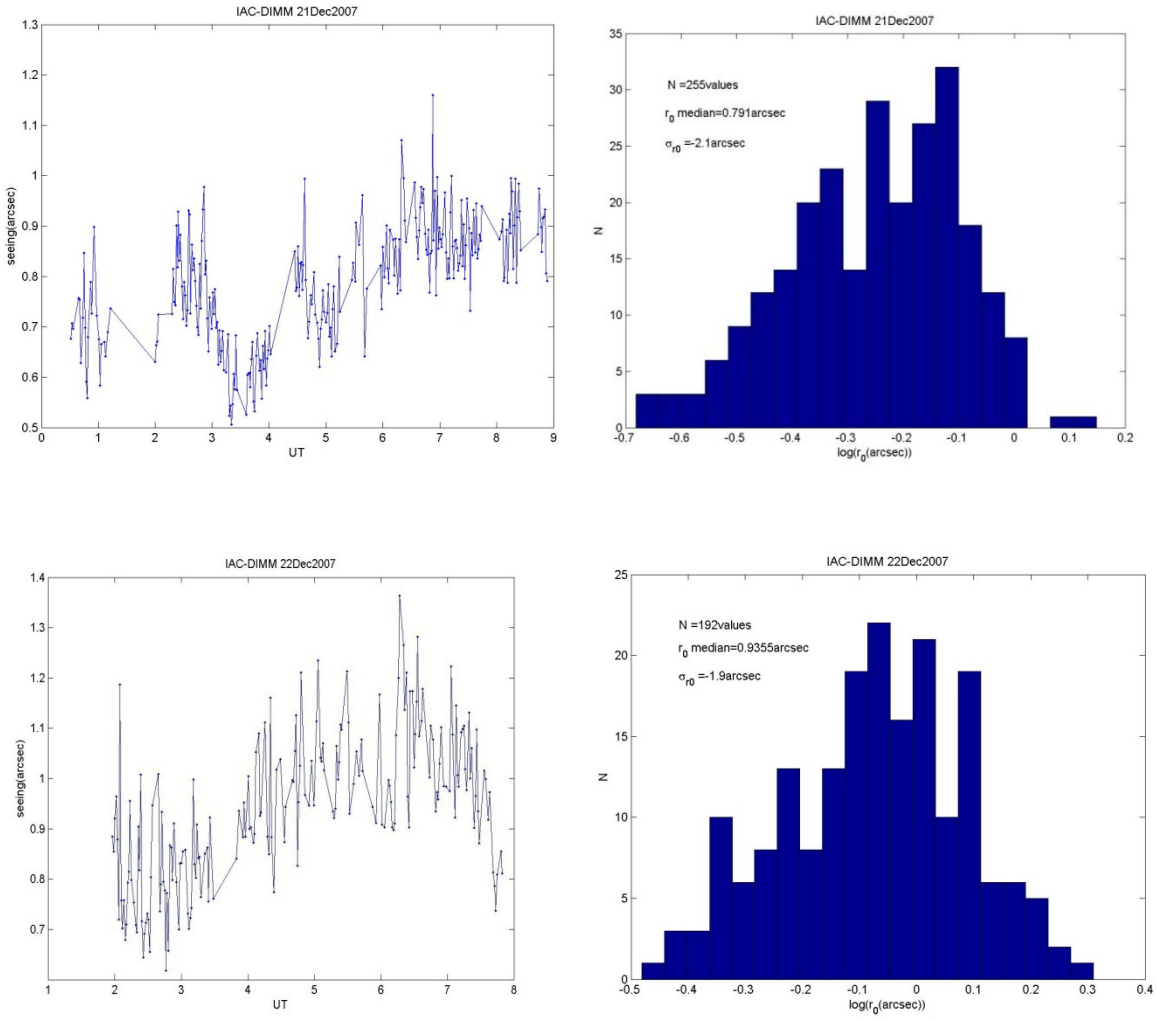

IAC-DIMM 21 Dec2007 at Paranal

night: 21 Dec2007	Median	Rang
seeing tot(arcsec)	0.791	0.506 -- 1.16

IAC-DIMM 22 Dec2007 at Paranal

night: 22 Dec2007	Median	Rang
seeing tot(arcsec)	0.936	0.618 -- 1.36

Figure 50: IAC-DIMM (seeing) 21-22 December 2007.

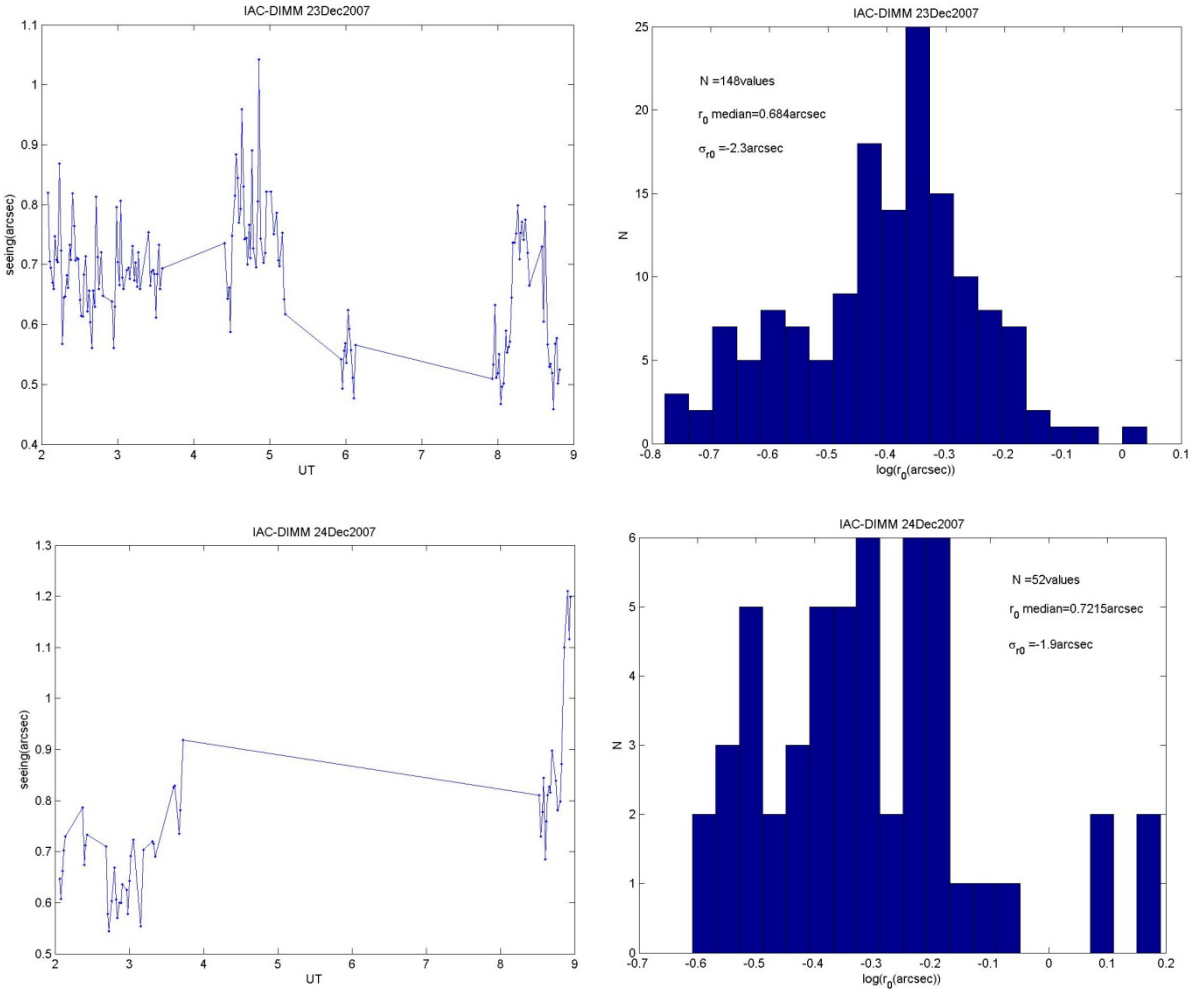

IAC-DIMM 23 Dec2007 at Paranal

night: 23 Dec2007	Median	Rang
seeing tot(arcsec)	0.684	0.459 -- 1.04

IAC-DIMM 24 Dec2007 at Paranal

night: 24 Dec2007	Median	Rang
seeing tot(arcsec)	0.722	0.544 -- 1.21

Figure 51: IAC-DIMM (seeing) 23-24 December 2007.

GSM results:

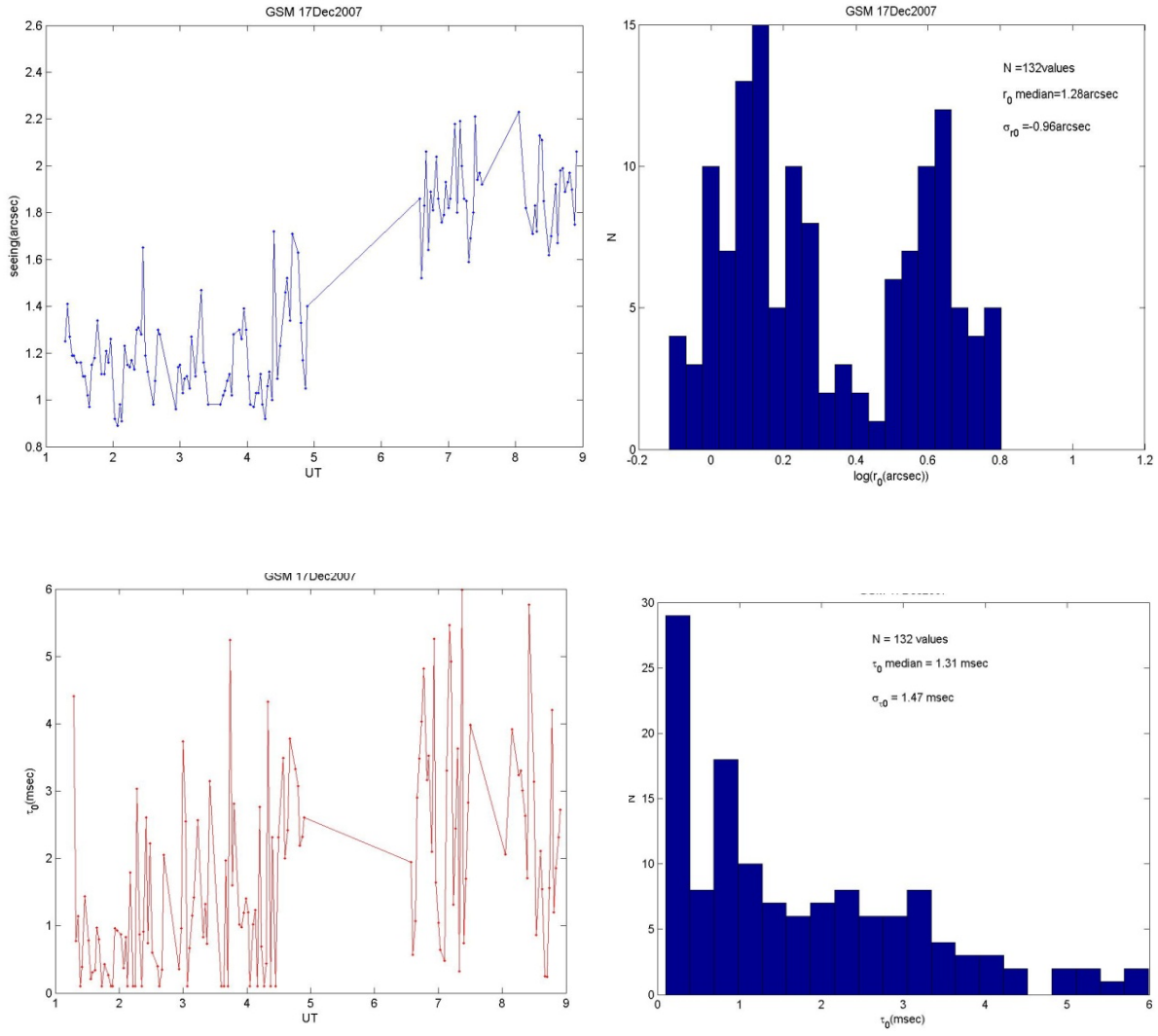

Figure 52: GSM (seeing and coherence time) 17 December 2007.

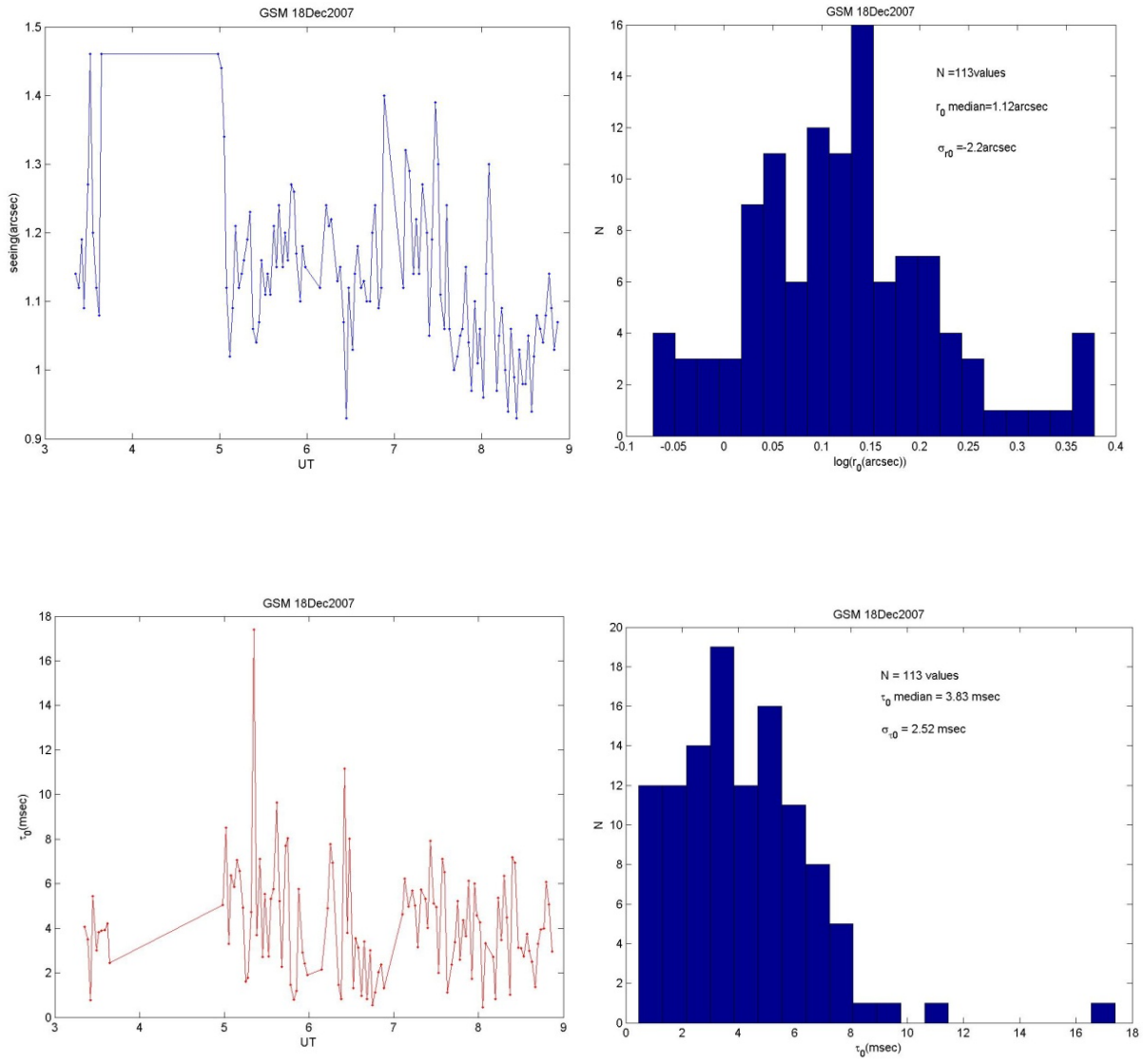

Figure 53: GSM (seeing and coherence time) 18 December 2007.

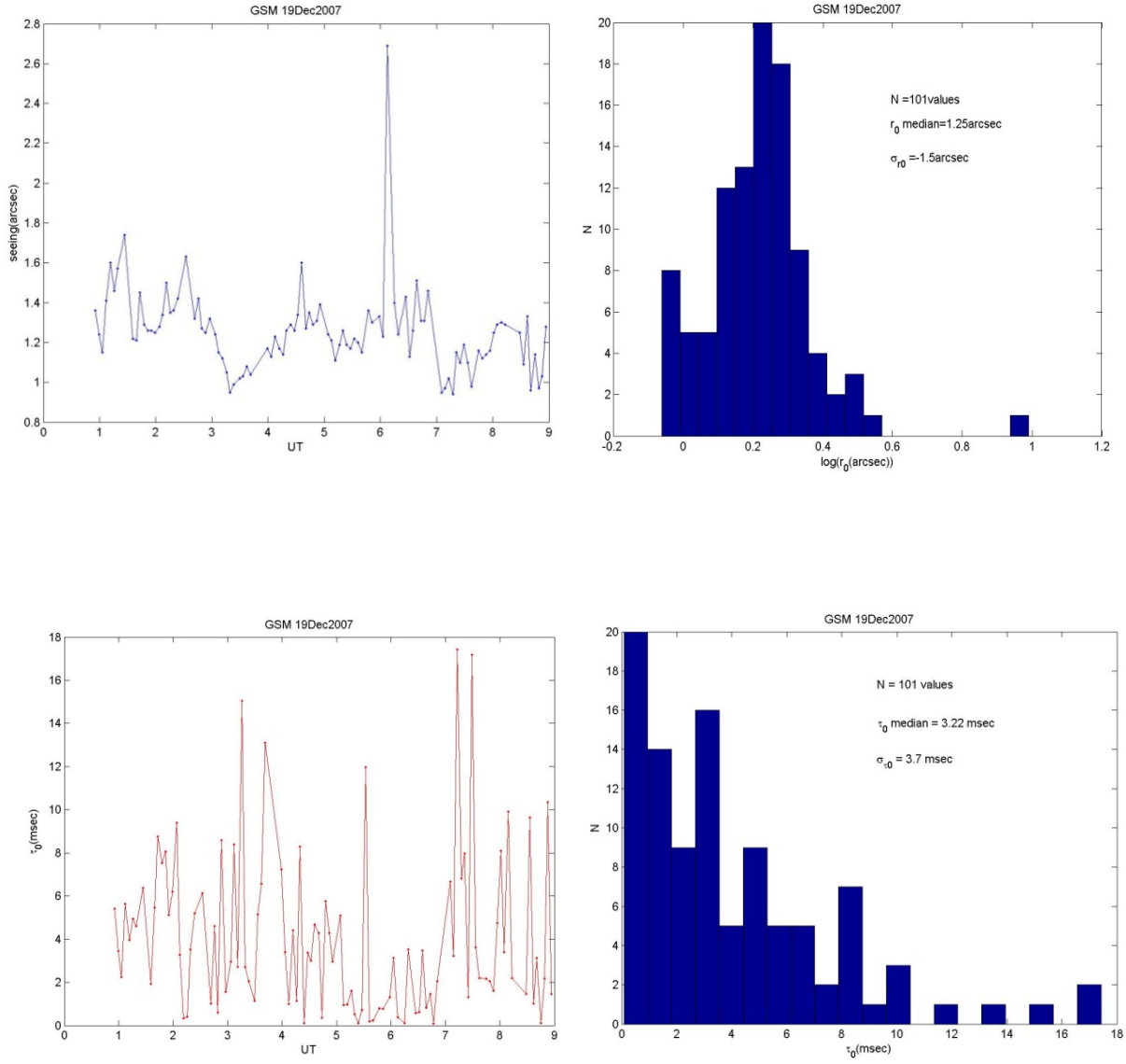

Figure 54: GSM (seeing and coherence time) 19December 2007.

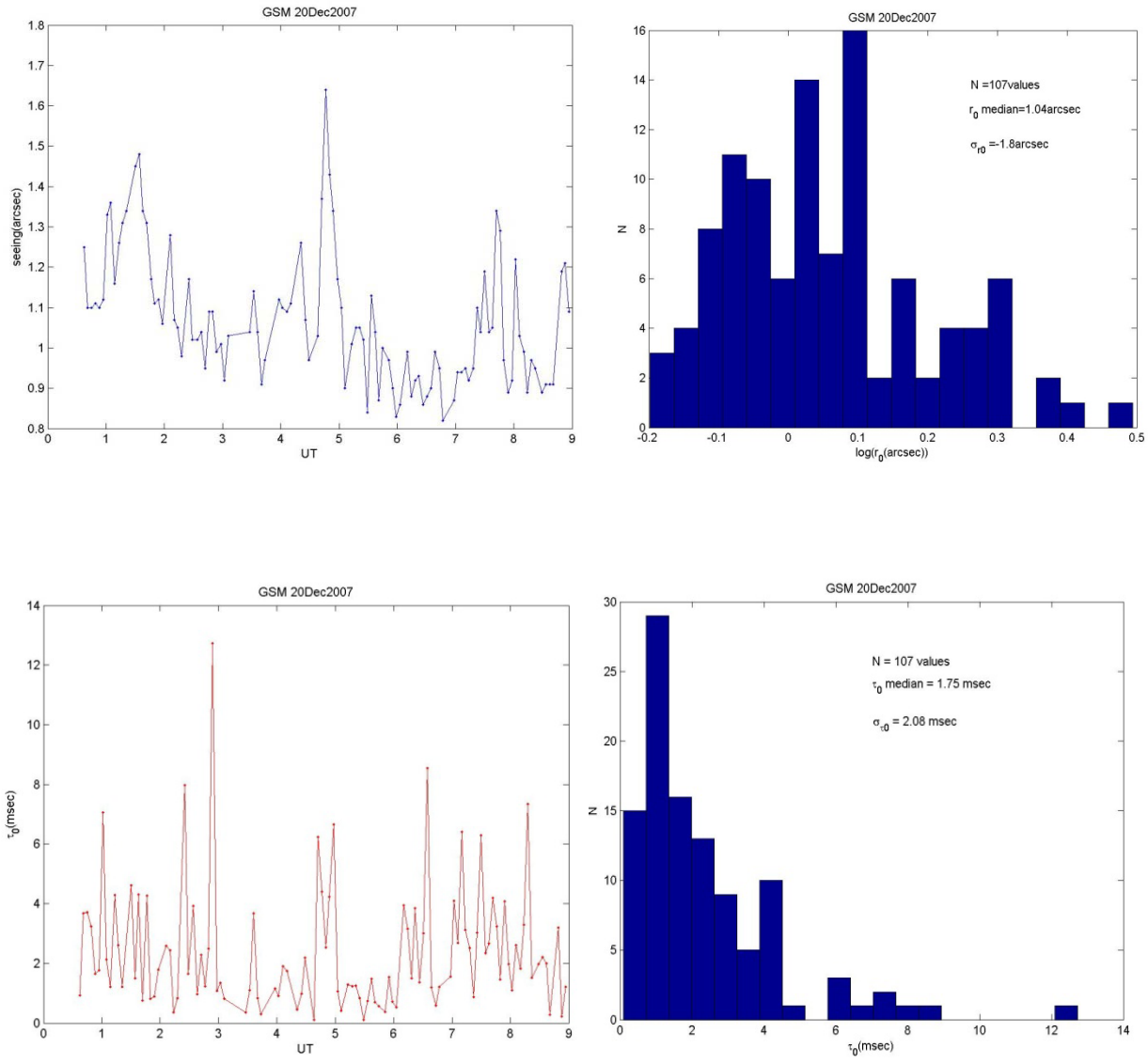

Figure 55: GSM (seeing and coherence time) 20 December 2007.

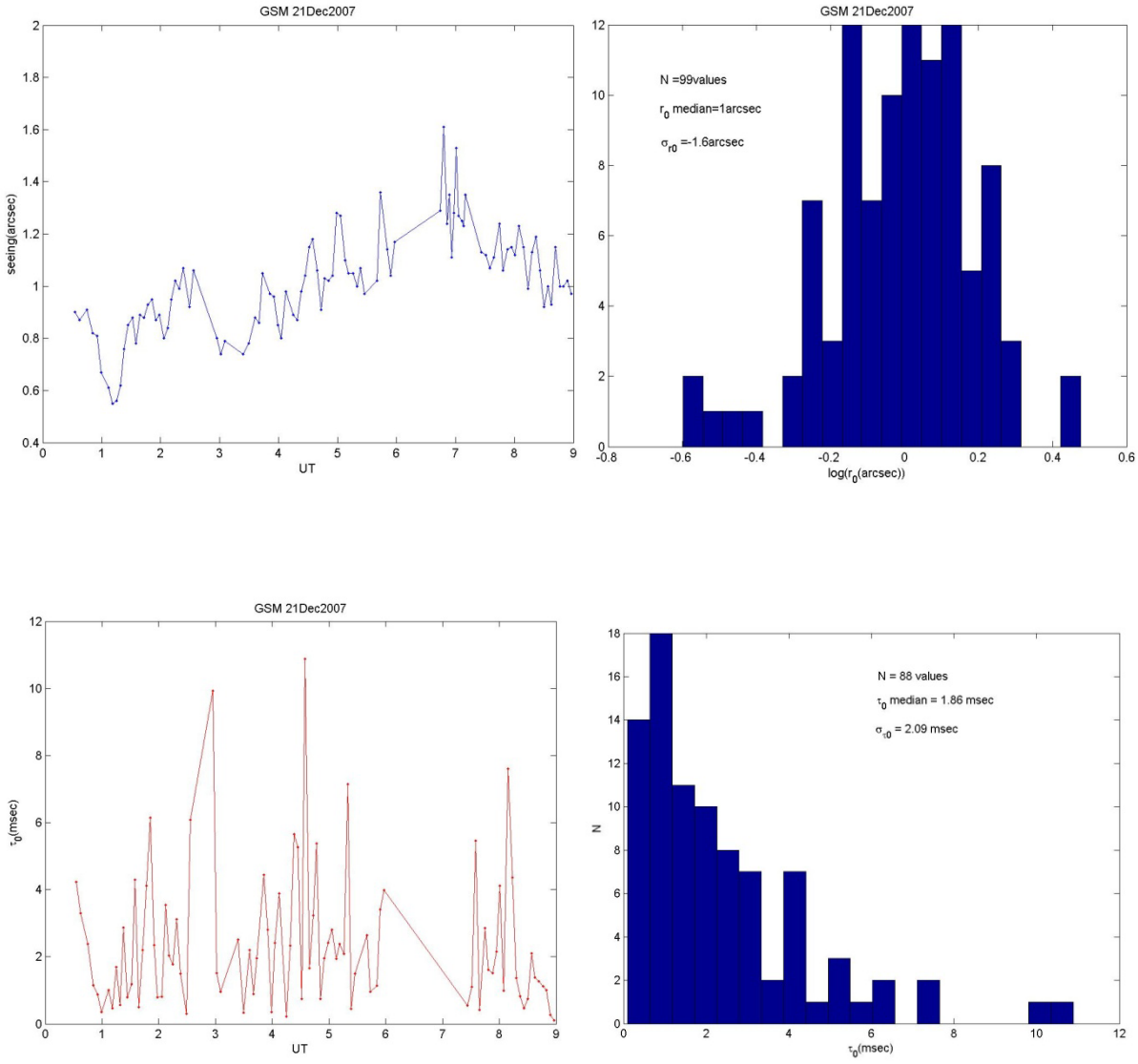

Figure 56: GSM (seeing and coherence time) 21 December 2007.

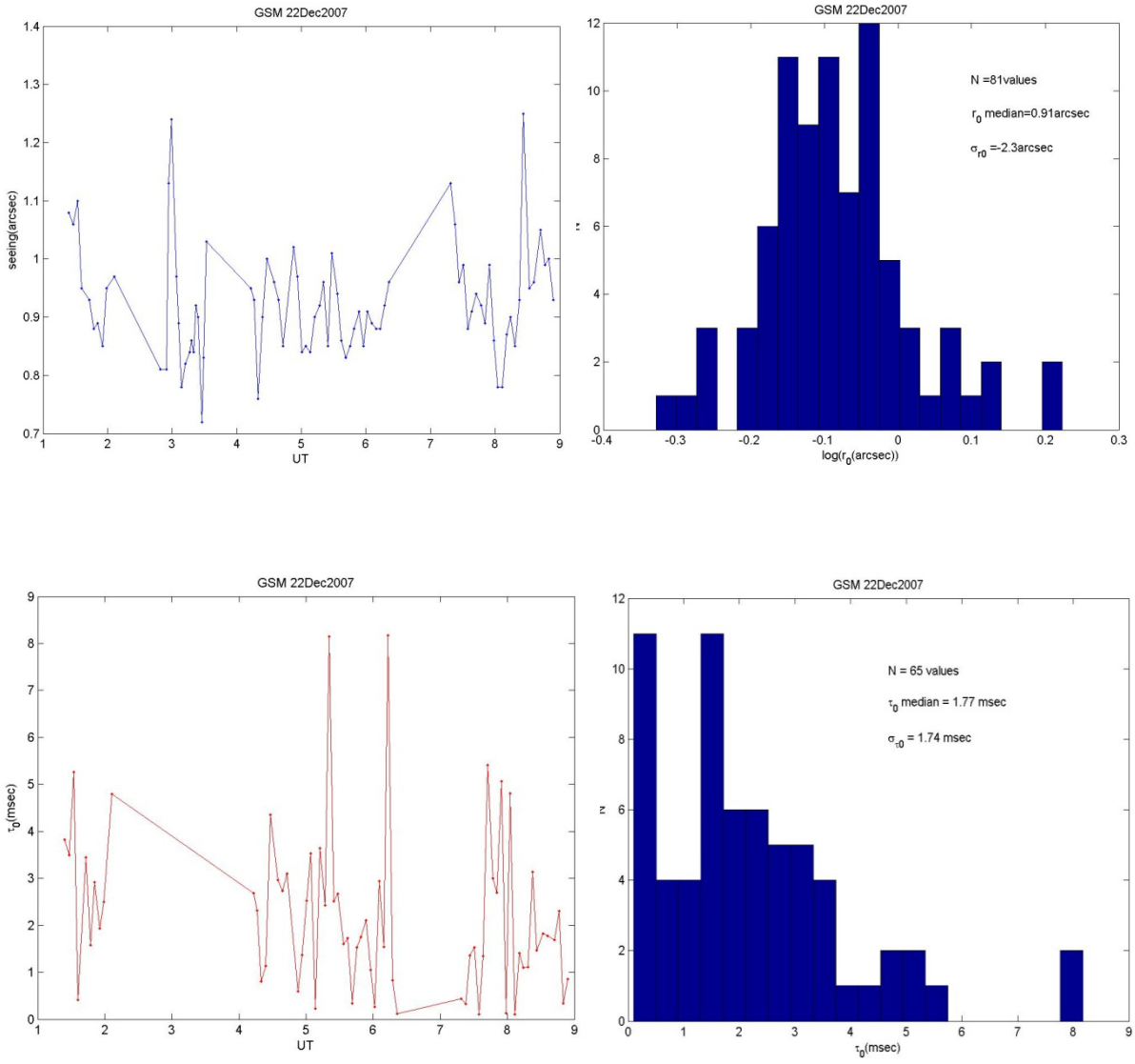

Figure 57: GSM (seeing and coherence time) 22 December 2007.

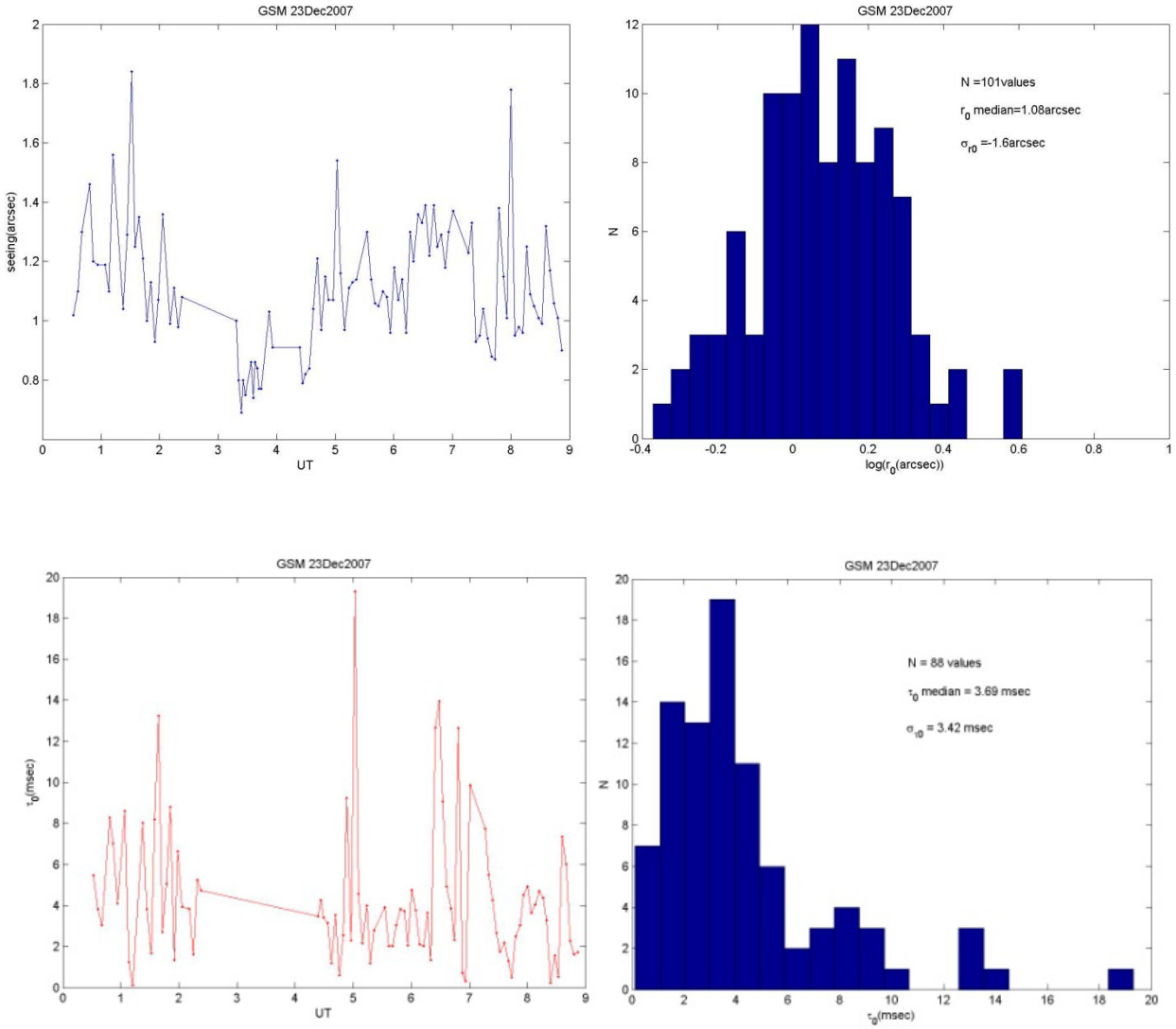

Figure 58: GSM (seeing and coherence time) 23 December 2007.

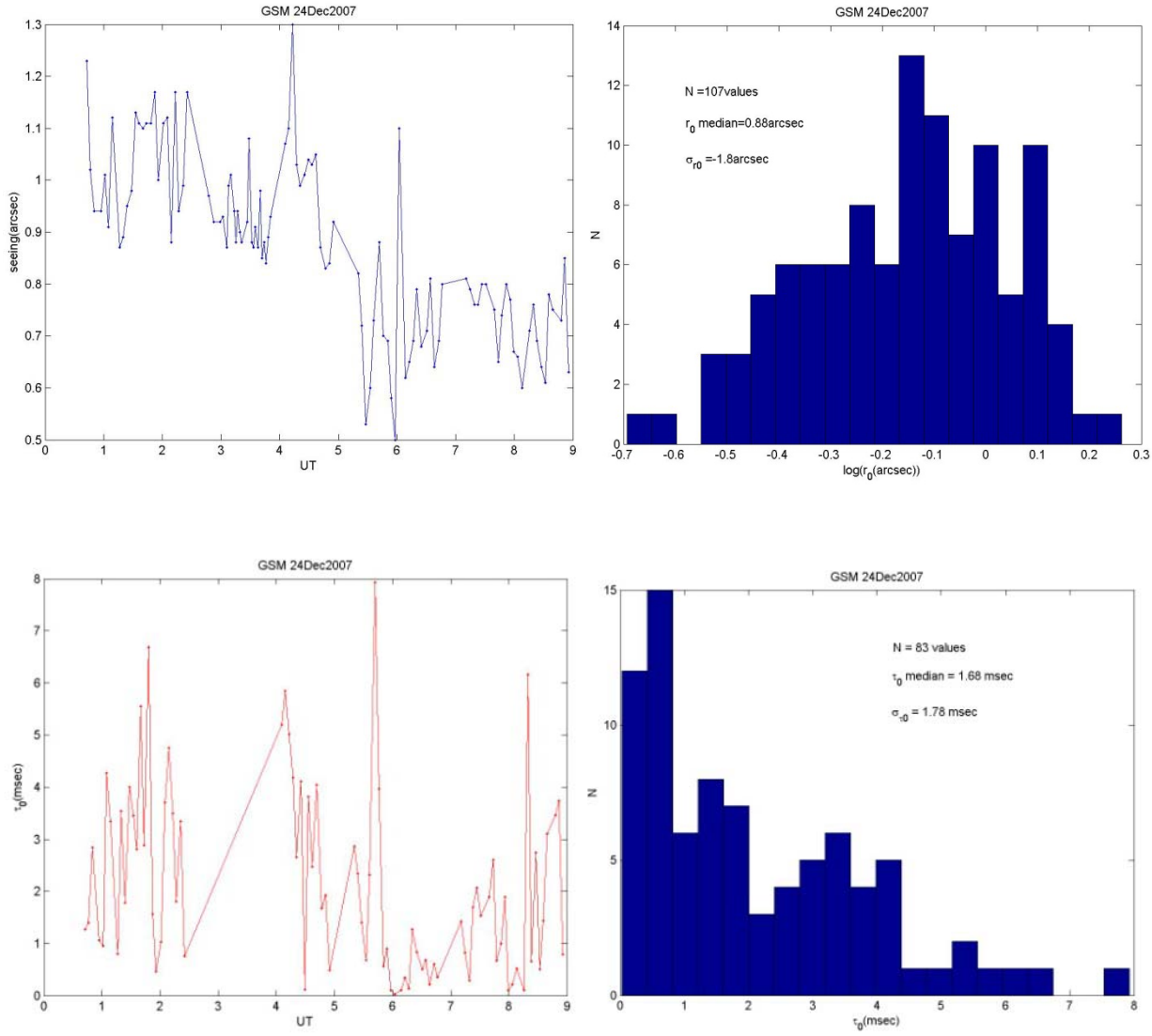

Figure 59: GSM (seeing and coherence time) 24 December 2007.

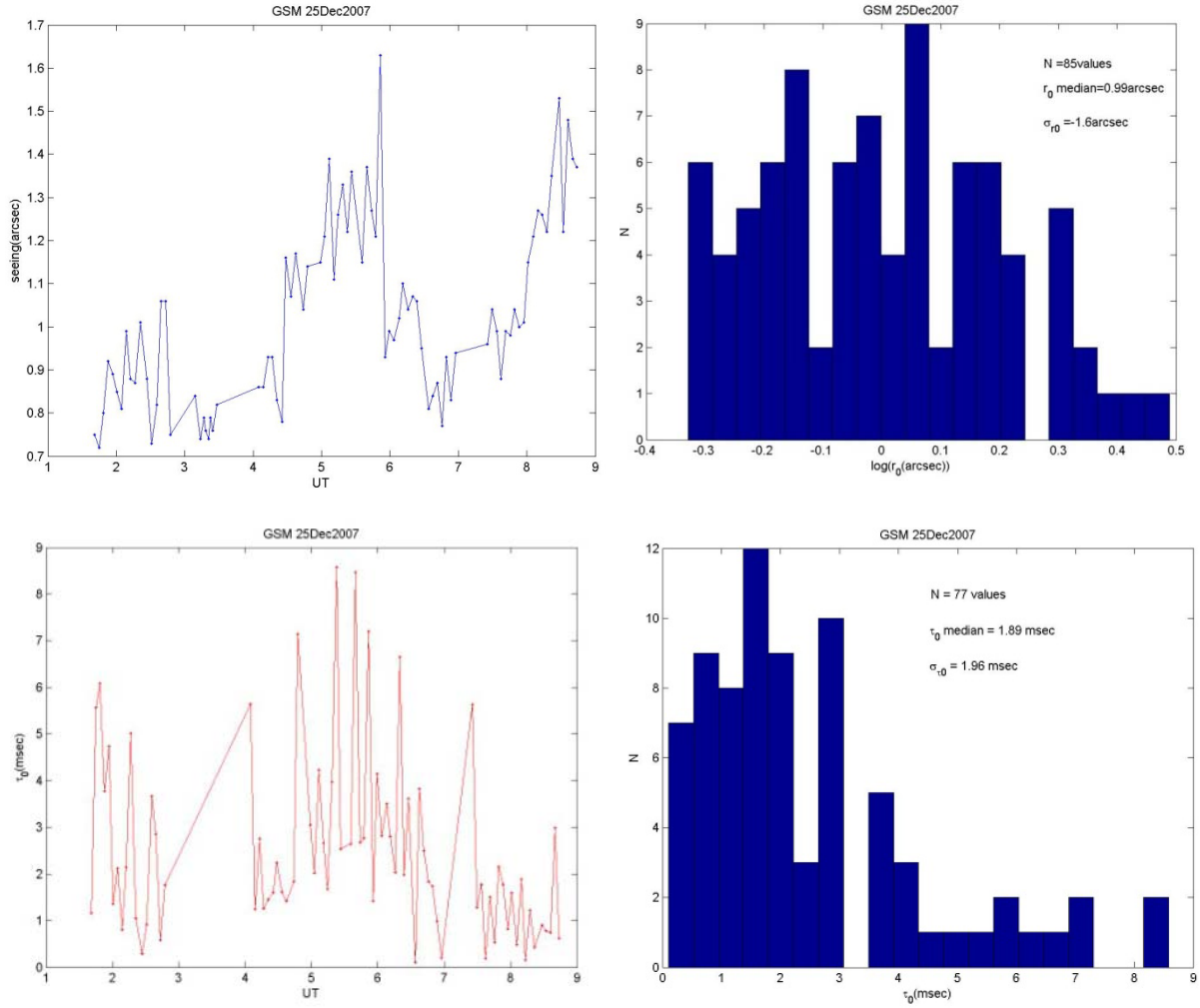

Figure 60: GSM (seeing and coherence time) 25 December 2007.

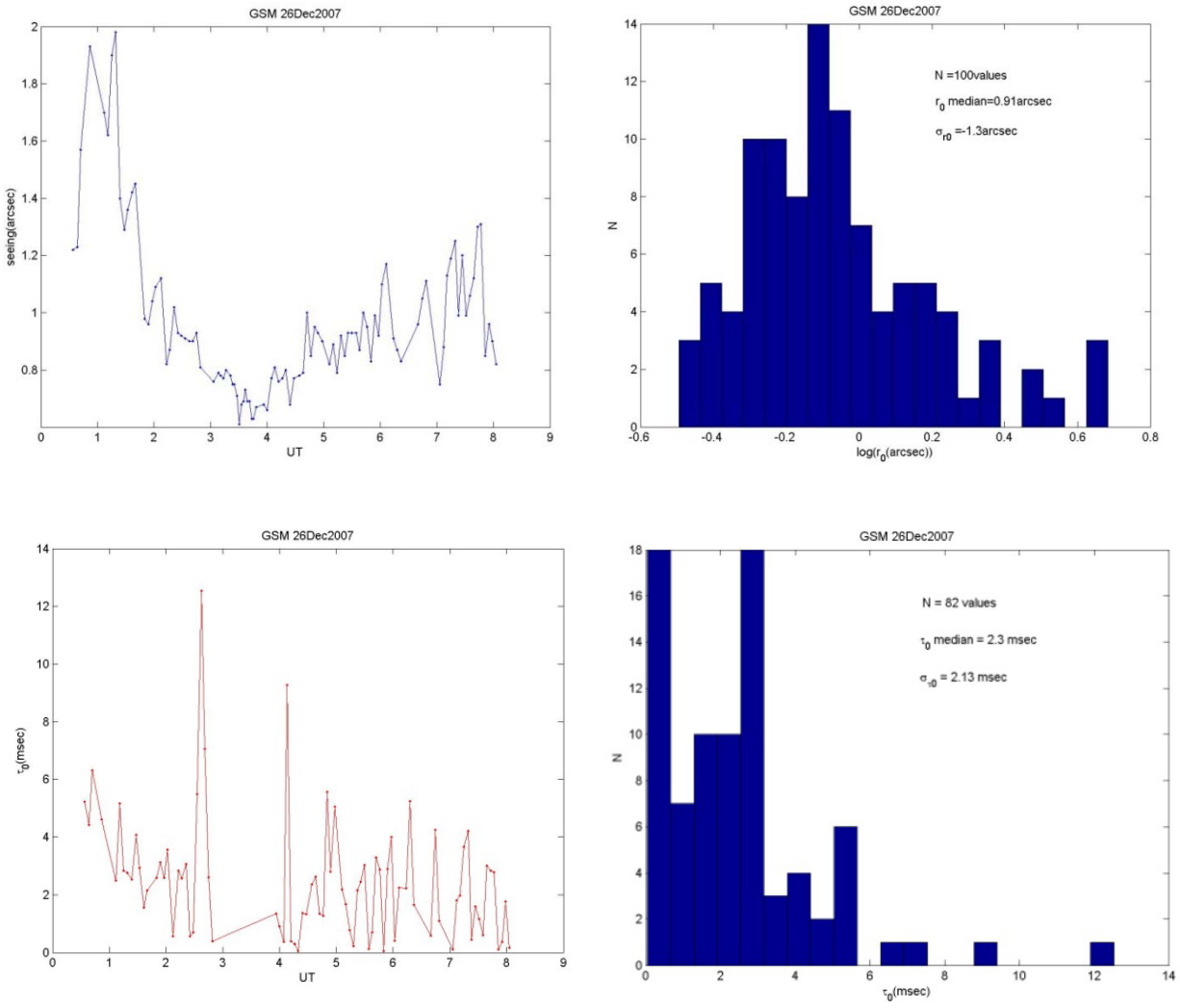

Figure 61: GSM (seeing and coherence time) 26 December 2007.

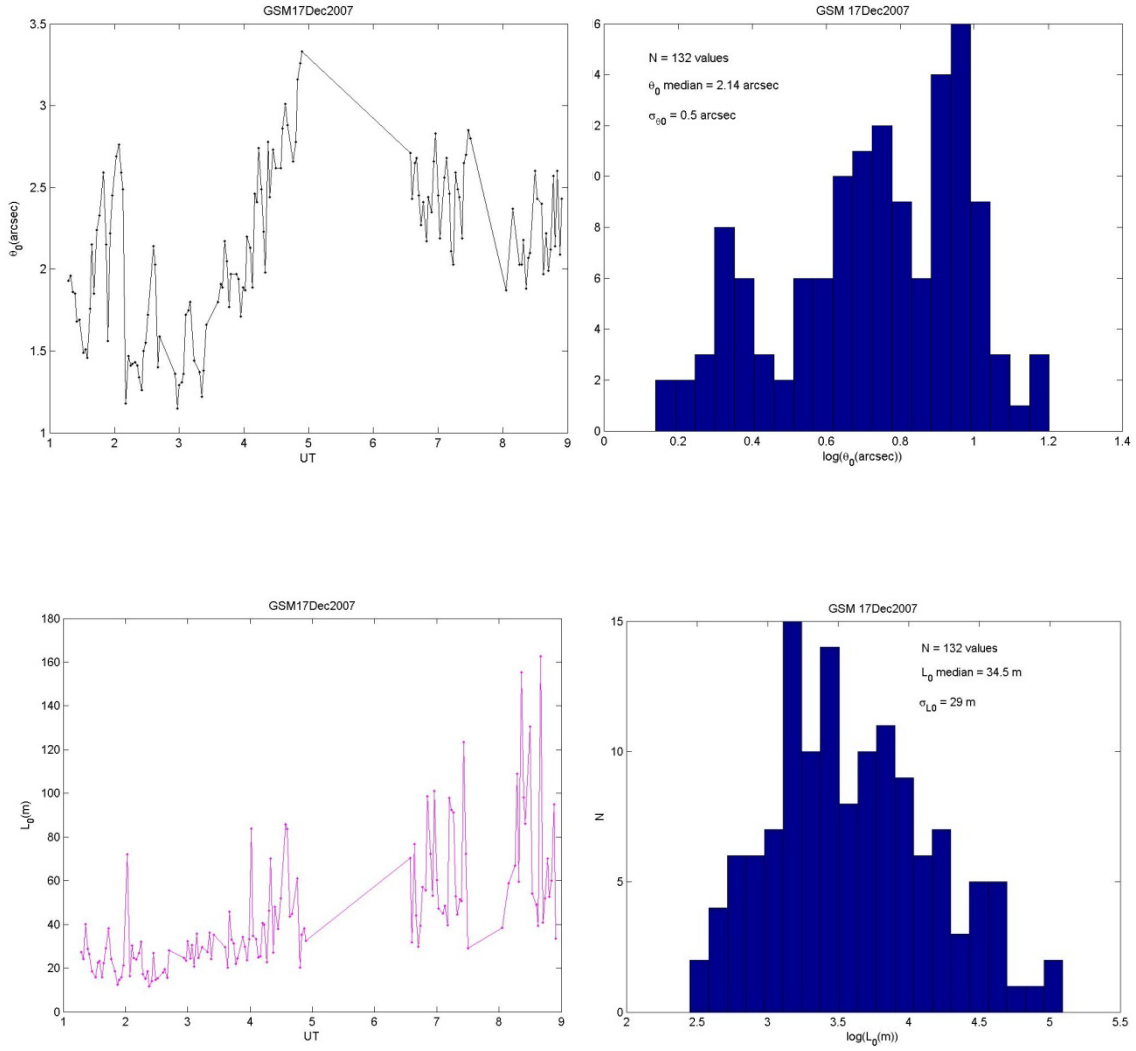

Figure 62: GSM (isoplanatic angle and outer scale) 17 December 2007.

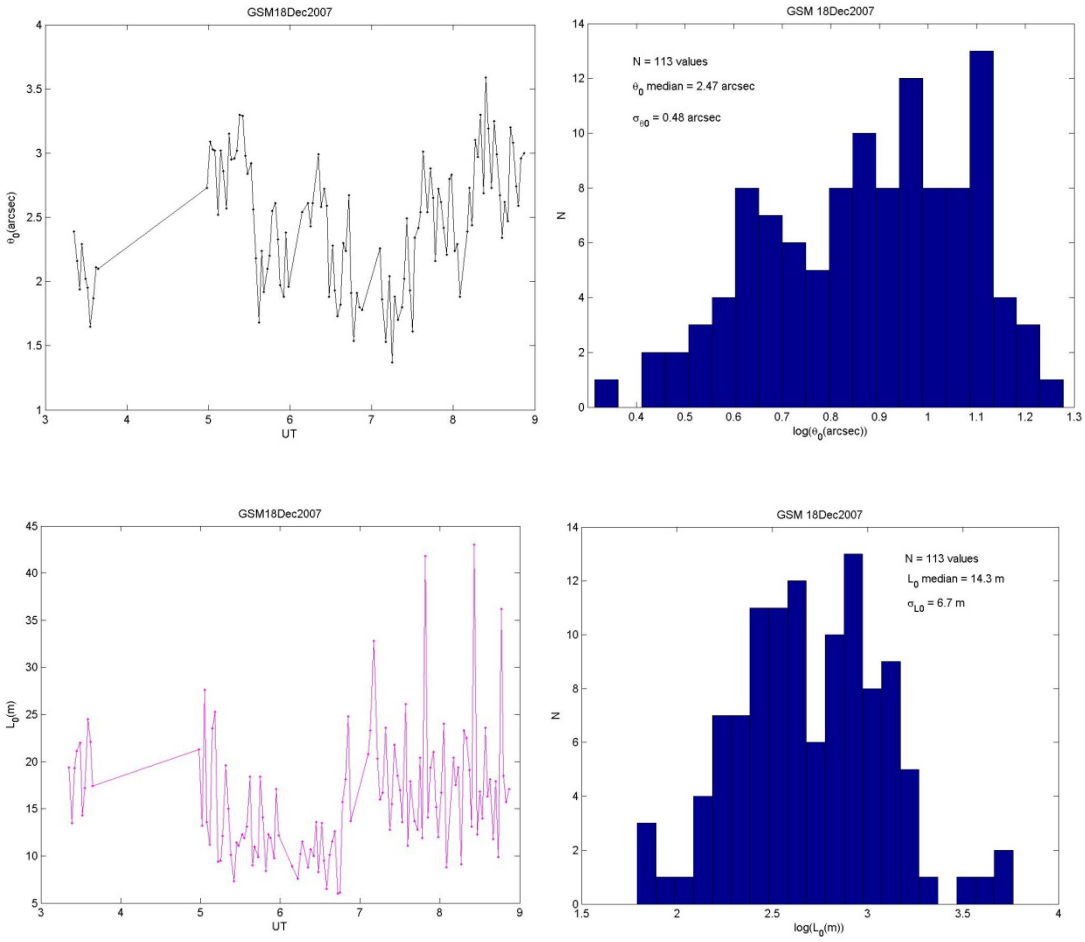

Figure 63: GSM (isoplanatic angle and outer scale) 18 December 2007.

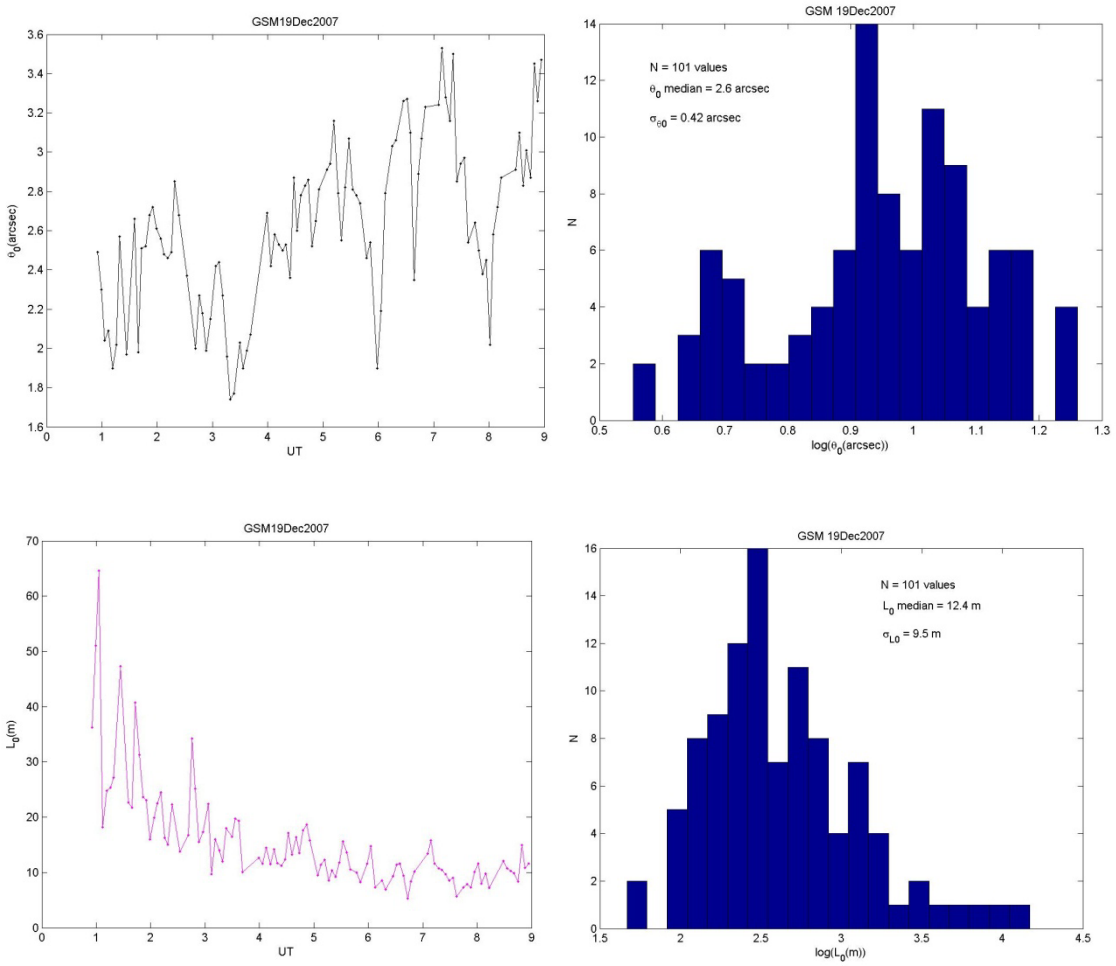

Figure 64: GSM (isoplanatic angle and outer scale) 19 December 2007.

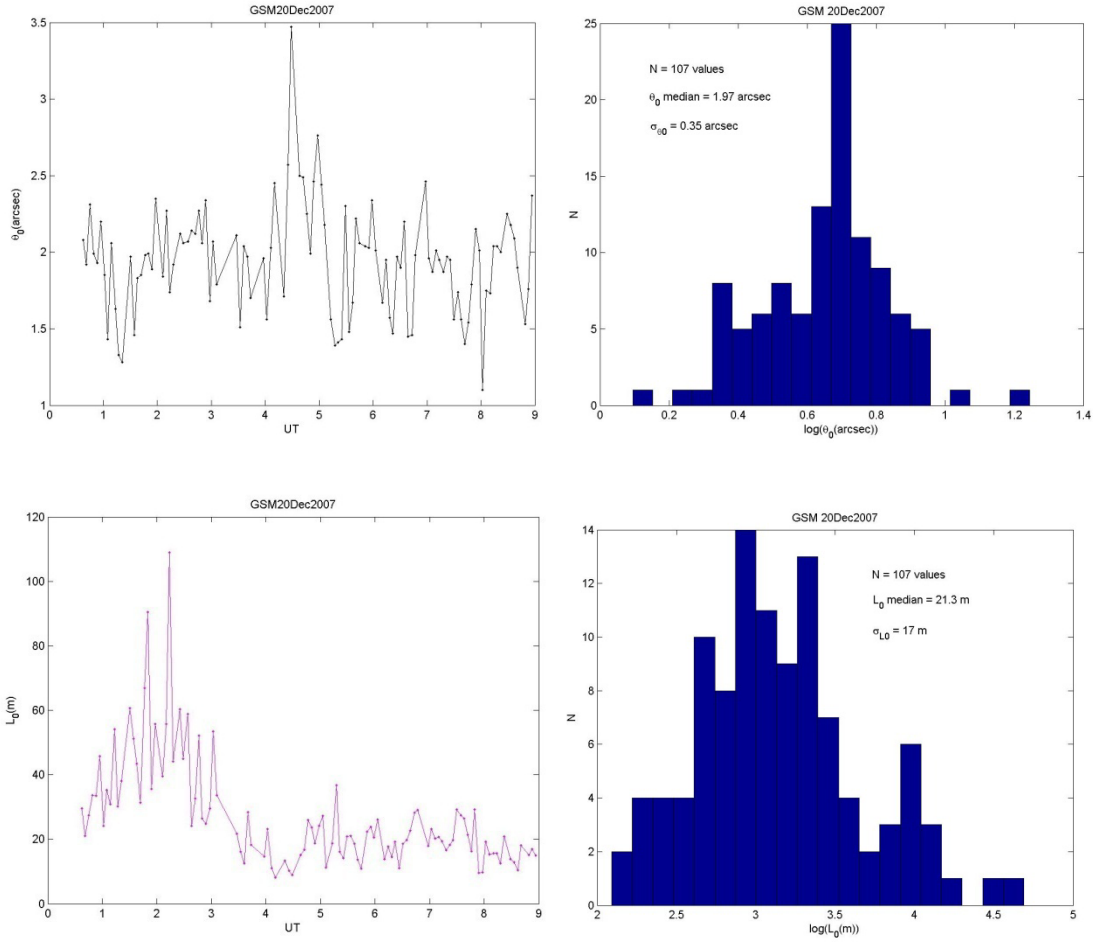

Figure 65: GSM (isoplanatic angle and outer scale) 20 December 2007.

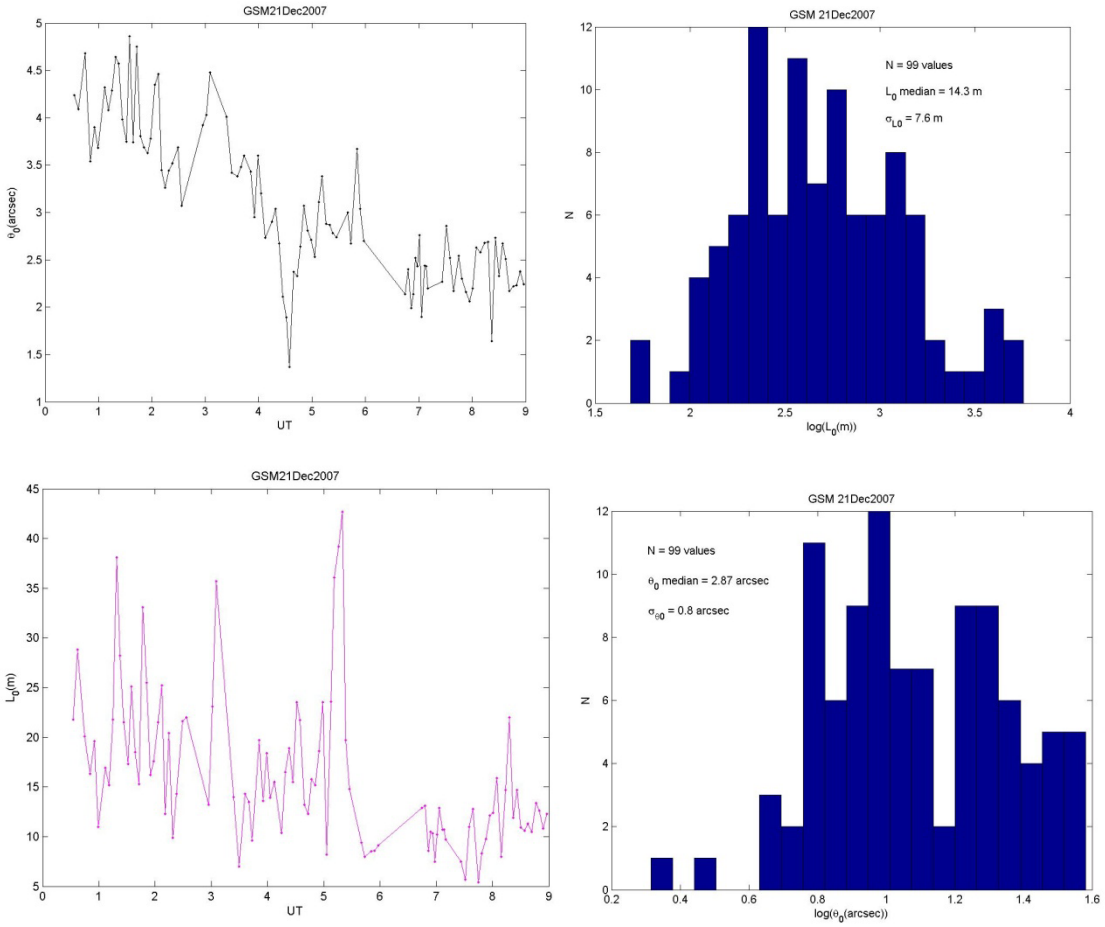

Figure 66: GSM (isoplanatic angle and outer scale) 21 December 2007.

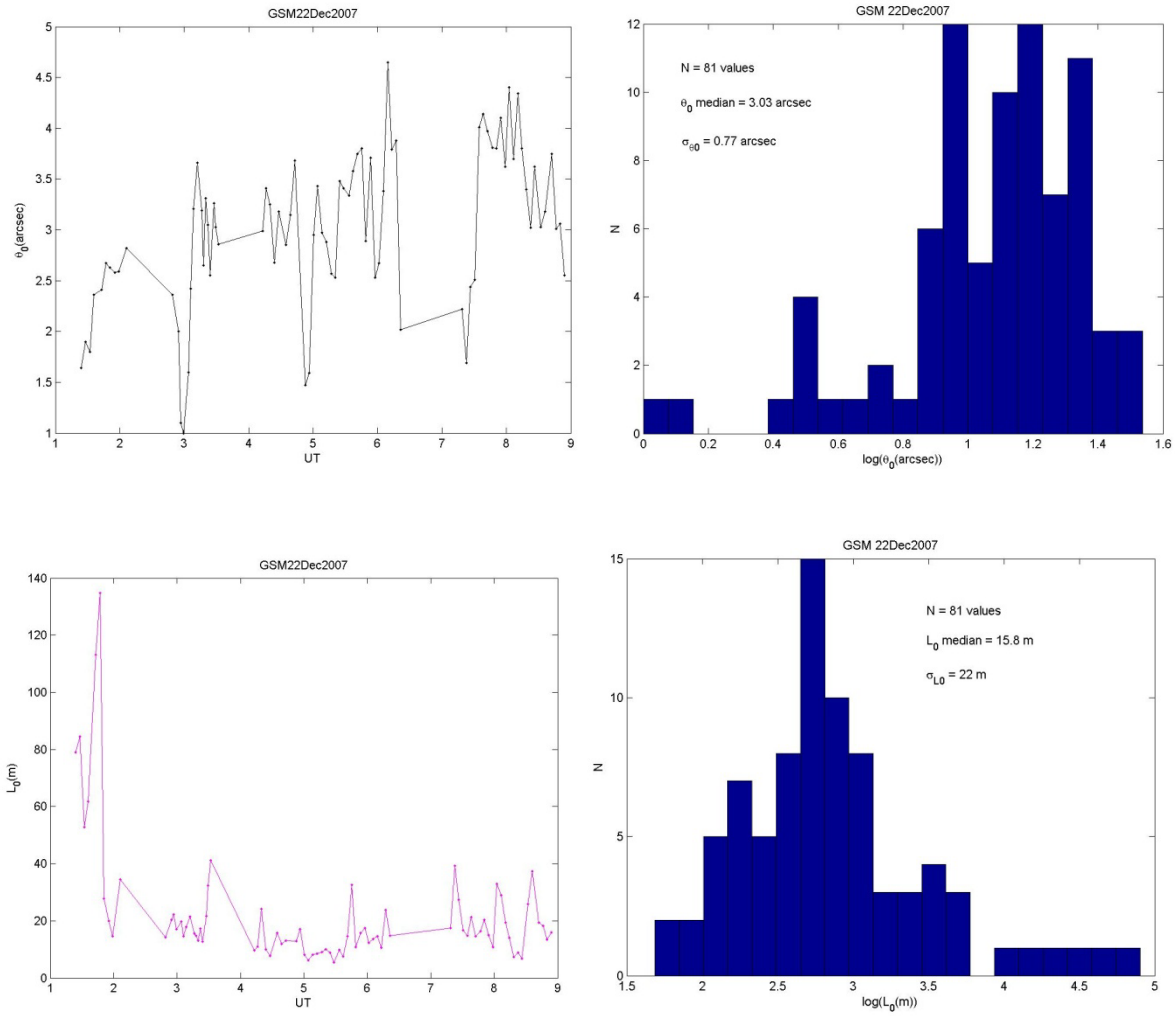

Figure 67: GSM (isoplanatic angle and outer scale) 22 December 2007.

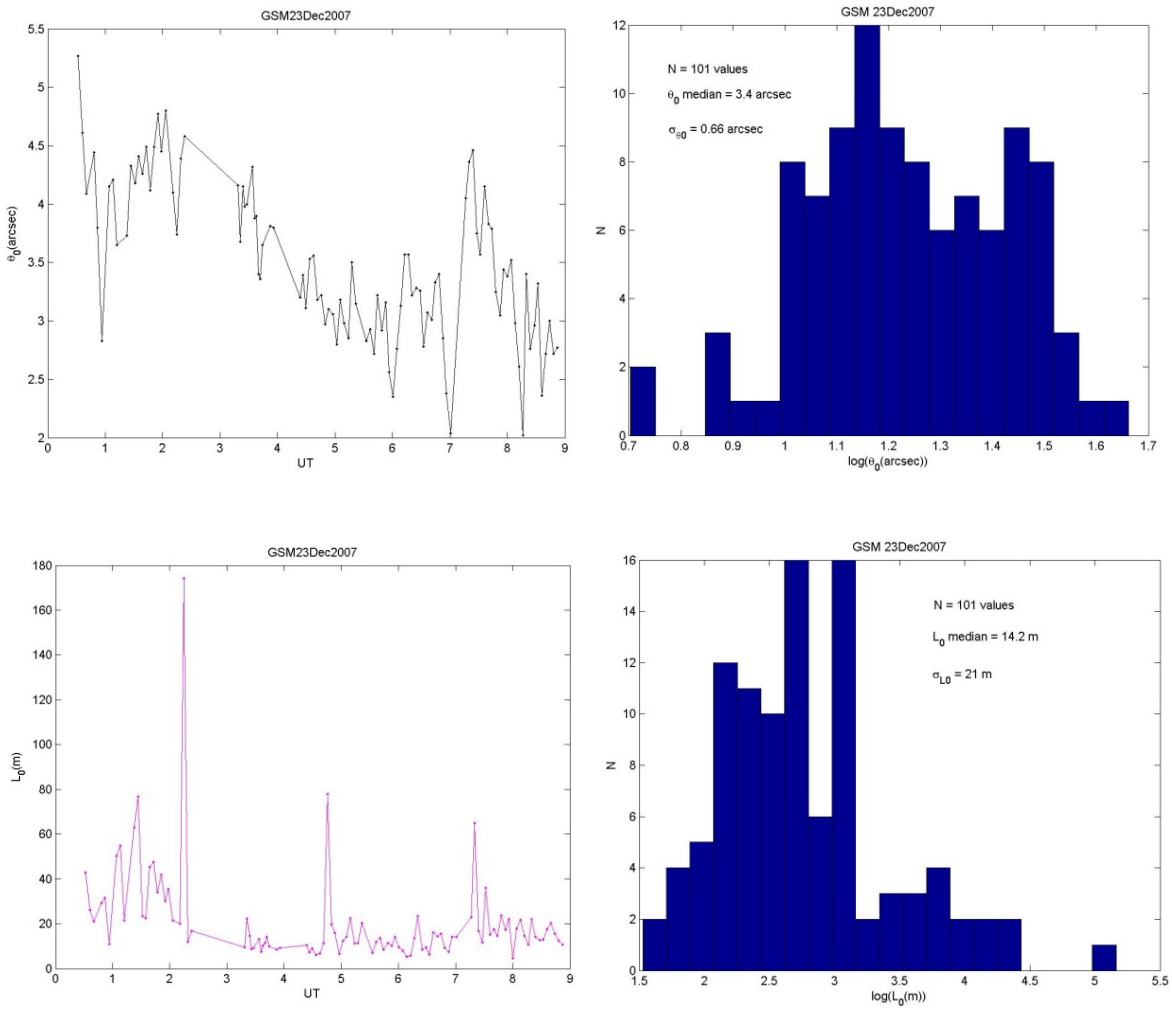

Figure 68: GSM (isoplanatic angle and outer scale) 23 December 2007.

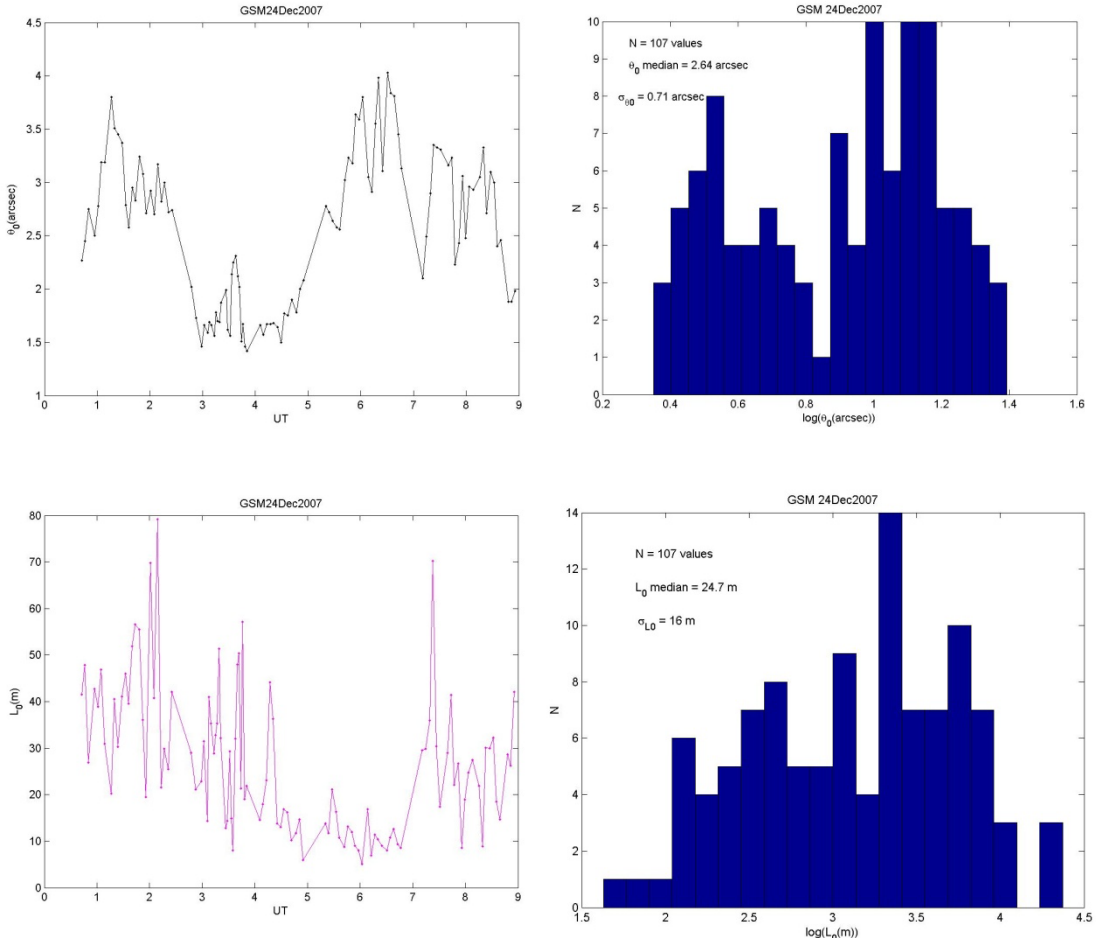

Figure 69: GSM (isoplanatic angle and outer scale) 24 December 2007.

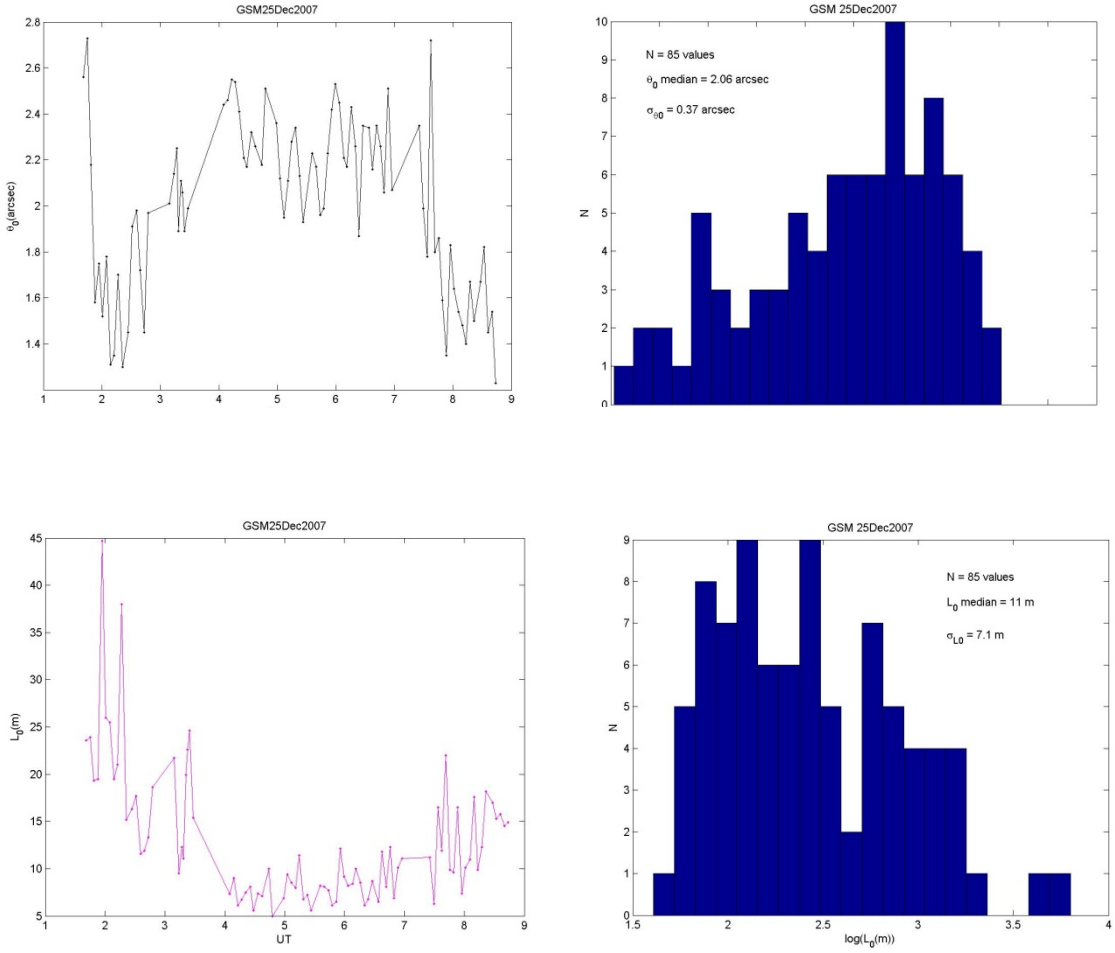

Figure 70: GSM (isoplanatic angle and outer scale) 25 December 2007.

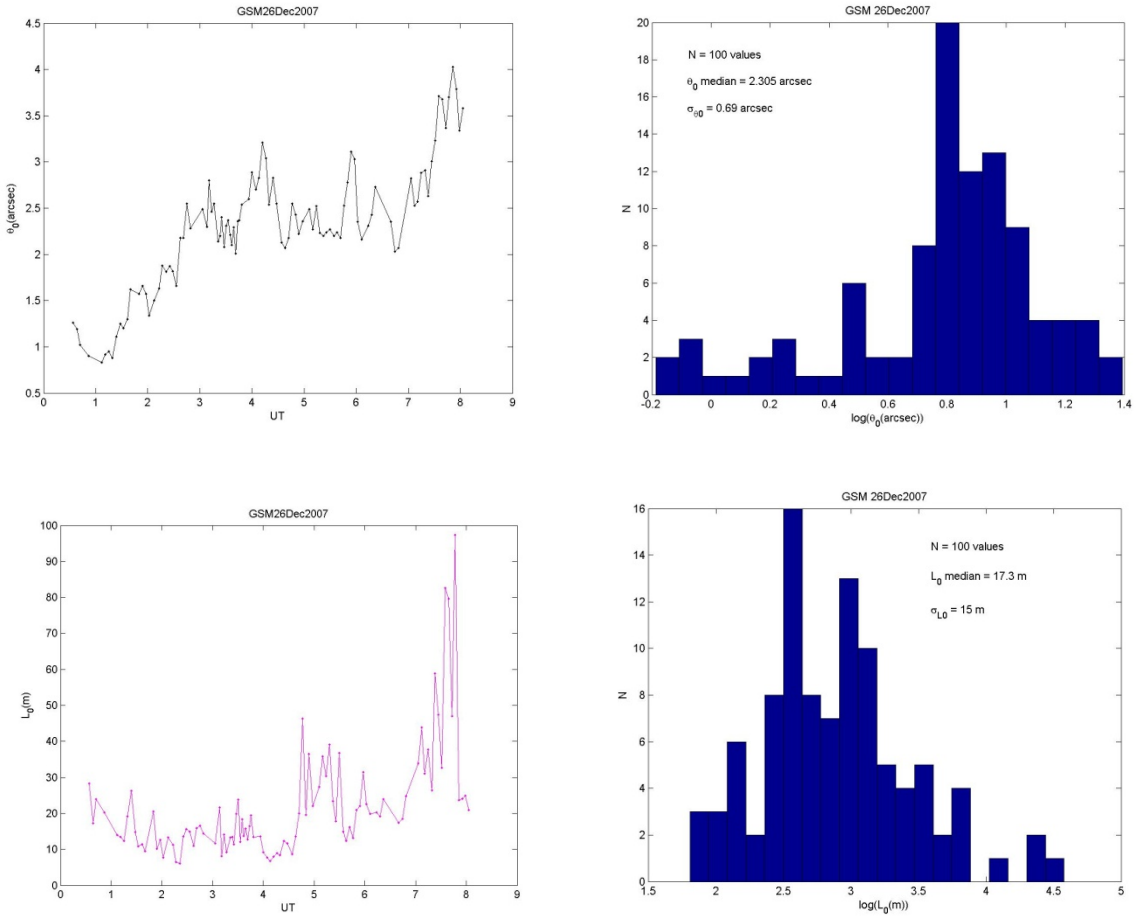

Figure 71: GSM (isoplanatic angle and outer scale) 26 December 2007.

GSM 17 Dec2007 at Paranal

night: 17 Dec2007	Median	Rang
seeing tot(arcsec)	1.28	0.89 -- 2.23
θ_0 (arcsec)	2.14	1.15 -- 3.33
τ_0 (msec)	1.31	0.1 -- 5.99
L_0 (m)	34.5	11.6 -- 163

GSM 18 Dec2007 at Paranal

night: 18 Dec2007	Median	Rang
seeing tot(arcsec)	1.12	0.93 -- 1.46
θ_0 (arcsec)	2.47	1.37 -- 3.59
τ_0 (msec)	3.83	0.46 -- 17.4
L_0 (m)	14.3	6 -- 43

GSM 19 Dec2007 at Paranal

night: 19 Dec2007	Median	Rang
seeing tot(arcsec)	1.25	0.94 -- 2.69
θ_0 (arcsec)	2.6	1.74 -- 3.53
τ_0 (msec)	3.22	0.08 -- 17.4
L_0 (m)	12.4	5.3 -- 64.6

GSM 20 Dec2007 at Paranal

night: 20 Dec2007	Median	Rang
seeing tot(arcsec)	1.04	0.82 -- 1.64
θ_0 (arcsec)	1.97	1.1 -- 3.47
τ_0 (msec)	1.75	0.1 -- 12.7
L_0 (m)	21.3	8.1 -- 109

GSM 21 Dec2007 at Paranal

night: 21 Dec2007	Median	Rang
seeing tot(arcsec)	1	0.55 -- 1.61
θ_0 (arcsec)	2.87	1.37 -- 4.86
τ_0 (msec)	1.86	0.1 -- 10.9
L_0 (m)	14.3	5.4 -- 42.7

GSM 22 Dec2007 at Paranal

night: 22 Dec2007	Median	Rang
seeing tot(arcsec)	0.91	0.72 -- 1.25
θ_0 (arcsec)	3.03	1 -- 4.65
τ_0 (msec)	1.77	0.1 -- 8.17
L_0 (m)	15.8	5.4 -- 135

GSM 23 Dec2007 at Paranal

night: 23 Dec2007	Median	Rang
seeing tot(arcsec)	1.08	0.69 -- 1.84
θ_0 (arcsec)	3.4	2.02 -- 5.27
τ_0 (msec)	3.69	0.12 -- 19.3
L_0 (m)	14.2	4.6 -- 174

GSM 24 Dec2007 at Paranal

night: 24 Dec2007	Median	Rang
seeing tot(arcsec)	0.88	0.5 -- 1.3
θ_0 (arcsec)	2.64	1.42 -- 4.03
τ_0 (msec)	1.68	0.03 -- 7.93
L_0 (m)	24.7	5.1 -- 79.2

GSM 25 Dec2007 at Paranal

night: 25 Dec2007	Median	Rang
seeing tot(arcsec)	0.99	0.72 -- 1.63
θ_0 (arcsec)	2.06	1.23 -- 2.73
τ_0 (msec)	1.89	0.1 -- 8.58
L_0 (m)	11	5 -- 44.7

GSM 26 Dec2007 at Paranal

night: 26 Dec2007	Median	Rang
seeing tot(arcsec)	0.91	0.61 -- 1.98
θ_0 (arcsec)	2.3	0.83 -- 4.03
τ_0 (msec)	2.3	0.05 -- 12.5
L_0 (m)	17.3	6.1 -- 97.4

LuSci:

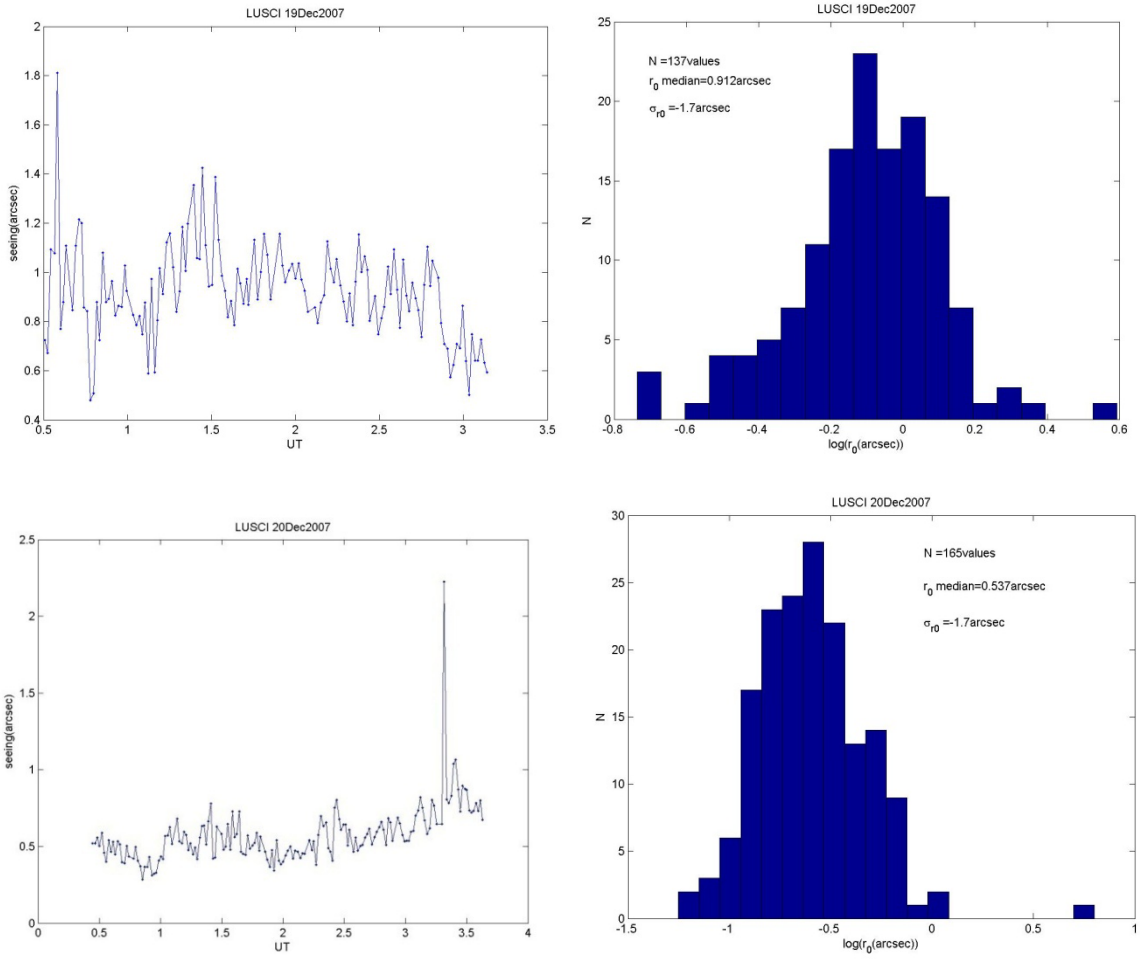

LuSci 19 Dec2007 at Paranal

night: 19 Dec2007	Median	Rang
seeing tot(arcsec)	0.91	0.48 -- 1.8

LuSci 20 Dec2007 at Paranal

night: 20 Dec2007	Median	Rang
seeing tot(arcsec)	0.54	0.29 -- 2.2

Figure 72: LuSci (seeing) 19-20 December 2007.

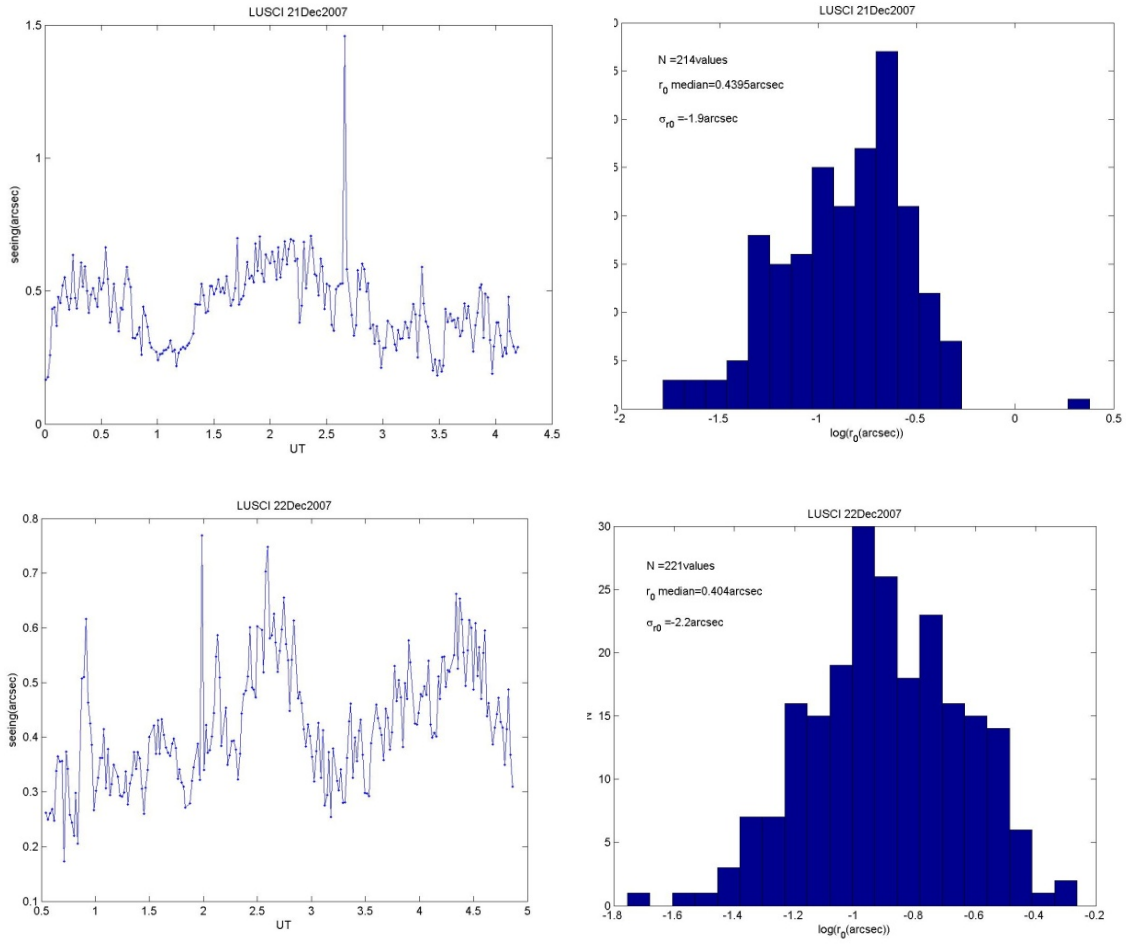

LuSci 21 Dec2007 at Paranal

night: 21 Dec2007	Median	Rang
seeing tot(arcsec)	0.44	0.17 -- 1.5

LuSci 22 Dec2007 at Paranal

night: 22 Dec2007	Median	Rang
seeing tot(arcsec)	0.4	0.17 -- 0.77

Figure 73: LuSci (seeing) 21-22 December 2007.

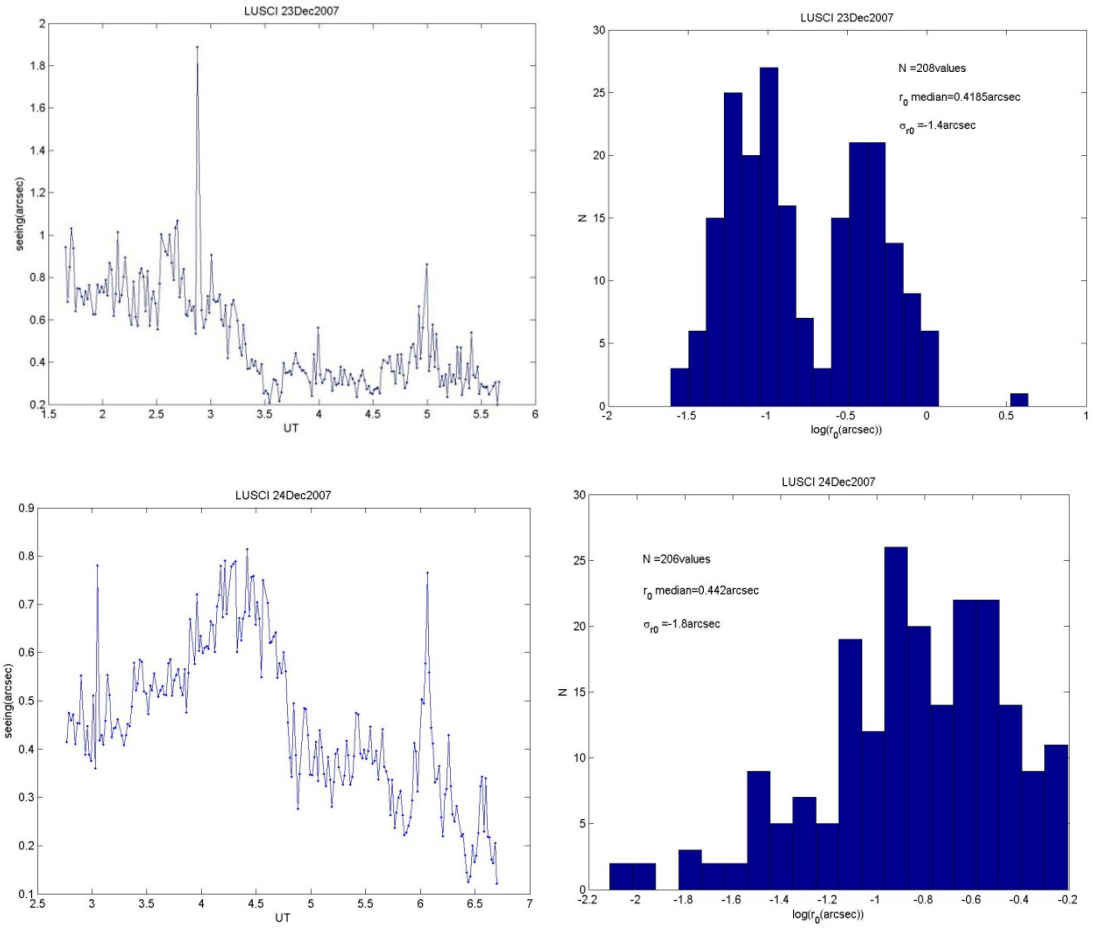

LuSci 23 Dec2007 at Paranal

night: 23 Dec2007	Median	Rang
seeing tot(arcsec)	0.42	0.2 -- 1.9

LuSci 24 Dec2007 at Paranal

night: 24 Dec2007	Median	Rang
seeing tot(arcsec)	0.44	0.12 -- 0.81

Figure 74: LuSci (seeing) 23-24 December 2007.

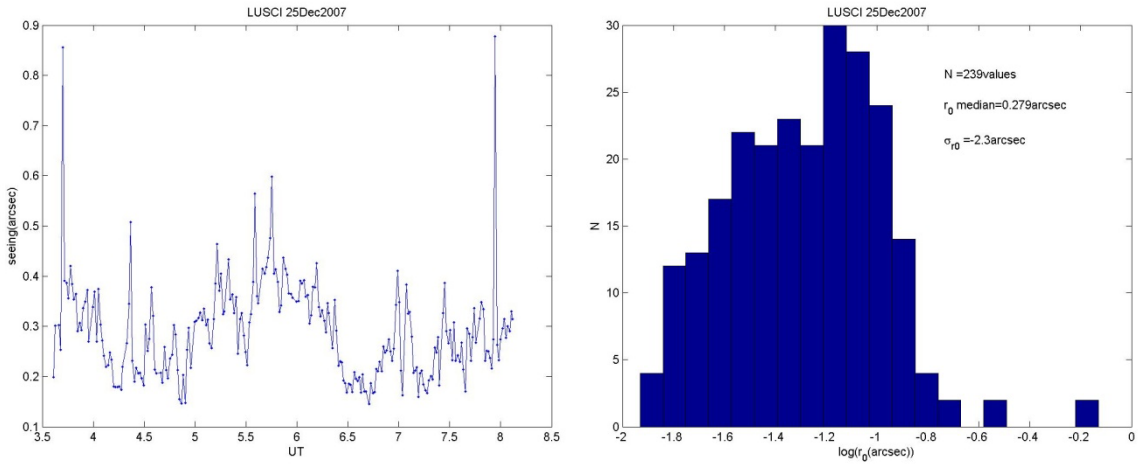

LuSci 25 Dec2007 at Paranal

night: 25 Dec2007	Median	Rang
seeing tot(arcsec)	0.28	0.14 -- 0.88

Figure 75: LuSci (seeing) 25 December 2007.

MASS:

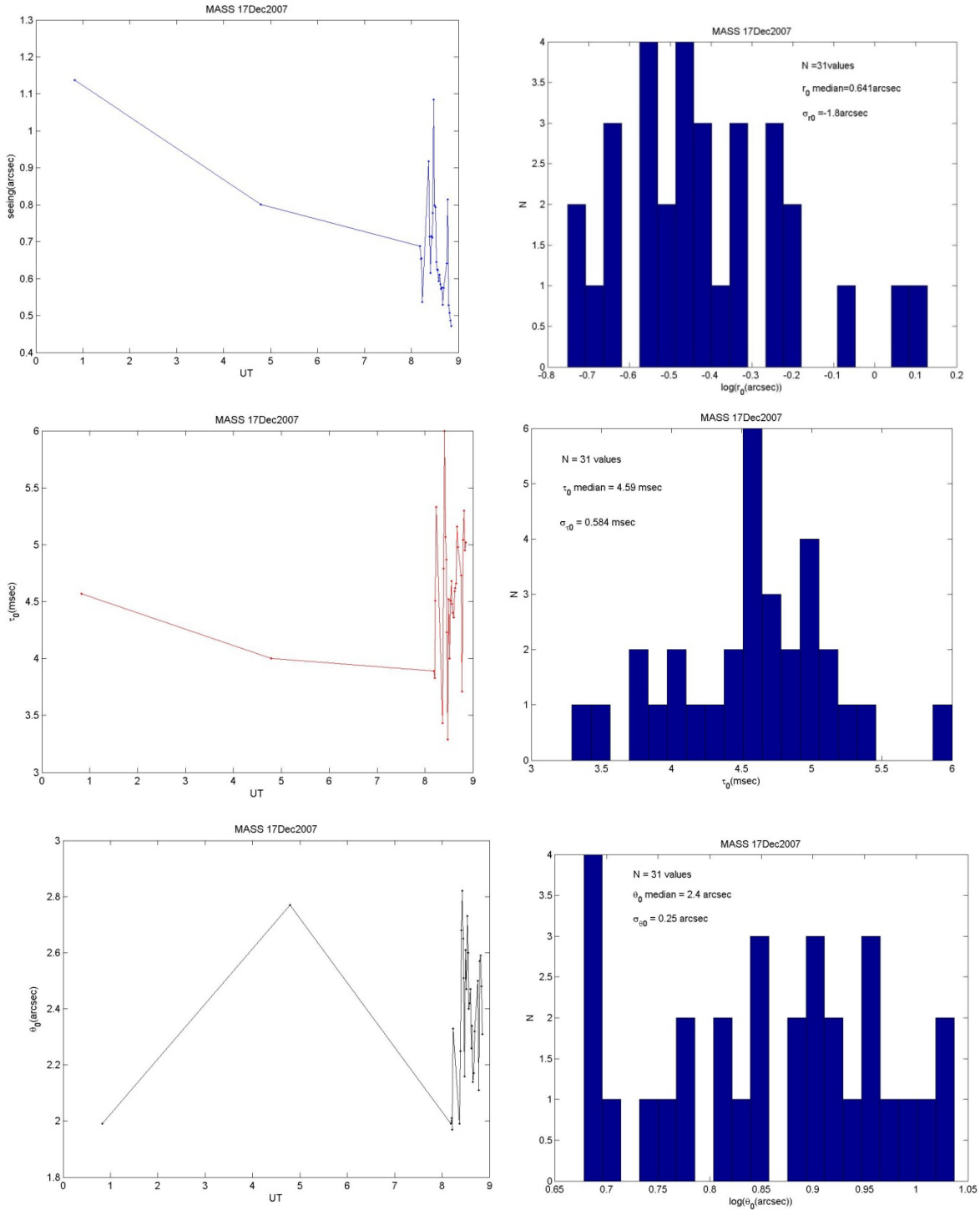

Figure 76: MASS (seeing, coherence time and isoplanatic angle) 17 December 2007.

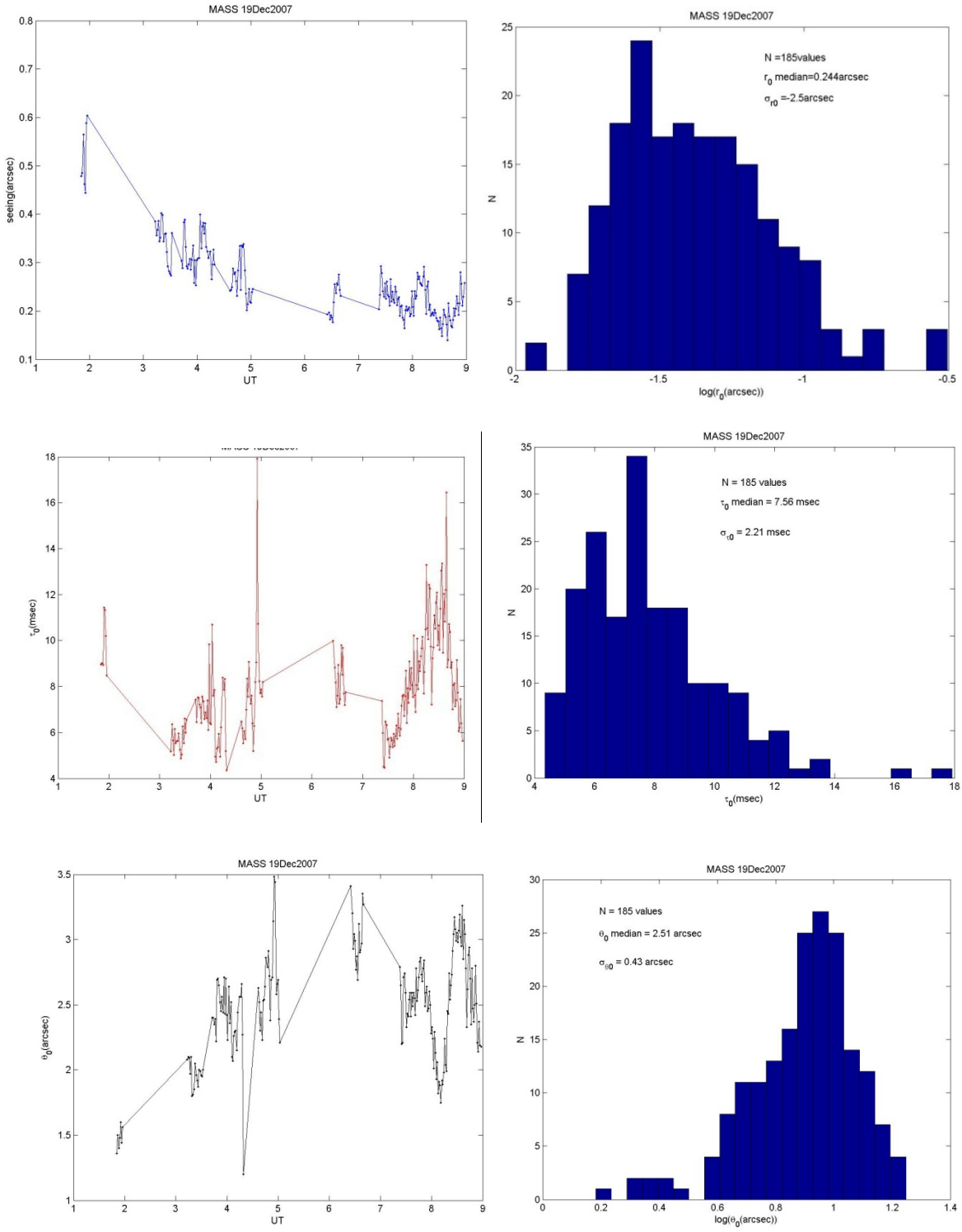

Figure 77: MASS (seeing, coherence time and isoplanatic angle) 19 December 2007.

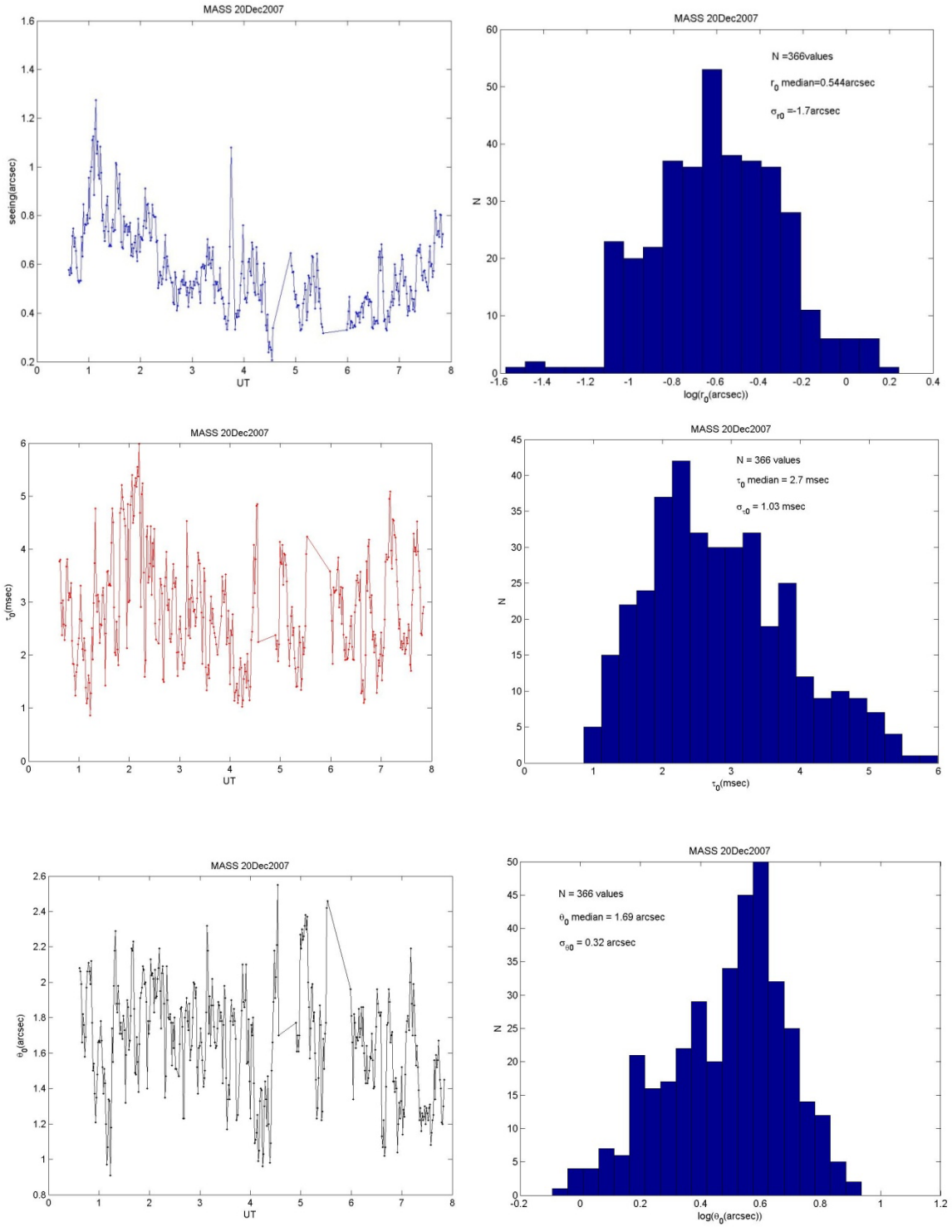

Figure 78: MASS (seeing, coherence time and isoplanatic angle) 20 December 2007.

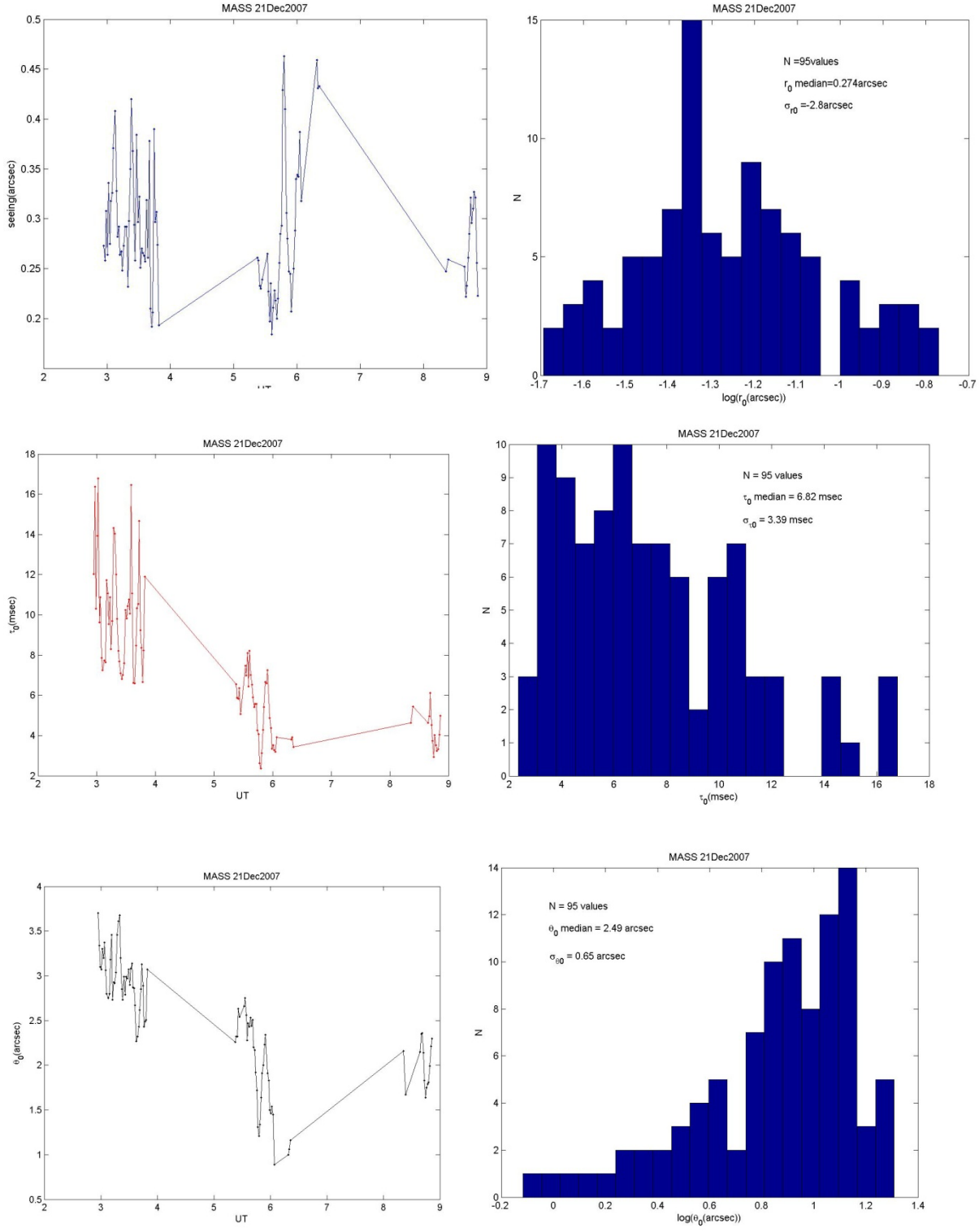

Figure 78: MASS (seeing, coherence time and isoplanatic angle) 21 December 2007.

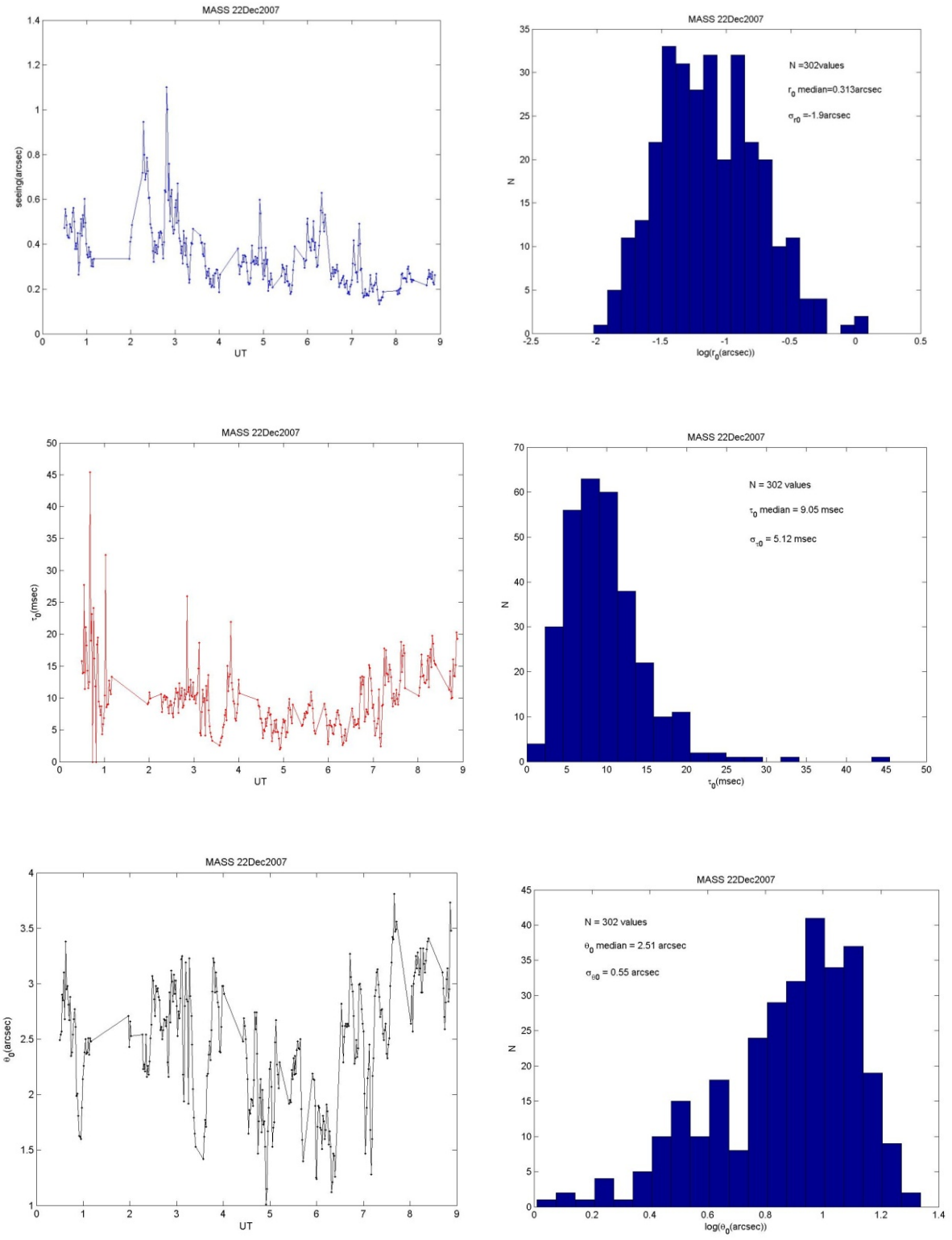

Figure 79: MASS (seeing, coherence time and isoplanatic angle) 22 December 2007.

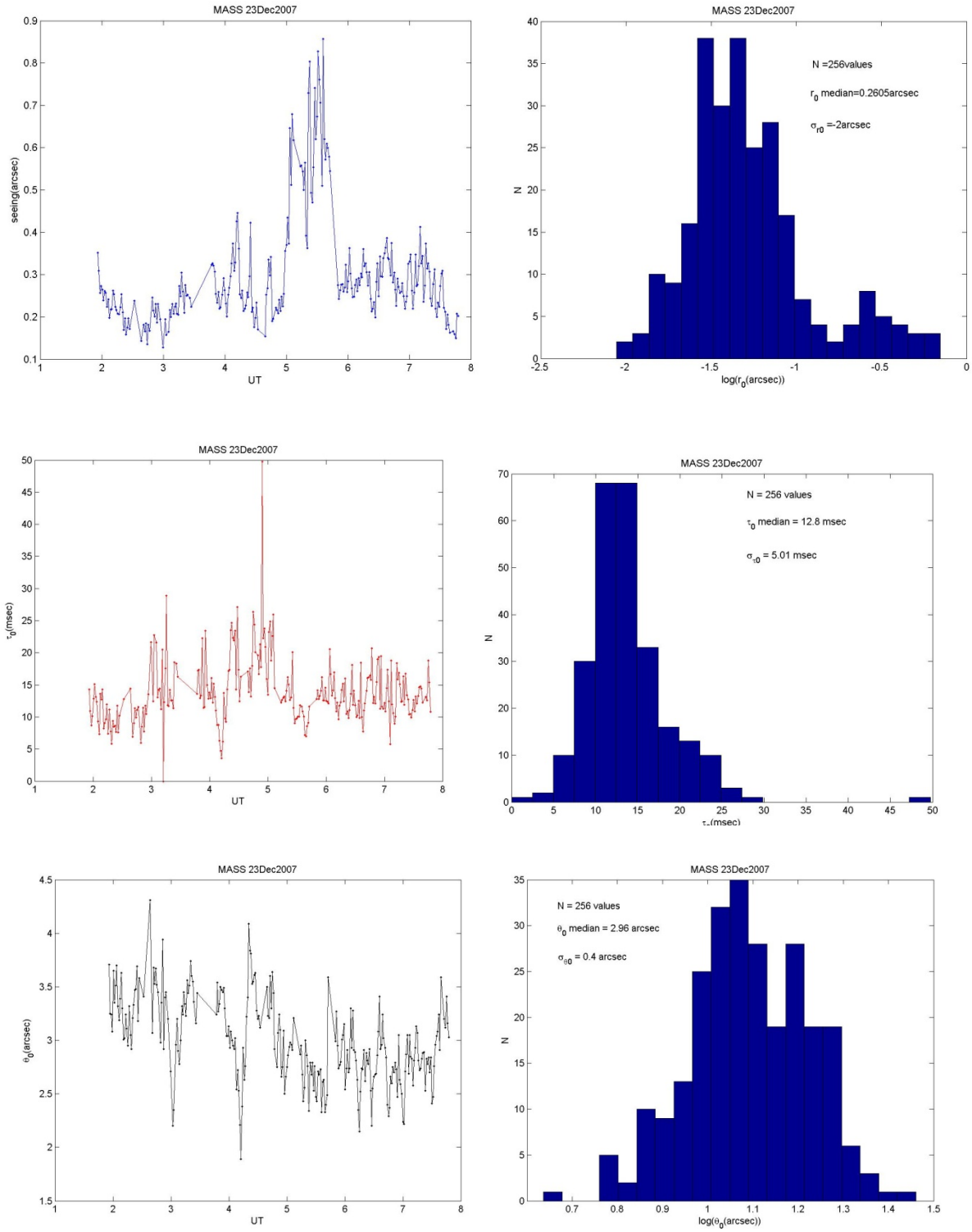

Figure 80: MASS (seeing, coherence time and isoplanatic angle) 23 December 2007.

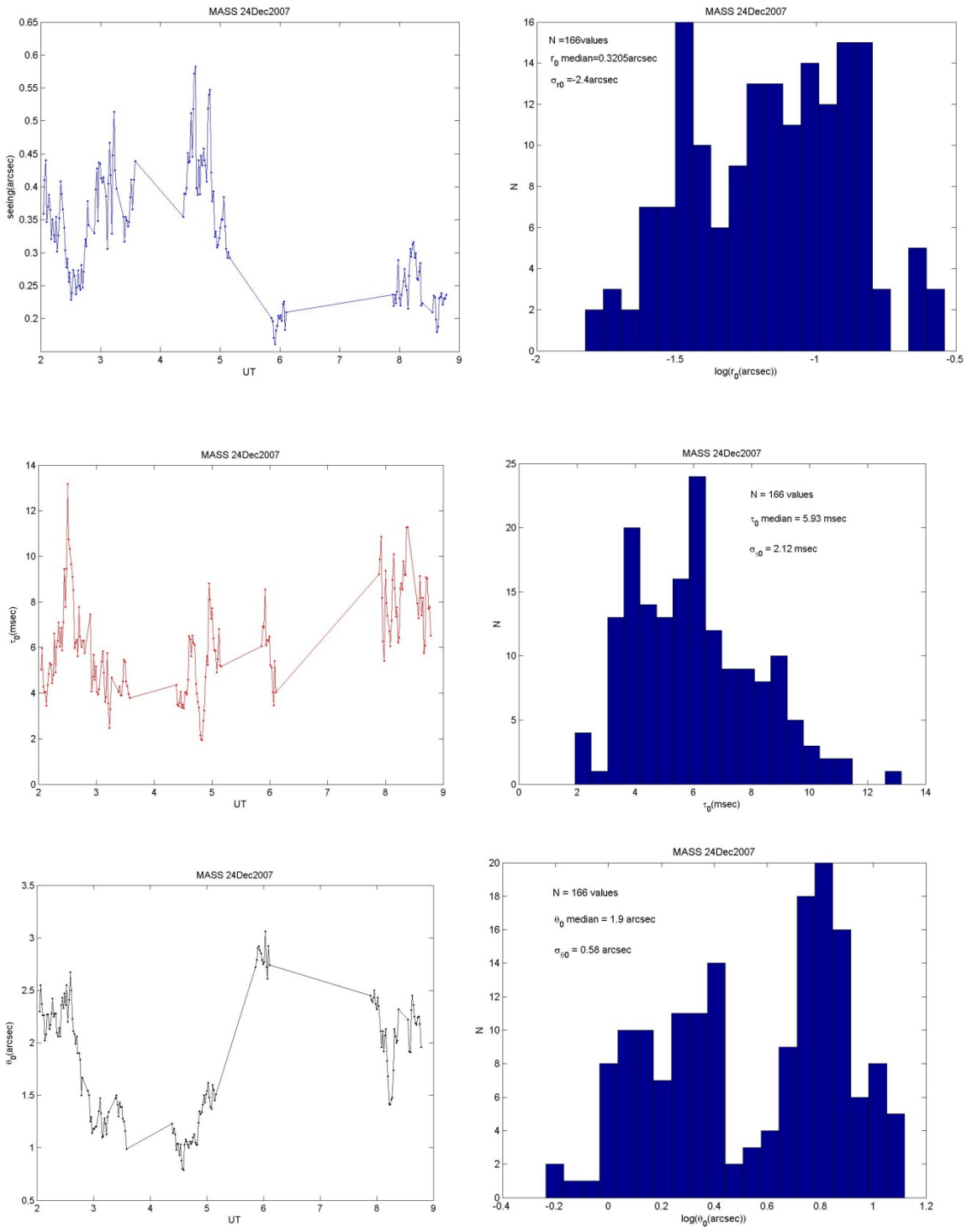

Figure 81: MASS (seeing, coherence time and isoplanatic angle) 24 December 2007.

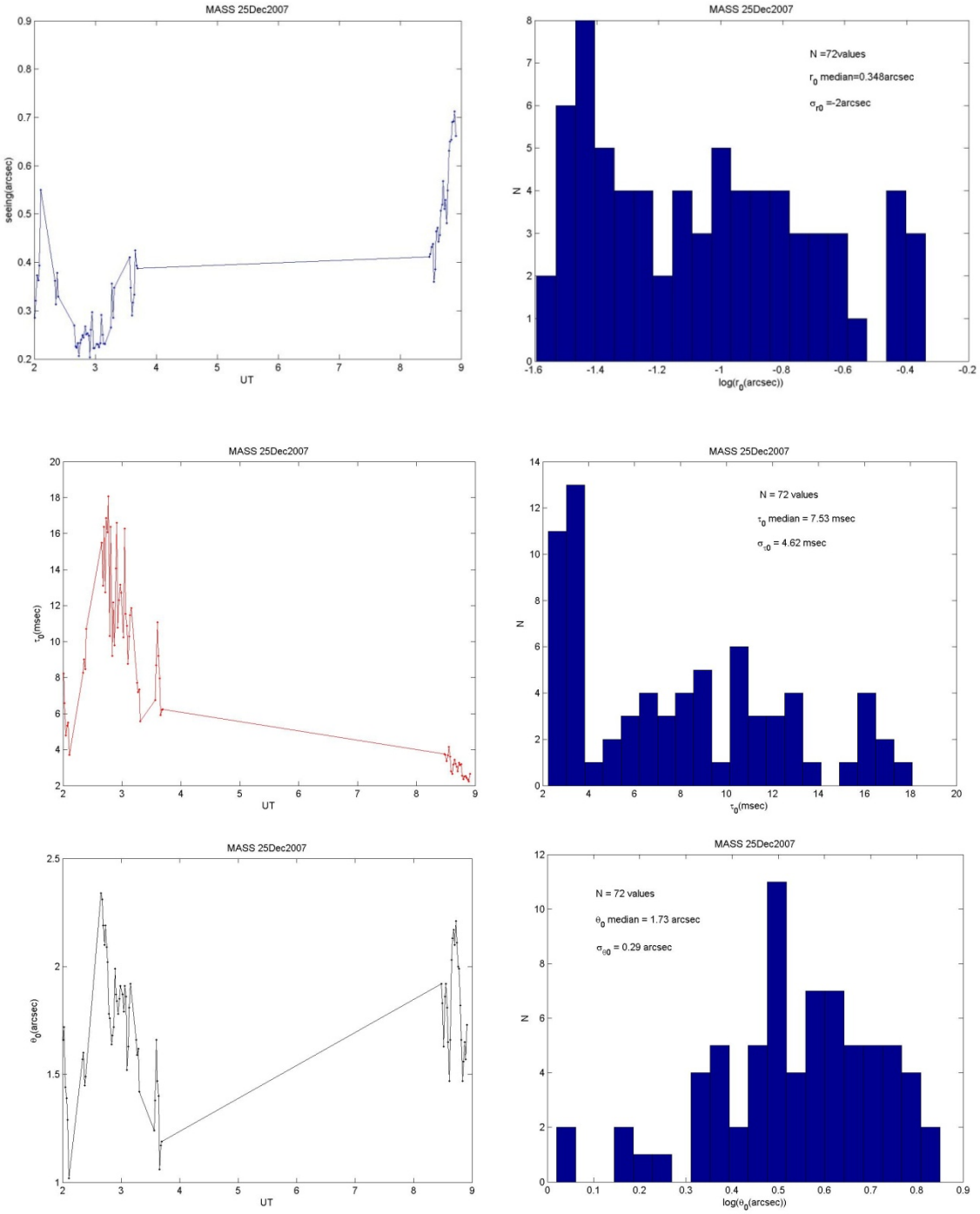

Figure 82: MASS (seeing, coherence time and isoplanatic angle) 25 December 2007.

MASS 17 Dec2007 at Paranal

night: 17 Dec2007	Median	Rang
seeing tot(arcsec)	0.64	0.47 -- 1.1
θ_0 (arcsec)	2.4	1.97 -- 2.82
τ_0 (msec)	4.59	3.29 -- 6

MASS 19 Dec2007 at Paranal

night: 19 Dec2007	Median	Rang
seeing tot(arcsec)	0.24	0.14 -- 0.6
θ_0 (arcsec)	2.51	1.2 -- 3.48
τ_0 (msec)	7.56	4.36 -- 17.9

MASS 20 Dec2007 at Paranal

night: 20 Dec2007	Median	Rang
seeing tot(arcsec)	0.54	0.21 -- 1.3
θ_0 (arcsec)	1.69	0.91 -- 2.55
τ_0 (msec)	2.7	0.86 -- 5.99

MASS 21 Dec2007 at Paranal

night: 21 Dec2007	Median	Rang
seeing tot(arcsec)	0.27	0.18 -- 0.46
θ_0 (arcsec)	2.49	0.89 -- 3.7
τ_0 (msec)	6.82	2.35 -- 16.8

MASS 22 Dec2007 at Paranal

night: 22 Dec2007	Median	Rang
seeing tot(arcsec)	0.31	0.13 -- 1.1
θ_0 (arcsec)	2.51	1.01 -- 3.81
τ_0 (msec)	9.05	0 -- 45.4

MASS 23 Dec2007 at Paranal

night: 23 Dec2007	Median	Rang
seeing tot(arcsec)	0.26	0.13 -- 0.86
θ_0 (arcsec)	2.96	1.89 -- 4.31
τ_0 (msec)	12.8	0 -- 49.7

MASS 24 Dec2007 at Paranal

night: 24 Dec2007	Median	Rang
seeing tot(arcsec)	0.32	0.16 -- 0.58
θ_0 (arcsec)	1.9	0.79 -- 3.06
τ_0 (msec)	5.93	1.93 -- 13.2

MASS 25 Dec2007 at Paranal

night: 25 Dec2007	Median	Rang
seeing tot(arcsec)	0.35	0.2 -- 0.71
θ_0 (arcsec)	1.73	1.02 -- 2.34
τ_0 (msec)	7.53	2.24 -- 18.1

Acknowledgements:

This document and the work described within are partly funded by the European Commission, Research Directorate, Sixth Framework Programme (EC FP6). The EC FP6 aims to contribute to the creation of a true European Research Area. The Extremely Large Telescope Design Study (ELT DS) is part of this initiative and the University of Nice is grateful for the financial support the ELT DS provides."

Bibliography:

Kornilov, V. G., & Tokovinin, A. A. (2001). Measurement of turbulence in the free Atmosphere above Mt. Maidanak. *Astronomy Report* .

Maire, j., & al. (2007). Comparaison between atmospheric turbulence models by angle-of-arrival covariance measurements. *MNRAS* .

Maire, J., & al. (2006). Measurments of wavefront outer scale profiles from Moon's linbe observations. *MNRAS* .

Maire, J., & al. (2005). Wavefront outer scale deduced from interferometric dipersed fringes. *A&A* .

Roddier, F. (1981). The effects of atmospheric turbulence in optical astronomy. *progress in optics* .

Sarazin, M. (1986). ESO-VLT Instrumention for site evaluation in Northern Chile. *SPIE* .

Sarazin, M., & Roddier, F. (1991). The ESO differential image motion monitor. *A&A* .

Tokovinin, A. (2007). Turbulence profiles from the scintillation of stars, Planets and Moon.

Tokovinin, A., & Kornilov, V. (2007). Accurate turbulence measurement with MASS and DIMM.

Vernin, J., & Munoz-Tunon, C. (1995). Measuring Astronomical Seeing: The DA/IAC DIMM. *PASP* .

Ziad, A., & al. (2000). from the grating scale monitor to the generalized seeing monitor. *App. Optics* .

Ziad, A., & al. (2004). Towards the monitoring of atmospheric turbulence model. *A&A* .